IMPERIAL COLLEGE OF SCIENCE, TECHNOLOGY AND MEDICINE

Faculty of Engineering

Department of Chemical Engineering

Dual-layer Functional Ceramic Hollow Fibre Membranes for Partial Oxidation of Methane

By

Zhentao Wu

Thesis Submitted for the Degree of Doctor of Philosophy and for the Diploma of Imperial College

March 2012

Declaration of Originality

I hereby declare that this thesis and the work reported herein was composed by and originated entirely from me. Information derived from the published and unpublished work of others has been acknowledged in the text and the relevant references are included in this thesis.

Zhentao Wu

Imperial College London,

March 2012

Abstract

Due to the unique mechanism of oxygen permeation through dense ceramic membranes with the mixed ionic-electronic conducting property, these membranes have been widely studied for oxygen separation. It has been several decades since the use of a dense ceramic membrane reactor for methane conversion was proposed. One of the major reasons for persistent worldwide research efforts to develop such dense ceramic membrane reactors is the advantages that result from combining oxygen separation and catalytic reactions within a single unit. Besides the significant progress that has been made to date, more and more effort has been directed towards the development of more stable membrane materials with higher oxygen permeation, more advanced membrane micro-structures, membrane configurations with higher surface area per unit volume and better membrane reactor designs. By improving the aforementioned membrane and membrane reactor properties, lower operating temperatures, longer life time and reduced costs can be achieved.

The evolution of membrane reactor designs has progressed through a number of stages, from an initial disk-type design to flat-sheet stack or tubular designs with higher surface areas. It is not until very recently that ceramic hollow fibre membrane with further increased surface area/volume ratios of up to 3000 m^2/m^3 has been developed. Although there has been a consistent progress in improving membrane configurations, the way that catalyst is employed in a membrane reactor is still based on packing catalyst particles on the membrane or inside the reactor. This occupies a considerable amount of space and as a consequence the actual surface area/volume ratio of a membrane reactor design is significantly lower than that of the membrane itself.

In order to develop a highly compact membrane reactor design for partial oxidation of methane (POM) with the maximum possible surface area/volume

ratio, this thesis focuses on the development of a functional ceramic hollow fibre membrane with a novel dual-layer structure. The outer layer is designed for oxygen separation while the inner layer can be considered as a catalytic substrate layer. Such dual-layer ceramic hollow fibre membranes can be fabricated by a novel single-step co-extrusion and co-sintering process. This new membrane fabrication process allows for the simultaneous formation of the dual-layer membrane structure with excellent adhesion between the two layers even at high operating temperatures. Moreover, as well as changes in the compositions of the membrane material, aspects of the membrane structure, such as the thickness of the outer oxygen separation layer, can be adjusted during the co-extrusion process, in order to achieve higher oxygen permeation and subsequently better reactor performance.

Although the functional dual-layer ceramic hollow fibre membranes discussed in this thesis are designed for POM, there are generic advantages of such membrane structures and the membrane fabrication process. Therefore, membranes of this type can be transferred to other membrane processes of great importance, such as oxygen separation and solid oxide fuel cells (SOFC).

Acknowledgements

First of all, I would like to thank Prof. Kang Li for his patient supervision and continuous strong support throughout my PhD study, and precious opportunities given to get access to different aspects of research activities by building up close collaborations with world-leading research groups. Scientific discussion with him has always been constructive and productive, which helps a great deal to pin down the crux of problems and generate new efficient solutions that significantly speed up the research progress. I am always grateful to benefit from his extensive knowledge and experience in academic research and many other aspects of life as a junior researcher in general, especially in the first two years of my PhD study.

I would also like to thank Dr. Benjamin F. K. Kingsbury and Dr. Bo Wang for the suggestions that they have offered throughout my PhD and for the many helpful discussions that covered lots of technique details of my work. They always made time to help with research and offer advice, which were greatly appreciated.

I also appreciate the help from the present and previous members of Prof. Li's group. Dr. Chiao-chien Wei and Dr. Sirichai Koonaphaapdeelert helped a lot to get me properly trained for membrane fabrication. The team with Dr. Ejirooghene Gbenedio, Dr. Krzystof Kanawka, Dr. Ifran Mohd Mohamed, Dr. Barbara Zydorczak, Dr. Mohd Hafiz Dzarfan Othman, Dr. Nur Hashim, Hashrina Hashbullah, Dr. Mohammad Reza Moghareh Abed, Dr. Mukhlis A Rahman and Dr Santosh Kumbharkar provides such a pleasant working environment where I was able to accumulate more experience in various aspects of membrane processes. Dr. Yutie Liu offered me a lot of practical help on the characterizations of different membranes. I would also like to thank Prof. Wanqin Jin, Dr. Xueliang Dong and their team members for their exceptional hospitality and great support during my time at Nanjing University of Technology, China.

I would also like to offer my thanks to Dr. Ardakani and Prof. Luckham for the provision and help with SEM and rheological characterization, respectively, and to Mrs. Patricia Carry for laboratory analysis. I also appreciate the work done by the technical and administrative staff to keep things running smoothly, especially Susi Underwood for processing my documentation over the course of my PhD and Keith Walker for supplying equipments and materials.

The research funding given by EPSRC for the duration of my PhD research is also greatly appreciated and finally, I would like to thank my friends and family who have been a constant source of encouragement throughout my PhD study, especially my wife and lovely son.

Table of Contents

Abstract…… 1

Acknowledgements…… 3

Table of contents…… 5

List of figures…….. 10

List of Tables…… 15

Chapter 1 Introduction…….. 16

1.1 Background…… 16

1.2 Objectives and thesis arrangement…… 23

1.2.1 Objectives and key research contents…….. 23

1.2.1.1 Selection of membrane materials…….. 24

1.2.1.2 Membrane fabrication process …….. 25

1.2.1.3 Membrane structures…… 27

1.2.1.4 Membrane reactor performance…… 27

1.2.2 Thesis arrangement…….. 28

Reference …….. 30

Chapter 2 Dense Ceramic Membrane Reactors for Methane Conversion…… 32

Abstract …….. 32

2.1 Introduction…… 33

2.2 Fundamentals of membrane materials 34

2.2.1 Crystal structure of perovskite-type materials…….. 34

2.2.2 Properties of MIEC materials…….. 37

2.2.3 Principles of developing MIEC materials…….. 38

2.2.4 Current status of MIEC materials…… 39

2.2.5 Summary of the development of MIEC materials…… 45

2.3 Fundamentals of MIEC membranes for oxygen separation…….. 45

2.3.1 Mechanism of oxygen permeation through MIEC

	membranes……	45
2.3.2	Classification of MIEC membranes for oxygen separation……..	47
2.3.2.1	Membrane configurations……	47
2.3.2.2	Membrane micro-structures……	49
2.3.3	Current status of MIEC membranes for oxygen separation……..	52
2.3.3.1	A phase inversion process producing ceramic hollow fibres……	52
2.3.3.2	MIEC hollow fibre membranes for oxygen separation….	54
2.4	MIEC membrane reactors for methane conversion…….	57
2.4.1	Fundamentals of MIEC membrane reactors …….	57
2.4.2	MIEC hollow fibre membrane reactors……..	59
2.5	Summarization……..	61
Reference	……..	63
Chapter 3	**A Single-Step Co-extrusion and Co-sintering Method for the Preparation of Dual-Layer Ceramic Hollow Fibre Membranes** …….	76
Abstract	……..	76
3.1	Introduction……	77
3.1.1	Objectives……..	78
3.2	Background……	78
3.2.1	Preparation of supported/asymmetric MIEC membrane.	78
3.2.2	Preparation of self-supported single layer MIEC hollow fibre membranes……	79
3.3	Experimental……..	87
3.3.1	Materials……	87
3.3.2	Co-extrusion of dual-layer hollow fibre membranes……	88
3.3.3	Characterizations……..	89
3.4	Results and discussion……	89
3.4.1	Preparation of LSCF/Al_2O_3 and LSCF/YSZ dual-layer hollow fibres……	89

3.4.2	Preparation of LSCF/LSCF-YSZ-8 dual-layer hollow fibres……	92
3.5	Conclusion……..	100
Reference	……..	102
Chapter 4	**A Novel Dual-Layer Ceramic Hollow Fibre Membrane Reactor for POM**…….....	104
Abstract	……..	104
4.1	Introduction…….	105
4.1.1	Objectives……...	106
4.2	Background…….	107
4.3	Experimental……..	110
4.3.1	Materials…….	110
4.3.2	Fabrication of LSM-YSZ/NiO-YSZ dual-layer hollow fibres…….	110
4.3.3	Characterizations of the dual-layer hollow fibres…….	112
4.3.4	Methane conversion using the DL-HFMR…….	113
4.4	Results and discussion…….	114
4.4.1	Co-extrusion of the dual-layer precursor hollow fibres…	114
4.4.2	Sintering behaviours of LSM-YSZ and NiO-YSZ …….	116
4.4.3	Mechanical property and microstructure of dual-layer hollow fibres…….	119
4.4.4	DL-HFMR for methane conversion…….	123
4.5	Conclusion……..	127
Reference	……..	128
Chapter 5	**Functional LSM-ScSZ/NiO-ScSZ Dual-Layer Hollow Fibres for Partial Oxidation of Methane**…….	132
Abstract	……..	132
5.1	Introduction…….	133
5.1.1	Objectives……...	135
5.2	Background…….	135
5.3	Experimental……..	137

5.3.1	Materials……..	137
5.3.2	Determination of membrane material compositions……	137
5.3.3	Fabrication of LSM-ScSZ/NiO-ScSZ dual-layer hollow fibres……	138
5.3.4	Characterizations of dual-layer hollow fibres…….	139
5.3.5	Partial oxidation of methane ……..	139
5.4	Results and discussion……	140
5.4.1	Compatibility of membrane materials…….	140
5.4.2	Adhesion between the separation and the catalytic layers……..	141
5.4.3	Sintering behaviour of membrane materials…….	143
5.4.4	Morphology and microstructure of LSM-ScSZ/Ni-ScSZ..	148
5.4.5	Partial oxidation of methane ……..	150
5.4.6	Comparison between DL-HFMR-YSZ and DL-HFMR-ScSZ……	153
5.5	Conclusions……	155
Reference	……..	156
Chapter 6	**Effects of Separation Layer Thickness on Oxygen Permeation and Mechanical Strength of DL-HFMR-ScSZ**……	160
Abstract	……..	160
6.1	Introduction……	161
6.1.1	Objectives……..	164
6.2	Background……	164
6.3	Experimental……..	166
6.3.1	Materials……	166
6.3.2	Fabrication of LSM-ScSZ/NiO-ScSZ dual-layer hollow fibres……	167
6.3.3	Characterizations of dual-layer hollow fibres…….	168

6.3.4	Oxygen permeation and methane conversion of DL-HFMR-ScSZ……..	168
6.4	Results and discussion……	169
6.4.1	Morphology of the precursor dual-layer hollow fibres…..	169
6.4.2	Microstructure of the co-sintered dual-layer hollow fibres……	170
6.4.3	Mechanical strength of the dual-layer hollow fibres……	177
6.4.4	Oxygen permeation of the dual-layer hollow fibre membranes……	178
6.5	Conclusions……	185
Reference	……..	186
Chapter 7	**Major Findings and Recommendations**…….	189
7.1	General conclusions……	189
7.1.1	Membrane fabrication – co-extrusion and co-sintering process……	190
7.1.2	Membrane functionalization – dual-phase membrane materials……	194
7.1.3	Application – Functional DL-HFMR for methane conversion ……	196
7.1.4	Approaches to improved DL-HFMR performance…….	196
7.2	Recommendations……	197
Reference	……..	200
Appendix I - List of symbols……....		202
List of publications……		203

List of Figures

Figure 1.1	Methane conversion routes	17
Figure 1.2	Indirect conversion routes for methane conversion	18
Figure 1.3	Operating principle of a catalytic membrane reactor for syngas production	20
Figure 1.4	Key research topics of the thesis	24
Figure 1.5	The overall arrangement of the thesis	29
Figure 2.1	Research topics on MIEC materials, membranes and membrane reactors	34
Figure 2.2	Schematic diagram of the ideal perovskite (ABO_3) structure	35
Figure 2.3	Schematic diagram of oxygen permeation through MIEC membranes	46
Figure 2.4	Classification of MIEC membranes in view of geometrical configurations	47
Figure 2.5	Classification of MIEC membranes in view of micro-structures	49
Figure 2.6	Operating principle of a MIEC membrane reactor for methane conversion	57
Figure 2.7	Schematic diagram of catalyst arrangement in a BCFZ hollow fibre membrane reactor for POM reaction: (a) blank reaction, (b) catalyst packed around membrane, (c) catalyst packed around & behind membrane	59
Figure 3.1	Schematic diagram of phase inversion/sintering process	81
Figure 3.2	Schematic diagram of sintering ceramic hollow fibre membranes	86
Figure 3.3	Co-extrusion of dual-layer hollow fibre membranes	88

Figure 3.4	SEM images of LSCF/ Al_2O_3 sintered at 1280 °C for 4 h (a) cross-section (b) separation layer surface	92
Figure 3.5	SEM images of LSCF-YSZ-8 sintered at 1280 °C for 4 h (a) cross-section (b) separation layer surface	92
Figure 3.6	Photographic pictures of LSCF/LSCF(30%)-YSZ-8(70%) precursor dual-layer fibres	94
Figure 3.7	SEM images of LSCF/LSCF-YSZ-8 dual-layer fibres co-sintered at 1280 °C for 4h (a) whole cross section (b) cross section (c) inner surface (d) outer surface	95
Figure 3.8	SEM image of the sponge-like layer in the inner layer	96
Figure 3.9	Temperature dependent oxygen permeation fluxes of LSCF and LSCF/LSCF-YSZ-8 hollow fibre membranes	96
Figure 3.10	SEM images of LSCF/LSCF-YSZ (63% 3 micron & 7% 0.3 micron) dual-layer hollow fibres sintered at 1280 °C for 4 h (a) whole view (b) cross-section (c) inner surface (d) outer surface	98
Figure 3.11	SEM images of LSCF/LSCF-YSZ (63% 3 micron & 7% 0.3 micron) dual-layer hollow fibres sintered at 1380 °C for 4 h (a) whole view (b) cross-section (c) inner surface (d) outer surface	99
Figure 4.1	Schematic diagram of preparing dual-layer hollow fibres using the co-extrusion process	112
Figure 4.2	Schematic diagram of experimental setting-up for POM reaction	113
Figure 4.3	Photographic and SEM images of the precursor dual-layer hollow fibres (a) photograph, (b) whole view (SEM), (c) cross section (SEM)	115
Figure 4.4	Sintering curves and sintering rates curves of the dual-layer hollow fibre materials, (a) sintering curves and (b)	

	sintering rates	118
Figure 4.5	SEM images of dual-layer hollow fibres after co-sintering (I) and after reduction (II), (a) whole view, (b) cross section, (c) outer layer cross section, (d) inner layer cross section, (e) outer layer surface, (f) inner layer surface	121
Figure 4.6	The time dependent performance of DL-HFMR at 750°C	124
Figure 4.7	The time dependent methane conversion (open symbols) and CO selectivity (solid symbols) of DL-HFMR between 800-950°C	125
Figure 4.8	The time dependent H_2/CO (open symbols) and oxygen permeation rate (solid symbols) of DL-HFMR between 800-950°C	126
Figure 5.1	Schematic diagram of a dual-layer membrane reactor for methane conversion	133
Figure 5.2	Temperature dependence of electrical conductivity for selected oxide ion conductors	134
Figure 5.3	Effects of membrane material on fabrication process and reactor performance	136
Figure 5.4	XRD patterns of LSM-ScSZ and NiO-ScSZ (1:1 by weight ratio) sintered at 1450 °C for 6 h	141
Figure 5.5	Schematic diagram of forming great adhesion between the two layers of LSM-ScSZ/NiO-ScSZ	143
Figure 5.6	Dilatometric curves of LSM, NiO and ScSZ (a) sintering curves and (b) sintering rate curves	144
Figure 5.7	Dilatometric curves of LSM-ScSZ and NiO-ScSZ (a) sintering curves and (b) sintering rate curves	147
Figure 5.8	SEM images of LSM-ScSZ/Ni-ScSZ (a) whole view (b) cross section (c) inner layer cross section (d) outer layer cross section (e) boundary between the two layers (f)	

	inner surface (g) outer surface	149
Figure 5.9	Time dependent (a) X_{CH4}, S_{CO} and S_C, (b) H_2/CO and F_{O2} between 920 and 1060 °C	152
Figure 5.10	Comparison between DL-HFMR-YSZ and DL-HFMR-ScSZ (a) X_{CH4}, S_{CO} and F_{O2} and (b) S_C	154
Figure 6.1	Change of oxygen permeation with the membrane thickness	163
Figure 6.2	Experimental set-up of measuring oxygen permeation and methane conversion	169
Figure 6.3	Photographic images of the precursor dual-layer fibres with different outer layer extrusion rates (0.5 to 5.0 ml/min)	170
Figure 6.4	SEM images of the co-sintered fibres – whole view (a) 0.5 ml/min, (b) 1.0 ml/min, (c) 2.0 ml/min, (d) 3.0 ml/min, (e) 4.0 ml/min, (f) 5.0 ml/min	171
Figure 6.5	SEM images of the co-sintered fibres – cross section (a) 0.5 ml/min, (b) 1.0 ml/min, (c) 2.0 ml/min, (d) 3.0 ml/min, (e) 4.0 ml/min, (f) 5.0 ml/min	172
Figure 6.6	SEM images of the co-sintered fibres – inner layer cross section (a) 0.5 ml/min, (b) 1.0 ml/min, (c) 2.0 ml/min, (d) 3.0 ml/min, (e) 4.0 ml/min, (f) 5.0 ml/min	172
Figure 6.7	SEM images of the co-sintered fibres – outer layer cross section (a) 0.5 ml/min, (b) 1.0 ml/min, (c) 2.0 ml/min, (d) 3.0 ml/min, (e) 4.0 ml/min, (f) 5.0 ml/min	173
Figure 6.8	SEM images of the co-sintered fibres – inner surface (a) 0.5 ml/min, (b) 1.0 ml/min, (c) 2.0 ml/min, (d) 3.0 ml/min, (e) 4.0 ml/min, (f) 5.0 ml/min	173
Figure 6.9	SEM images of the co-sintered fibres – outer surface (a) 0.5 ml/min, (b) 1.0 ml/min, (c) 2.0 ml/min, (d) 3.0 ml/min,	

(e) 4.0 ml/min, (f) 5.0 ml/min 174

Figure 6.10 (a) ID and OD and (b) thickness of the inner and outer layers of the co-sintered dual-layer hollow fibres with different outer layer extrusion rate 175

Figure 6.11 Photographic image of precursor dual-layer hollow fibres with finger-like voids developed from both the inner and outer surfaces 176

Figure 6.12 Effects of the outer layer extrusion rate on the mechanical strength of the dual-layer hollow fibres 178

Figure 6.13 Effects of temperature on the oxygen permeation of dual-layer hollow fibre membranes with different separation layer thicknesses 180

Figure 6.14 Effects of separation layer thickness on oxygen permeation at different temperatures 181

Figure 6.15 Methane conversion, coke deposition and oxygen permeation rate of DL-HFMR-ScSZ with the separation layer of 8.0 μm (blank symbols) and 63.8 μm (solid symbols) at 820 °C 185

Figure 7.1 Photographic image of a triple-layer hollow fibre fabricated by co-extrusion and co-sintering process 199

List of Tables

Table 2.1	Oxygen permeation of MIEC hollow fibre membranes	56
Table 3.1	Compositions of LSCF/ Al_2O_3 spinning suspensions and co-extrusion parameters	90
Table 3.2	Compositions of LSCF/ YSZ-8 spinning suspensions and co-extrusion parameters	90
Table 3.3	Compositions of LSCF/ LSCF(30%)-YSZ-8(70%) spinning suspensions and co-extrusion parameters	93
Table 3.4	Summarization of the shrinkages of the hollow fibres membranes	100
Table 4.1	Compositions of the spinning suspensions and co-extrusion parameters	111
Table 4.2	Three-point bending of single-layer and dual-layer hollow fibres	120
Table 5.1	Compositions of spinning suspensions and co-extrusion parameters	138
Table 5.2	Operating conditions and the differences in membrane reactor structure	153
Table 6.1	Compositions of spinning suspensions and co-extrusion parameters	167

Chapter 1
Introduction

1.1 Background

Methane conversion

Natural gas is one of the cleanest, safest, and most useful natural energy sources of huge reserves, and is one of the essential components of global energy supply. However, the major reserves of natural gas are located in remote areas, and as a consequence it is difficult to justify the economical transportation of natural gas from wellheads to consumers due to the low energy content per unit volume, unless it can be physically liquefied or economically chemically converted to other liquid products. Up to date, most of global production of methane, the major component of natural gas, is consumed directly as a fuel for heating or for power generation, instead of being utilized for the production of higher value-added chemicals and cleaner fuels (such as hydrogen). Methane flaring or emission not only causes wastage of valuable raw materials, but also raises concerns over global warming due to the release of a large quantity of carbon dioxide into atmosphere. Following the oil crisis in 1970s and other environmental and political issues, there have been considerable world-wide efforts for commercially viable routes to convert methane into more valuable and more transportable chemicals and fuels, which is briefly summarized in Figure 1.1. Technologies for methane conversion have also been recognized as one of the most technologically important and challenging issues facing the industrialized nations.

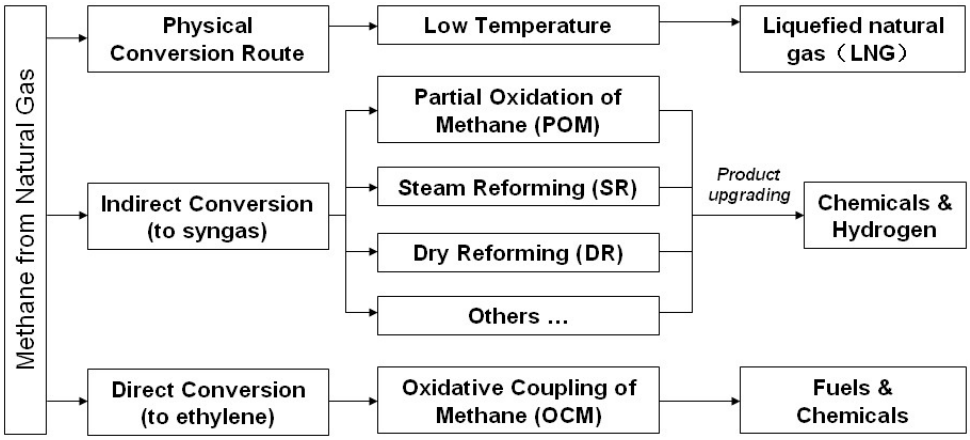


Figure 1.1 Methane conversion routes

Products of great importance, such as C_1 compounds (methanol and formaldehyde), C_2 hydrocarbons (ethane and ethylene), and syngas (a mixture of CO and H_2) etc., can be obtained through a catalytic oxidation or a dehydrogenation of methane. Except for the one involving syngas synthesis, other methane conversion routes have not yet found large scale commercial applications due to the limited reactivity or low selectivity to the desired products [1]. In contrast to C_1 products or indirect conversion technologies, direct methane coupling to higher hydrocarbons can be more economically beneficial if C_2 yields higher than 30% can be achieved [1]. In the last three decades, considerable efforts have been involved in the development of highly active and selective OCM catalysts, catalytic reactors and reaction mechanism, in order to achieve commercially feasible product selectivity and yields, and operation at a mild environment [1]. However, the commercialization of OCM process is still challenged by the low methane

conversion and C_2 yields, high operating temperatures and separation of low concentration ethylene from the product stream etc..

Alternatively, indirect conversion routes, in which methane is converted into syngas prior to the subsequent product upgrading, are considered to be more productive and flexible. Syngas can be produced from methane by a series of reactions, as shown in Figure 1.2, and be subsequently turned into other chemicals and fuels by well developed engineering processes. In the indirect conversion routes, syngas production normally takes around 60% of the overall cost, while products upgrading together with post-treatments have been industrially and commercially well developed and take the rest 40% of cost.

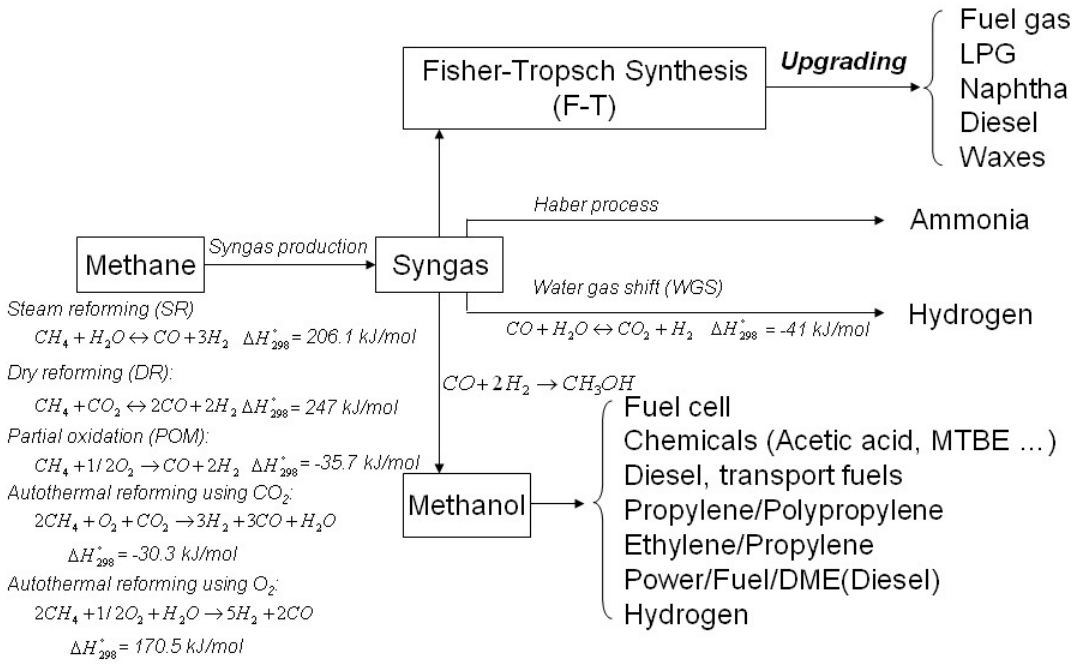


Figure 1.2 Indirect conversion routes for methane conversion

As a result, extensive efforts have been directed to the development of new techniques to reduce the cost of syngas production. So far, the highly endothermic steam-reforming (SR) reaction still dominates syngas production from methane, but a substantial energy input and an additional optimization of the molar ratio between hydrogen and carbon monoxide in the product stream (prior to the subsequent product upgrading) have to be compromised. Although the advantages of autothermal reforming (ATR) processes, such as coupling exothermal and endothermic reactions for less overall energy consumption, can be used to lower the energy cost and adjust the H_2/CO ratio, large-scaled equipments and complicated controlling systems have to be employed.

In comparison with SR and ATR processes, partial oxidation of methane (POM) to syngas needs much less energy, as a result of the mild exothermal nature of the reaction. Moreover, the ratio of H_2/CO in the product stream is 2, which is ideal for the production of methanol via the F-T process. All these advantages contribute to reduce the cost of syngas production by as much as 10-15%. However, pure oxygen (normally produced from large oxygen plants) has to be employed, and the direct pre-mixing of oxygen and methane at high temperatures raises serious safety concerns for most of the conventional catalytic reactor designs, in additional to the possible over oxidation of methane to other by-products. As a consequence, the challenges for POM routes are how to obtain pure oxygen in a more economical way and how to uniformly distribute oxygen inside the reactor, instead of pre-mixing with methane.

Membrane technology for methane conversion

Benefiting from the significant development of membrane technology, the concept of catalytic membrane reactor coupling reaction and membrane separation into one unit [2, 3] has been developed and widely studied. For those reactions limited by thermodynamics, higher conversion rate and reaction yield can be achieved by selectively removing one or more products from reaction zone [4-6]. In another case, membrane can be used to control the reaction pathway by introducing/distributing one or more reactants into the reactor in a controllable manner [2, 7-9]. By using oxygen permselective membranes made of ceramic oxides with fluorite, perovskite or perovskite-related structures, air can be, in this case, directly utilized as oxygen source for POM reaction in a catalytic membrane reactor, as shown in Figure 1.3.

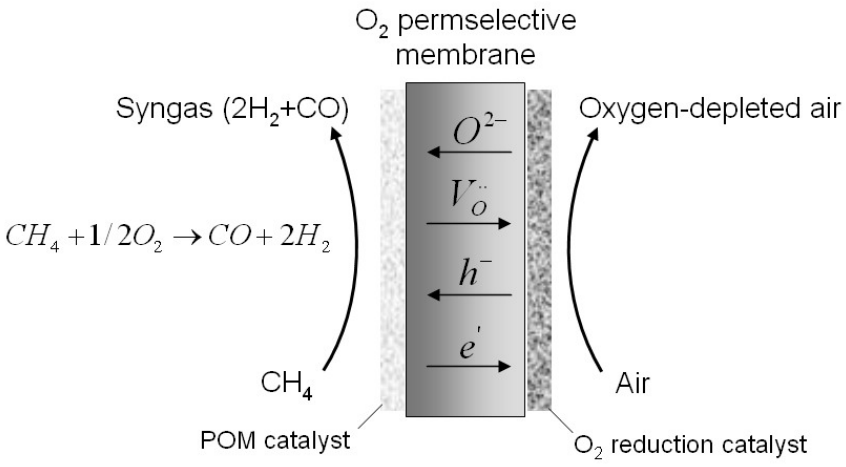


Figure 1.3 Operating principle of a catalytic membrane reactor for syngas production

This saves approximately 30% of investments by eliminating oxygen separation in large scale oxygen plants [10]. In addition, pure oxygen can be uniformly distributed within the membrane reactor by controlling the oxygen permeation process through the membranes, enhancing the reaction yield and safety [7].

Two of the most important, and often the most expensive, steps in a chemical process are usually chemical reactor and purification of feed stream and/or separation of product stream [4]. Coupling of these two steps into a single unit leads to significant savings in energy and reactant consumption, and reduces by-product formation. Extensive efforts have been carried out to develop membrane reactors of this type for methane conversion. Two industrial alliances have been formed in America to promote R&D work aiming at commercialization of ceramic membrane technology for syngas production [11, 12]. One includes five large global oil and gas companies, i.e. BP/Amoco, Praxair, Sasol, Statoil and Phillips Petroleum, cooperating with universities, and the other one is headed by Air Products and Chemicals and Ceramatec, and works together with other industrial partners. Although significant progress has been achieved in the last several decades, experimentally and theoretically demonstrating the feasibility as well as the advantages of using catalytic membrane reactor for syngas production [11], there are still a number of technological challenges limiting the applications of this methane conversion technique:

1) Trade-off between oxygen permeation and chemical and thermal stabilities of the membrane materials.

2) High operating temperatures (800-950 °C) needed for a reasonable oxygen permeation flux.

3) Lack of reliable high temperature seals and/or sealing methods for the ceramic membranes in a disk/flat-sheet or a short tubular configuration.

4) Lack of reliable techniques allowing large-scale production of uniform oxygen permselective membranes and flexible control over the membrane microstructures.

5) Lack of achievable techniques for the fabrication of uniform and defect free thin oxygen permselective films supported on stable substrates. Such composite membrane configuration will promote oxygen permeation flux and reduce membrane cost.

6) Necessity of developing oxygen permselective membranes with higher surface area/volume ratio, increasing oxygen production rate of per unit volume.

7) Necessity of developing catalytic membrane reactor designs with higher volume productivity.

Dual-layer ceramic hollow fibre membranes for methane conversion

In terms of membrane configurations and membrane reactor designs, disk/flat-sheet or short tubular supported/asymmetric membranes composed of a thin dense oxygen separation layer supported on a highly porous substrate always show greater oxygen permeation flux, as a result of the significantly reduced membrane thickness. In the mean time, ceramic hollow fibre membranes possess to date the highest surface area/volume ratio.

However, there is still a lack of ceramic membrane configuration or a membrane reactor design that is able to combine the advantages of the two membrane configurations above, mainly due to the fact that it is hardly achievable by the conventional membrane fabrication processes.

In this thesis, a novel single-step co-extrusion and co-sintering fabrication process is going to be employed to develop dual-layer ceramic hollow fibre membranes, a membrane configuration that has yet to be achieved experimentally in oxygen separation and membrane reactor for POM reaction. The membranes of this type are directly used as a multifunctional catalytic hollow fibre membrane reactor for methane conversion. The main objective of this thesis is to gain knowledge and understanding in different aspects of the newly developed oxygen permselective hollow fibre membranes, as well as the use of such membranes as a new membrane reactor design for methane conversion. Principles of how to select membrane materials and the key factors of fabricating such membranes with controlled macro/microstructures are addressed, together with the systematic characterizations and the evaluation of such membrane reactor design for methane conversion.

1.2 Objectives and thesis arrangement

1.2.1 Objectives and key research contents

The main objective of this thesis is to develop a compact multifunctional ceramic hollow fibre membrane reactor design for methane conversion. A new single-step membrane fabrication process, i.e. a co-extrusion and co-sintering

process, is used for the production of the hollow fibre membranes with a novel dual-layer structure for such purpose. The thin dense outer layer is for oxygen separation while the other highly porous inner layer functions not only as a support, but also a catalytic layer in the reactor, significantly increasing the surface area/volume ratio of the membrane reactor design of this type by eliminating additional catalyst packing. In order to achieve this, a series of technical difficulties need to be solved, and they are presented in Figure 1.4. These difficulties majorly cover 3 interactive aspects, which are membrane material, membrane fabrication and membrane structure. All these will finally determine the performance of the resultant membrane reactor for methane conversion.

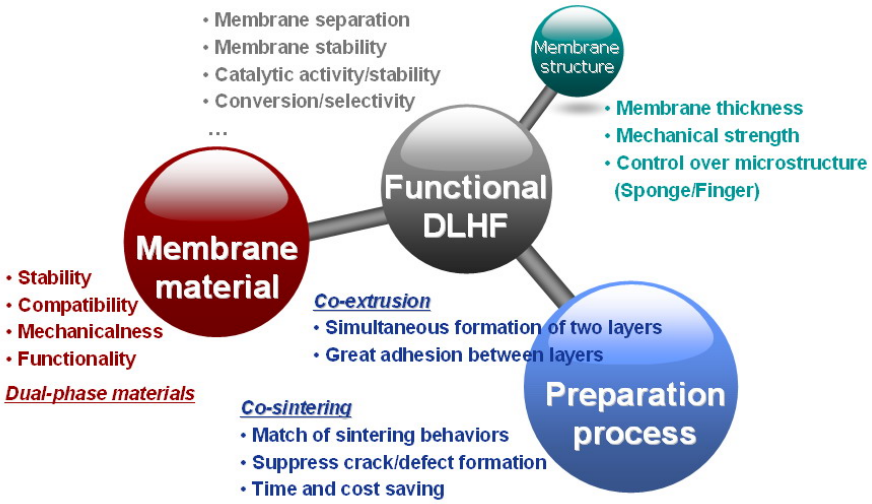


Figure 1.4 Key research topics of the thesis

1.2.1.1 Selection of membrane materials

In most cases, single-phase mixed ionic-electronic conducting (MIEC) ceramics are studied for oxygen separation, ceramic membrane reactor and solid oxide fuel cell (SOFC), due to the much higher mixed conductivity than the other ceramic materials and the adjustable oxygen permeation via doping. It has been widely accepted that in a membrane reactor for methane conversion, a membrane material with higher oxygen permeation flux is less stable at high temperatures, especially in the presence of reducing products such as H_2 and CO. In fact, it is still one of the major challenges limiting the development and application of MIEC membranes. Although dual-phase ceramic materials consisting of a separate ionic-conductive phase and an electronic-conductive phase are more chemically and thermally stable, its oxygen permeation fluxes are normally much lower than the single-phase counterparts. Moreover, the selection of membrane materials for ceramic membranes in a hollow fibre configuration with a dual-layer structure inevitably raises additional concerns such as the compatibility and mechanical property of membrane materials, because both of these two can cause malfunction of the resultant membrane reactor. Furthermore, the selected membrane materials need to deliver certain functionalities to achieve a multi-functional membrane reactor design. Taken all these into consideration, dual-phase/composite membrane material seems to be the only possible candidate, because few single-phase MIEC ceramics can simultaneously meet all the requirements mentioned above.

1.2.1.2 Membrane fabrication process

Although there have been a number of processes fabricating multi-layer ceramic membranes (flat-sheet or tubular), the fabrication processes normally consist of a number of steps with repeated coating and sintering. This is not only time-consuming, but also less preferred with regards to quality control. Moreover, due to the much higher surface curvature than tubular and flat-sheet counterparts, uniform and controllable coating free of defects on ceramic hollow fibres is more challenging to the conventional fabrication processes. As a result, a phase-inversion based single-step co-extrusion and co-sintering process is going to be employed in this thesis to fabricate ceramic dual-layer ceramic hollow fibre membranes.

Co-extrusion: different from the conventional fabrication processes for a dual-layer ceramic membrane, where a coating is normally carried out on a pre-sintered support followed by another sintering process, the two layers of the hollow fibre membranes can be simultaneously formed during the preparation process, contributing to form greater adhesion between the layers even if the curvature of hollow fibre membranes is much higher. By adjusting the co-extrusion parameters such as suspension viscosity, extrusion rate and air-gap etc., thickness of the outer layer and macrostructure of the hollow fibre membrane can be controlled and adjusted for different purposes.

Co-sintering: Besides time- and cost-saving, one of the main advantages of co-sintering over the conventional counterparts is that, the possibility of forming cracks or defects is significantly reduced or suppressed by avoiding

repeated high temperature sintering. However, as a prerequisite to this advantage, sintering behaviours and thermal expansion of the two layers, which are largely determined by materials and phase composition, should be investigated and well matched during the co-sintering step.

1.2.1.3 Membrane structures

For the dual-layer ceramic hollow fibre membranes to be developed in this thesis, membrane structures indicate both the macro- and micro-structures of the membrane, and they both affect the membrane performance. Macro-structure means the morphology of the membrane, such as thickness of each layer, as well as the finger-like voids and sponge-like structure in each layer. In contrast to tubular membranes, there are more concerns over the mechanical strength of ceramic hollow fibre membranes that is closely related to the macro-structure. The macro-structure can be well controlled and adjusted by the co-extrusion and co-sintering process. The micro-structure of the membrane (porosity of the porous substrate layer, boundaries between the two layers and between the two phases in each layer etc.) is more dependent on the membrane materials, such as particle size and phase composition, although the co-sintering step also plays a very important role.

1.2.1.4 Membrane reactor performance

With regards to the advantages of the functional dual-layer hollow fibre membrane reactor design, an extremely high surface area/volume ratio can be achieved by avoiding extra catalyst packing inside the reactor. This is quite

unique from the conventional membrane reactor design. However, the performance of such membrane reactor is still dependent on a number of other factors: 1) oxygen permeation flux of the outer oxygen separation layer, which is determined by the membrane materials as well as their phase composition and the minimum thickness of the outer layer that can be achieved; 2) catalytic activity and stability of the inner catalytic support layer and 3) porosity and average pore size of the inner layer, which determine how efficiently methane is able to diffuse into this layer and reacts with the permeated oxygen. Besides the fabrication process, the phase composition of the membrane material determines the porous structure of the inner layer, which also considerably affects the mechanical property of the resultant hollow fibre.

In brief, membrane materials and their phase composition, structure and fabrication of dual-layer hollow fibre membranes and performance of the resultant membrane reactors are highly interactive factors, and constitute the major content of this thesis. As a result, the research work is divided into several parts following the layout introduced in the subsequent section.

1.2.2 Thesis arrangement

This thesis consists of 7 chapters in total, addressing different aspects of the development of a compact multifunctional ceramic dual-layer hollow fibre membrane reactor for methane conversion. Each chapter begins with an abstract followed by a brief introduction part, capturing fundamental findings in

the sub-research and building up connections with previous chapters. The overall arrangement of the thesis is shown in Figure 1.5.

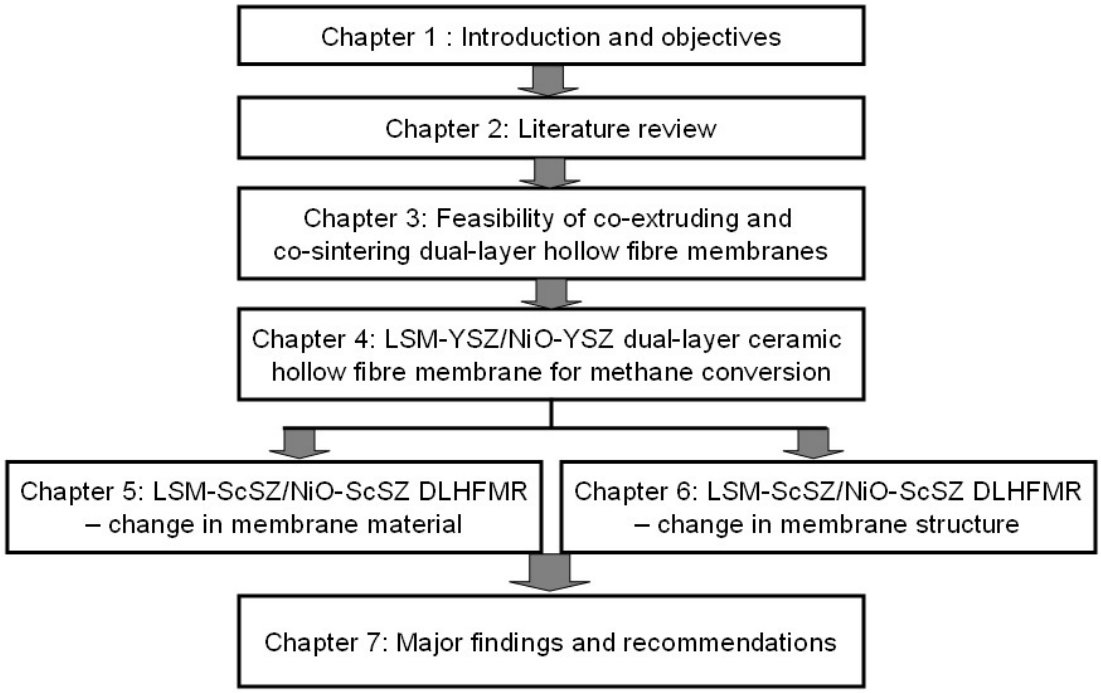


Figure 1.5 The overall arrangement of the thesis

Chapter 1 briefly introduces the background and major objectives of the research. A systematic literature review in Chapter 2 gives an insight into the fundamental knowledge of MIEC materials for oxygen separation, membrane configurations as well as fabrication processes, and related membrane reactor designs for methane conversion. Chapter 3 investigates the technical feasibility of using the single-step co-extrusion and co-sintering process to fabricate dual-layer ceramic hollow fibre membranes, addressing more on the fabrication process with less effort on the selection of membrane materials. Based on Chapter 3, proper membrane materials are employed in Chapter 4

to functionalize the two layers of the fibre and a functional dual-layer hollow fibre membrane reactor for methane conversion is developed and characterized. In order to improve the reactor performance, different measures to improve oxygen permeation and reduce coke-formation are carried out in Chapter 5 and Chapter 6. The improvement in Chapter 5 is to replace YSZ by ScSZ, a better ionic-conductive phase for higher oxygen permeation (from the point of view of membrane material). While the one in Chapter 6 is to reduce the thickness of the outer oxygen separation layer in order for higher oxygen permeation (from the point of view of membrane structure). Finally, Chapter 7 summarizes general conclusions of the research and gives recommendations for the future work.

References

1. S.M. Liu, X.Y. Tan, K. Li, R. Hughes, Methane coupling using catalytic membrane reactors, Catal. Rev.-Sci. Eng., 43 (2001) 147-198.
2. K. Li, *Ceramic Membranes for Separation and Reaction*. 2007: Wiley.
3. T. Westermann, T. Melin, Flow-through catalytic membrane reactors--Principles and applications, Chemical Engineering and Processing: Process Intensification, 48 (2009) 17-28.
4. A.G. Dixon, Recent Research in Catalytic Inorganic Membrane Reactors, International Journal of Chemical Reactor Engineering, 1 (2003) 1-34.
5. J.A. Ritter, A.D. Ebner, State-of-the-art adsorption and membrane separation processes for hydrogen production in the chemical and petrochemical industries, Sep. Sci. Technol., 42 (2007) 1123-1193.

6. S.N. Paglieri, J.D. Way, Innovations in palladium membrane research, Separation and Purification Methods, 31 (2002) 1-169.

7. H.J.M. Bouwmeester, Dense ceramic membranes for methane conversion, Catalysis Today, 82 (2003) 141-150.

8. W.S. Yang, H.H. Wang, X.F. Zhu, L.W. Lin, Development and application of oxygen permeable membrane in selective oxidation of light alkanes, Topics in Catalysis, 35 (2005) 155-167.

9. A. Thursfield, I.S. Metcalfe, The use of dense mixed ionic and electronic conducting membranes for chemical production, Journal of Materials Chemistry, 14 (2004) 2475-2485.

10. Y.Y. Liu, X.Y. Tan, K. Li, Mixed conducting ceramics for catalytic membrane processing, Catal. Rev.-Sci. Eng., 48 (2006) 145-198.

11. P.N. Dyer, R.E. Richards, S.L. Russek, D.M. Taylor, Ion transport membrane technology for oxygen separation and syngas production, Solid State Ionics, 134 (2000) 21-33.

12. Y.S. Lin, Microporous and dense inorganic membranes: current status and prospective, Separation and Purification Technology, 25 (2001) 39-55.

Chapter 2

Dense Ceramic Membrane Reactors for Methane Conversion

Abstract

This chapter presents a review on the recent development of mixed ionic-electronic conducting (MIEC) ceramic materials, membranes, and their applications in oxygen separation and methane conversion. Basic concepts of MIEC material structure, composition and property are first introduced briefly, followed by an introduction on the use of MIEC membranes for oxygen separation and the corresponding designs of catalytic membrane reactors for methane conversion. Achievements as well as progresses in the development of membrane materials, fabrication of MIEC membranes of different configurations and use of these membranes in methane conversion are addressed, and future technology challenges are also outlined.

Keywords: mixed ionic-electronic conducting (MIEC) material, ceramic membrane, membrane reactor, oxygen separation, methane conversion

2.1 Introduction

In 1899, Nernst [1] reported the ionic conductivity of a $ZrO_2(Y_2O_3)$ solid solution. Around 80 years later, Takahashi et. al. [2] initiated the development of mixed ionic-electronic conducting (MIEC) oxides such as Bi_2O_3-BaO. The concept of using MIEC oxides to fabricate oxygen permselective membranes was introduced by Cales et. al. [3, 4] about 25 years ago, after which extensive researches and efforts have been carried out utilizing MIEC materials for oxygen separation [5-8], solid oxide fuel cell (SOFC) [9-11] and methane conversion [6, 7, 12, 13] etc., due to the unique mixed conducting property of the materials of this type [14].

Up to date, huge amounts of studies have been reported, majorly covering the three topics of membrane material, membrane separation and membrane reactor, as shown in Figure 2.1. Although each topic seems to focus on a number of separate and specific scientific and technological issues, a breakthrough in any of them may lead to a significant progress of the whole process because of the close interactions between the three major topics.

As a result, the literature review in this chapter is also comprised of three major parts addressing the development of MIEC materials, the fabrication of MIEC membranes with different geometrical configurations and the design of MIEC membrane reactors for methane conversion, respectively. Instead of expatiating on every detail of the progress achieved, the following review focuses on the most concerning issues of every research topic.

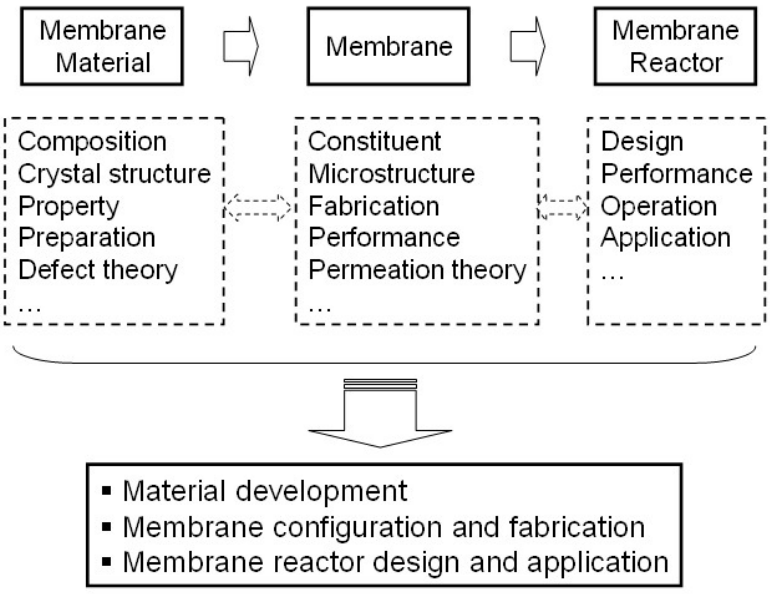


Figure 2.1 Research topics on MIEC materials, membranes and membrane reactors

2.2 Fundamentals of membrane materials

2.2.1 Crystal structure of perovskite-type materials

Although most ceramic oxides exhibit to some extent mixed conducting property, dense ceramic oxygen permselective membranes are usually made of mixed ionic-electronic conducting (MIEC) materials with perovskite or perovskite-related structures, and sometimes ion conductive materials such as fluorite oxides [15], due to the significant mixed conducting capabilities. The basic crystal structure of perovskite-type materials, which is originally named from the mineral oxide of $CaTiO_3$, was first thought to be cubic although it was later found to be orthorhombic. However, the name of perovskite has been retained for the structure of this type. The ideal perovskite structure (ABO_3) illustrated in Figure 2.2 consists of a cubic array

of corner-sharing BO_6 octahedra, where B is a transition metal cation. A-site ions (interstitial between the BO_6 octahedra) may be occupied by either an alkali, alkaline earth or a rare earth ion. In many cases, the BO_6 octahedra is distorted or tilted due to the presence of A-site cations, which is normally larger in size than B cations. When the distortion becomes too large, other crystal symmetries such as orthorhombic and rhombohedral may appear. Alternatively, the perovskite structure can be regarded as a cubic close-packing of AO_3 layers with B cations placed in the interlayer octahedral interstices. The latter one turns out to be more useful in distinguishing different structural arrangements (stacking sequences) of perovskite blocks. Although an ideal perovskite structure only consists of a series of ABO_3 units, the chemical composition of materials can vary a lot with the different valence of the A- and B-site cations. The most common combinations are $A^{1+}B^{5+}O_3$, $A^{2+}B^{4+}O_3$ and $A^{3+}B^{3+}O_3$, where the A site is generally occupied by larger 2+ alkali earth metals such as Ba, La or Sr, while smaller 4+ first-row transition elements such as Ce, Co or Fe for the B site [16].

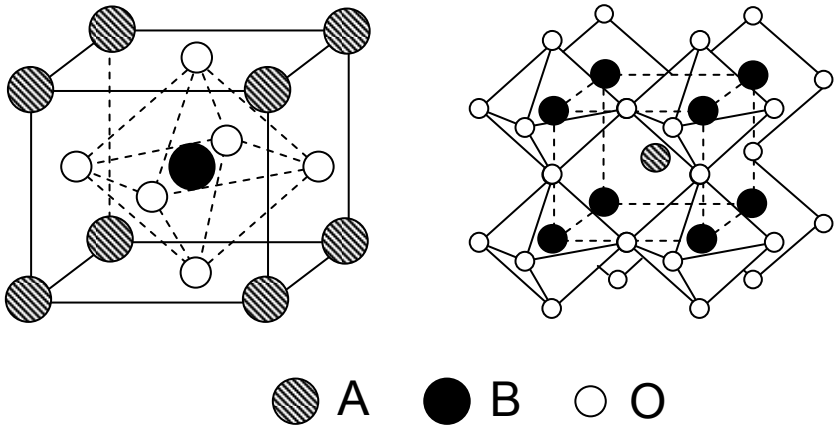


Figure 2.2. Schematic diagram of the ideal perovskite (ABO_3) structure

Selection of elements on A and B sites can be physically determined by a number of structural parameters, such as tolerance factor (*t*) and specific free volume etc., both of which are a function of ionic radius [17]. *t* of stable perovskite structure (0.75-1.0) can be calculated using the following equation:

$$t = \frac{(r_A + r_O)}{\sqrt{2}(r_B + r_O)} \tag{2-1}$$

where r_A, r_B and r_O are the mean ionic radii of A-site cations, B-site cations and oxygen ion, respectively. While specific free volume is defined as the ratio between free volume and unit cell volume [18, 19]. In addition, it has been proved that these structure-related parameters can be correlated to the electrical conductivity of MIEC materials [17], and can be used as a guidance for the selection of materials [20].

However, the ideal perovskite structure in Figure 2.2 is too “perfect” to exhibit any mixed ionic-electronic conducting property, because oxygen ions or electrons cannot move across the lattices without certain sort of “mobile carriers”. This means that a number of imperfections or defects has to be “created” according to the non-stoichiometry for the conduction or diffusion to take place [13, 21]. The most important defects for MIEC materials are ion defects and electron defects. Ion defects may take the form of vacancies, interstitial ions, impurities or dopants with charges different from those expected from the overall stoichiometry. Electron defects may be in the form of ions with charges deviating from the normal lattice ions, as a consequence of the transition of electrons from normally filled energy levels to normally empty levels [16]. Defect theory has been used to explain conductive

properties of MIEC materials, which has been systematically reviewed by Liu et. al [16] and Sunarso et. al. [8].

2.2.2 Properties of MIEC materials

In the presence of defects, MIEC materials are able to exhibit the mixed conducting property, which is usually expressed by ionic conductivity and electronic conductivity, the sum of which gives the total conductivity:

$$\sigma_{total} = \sigma_{ion} + \sigma_{electron} \tag{2-2}$$

Measurements of total and ionic conductivities can be achieved by using the four-probe method and the electron-blocking four-probe method [22], respectively. Electronic conductivity can, thus, be obtained by subtracting the ionic conductivity from the total conductivity.

Another useful and more frequently used concept to describe the mixed conducting property of MIEC materials is transport (or transference) number t_k. For a certain type of carrier k, t_k is defined as:

$$t_k = \sigma_k / \sigma_{total} \tag{2-3}$$

In the case of mixed conduction,

$$\sigma_{total} = \sigma_{ion} + \sigma_{electron} = \sigma_{total}(t_{ion} + t_{electron}) \tag{2-4}$$

where t_{ion} and $t_{electron}$ represent the transport numbers of ionic and electronic defects respectively. t_{ion} plus $t_{electron}$ always equals unity to retain electron neutrality. For an ideal MIEC material, t_{ion} and $t_{electron}$ are both preferred to be

0.5 so as to achieve the highest total conductivity, although in many cases $t_{electron}$ is much smaller than t_{ion} [16]. When $t_{electron}$ is too low, an external circuit is needed to assist electronic conduction so that the ions' transport can take place in an ionic conducting phase. The enhancement of t_{ion} and $t_{electron}$ values can be achieved by doping appropriate elements, which is one of the most efficient strategies in the development of new MIEC materials.

2.2.3 Principles of developing MIEC materials

Generally, both A- and B-site cations strongly affect the mobility of oxygen ions in the bulk phase [23], while B-site cations are, in the mean time, critically important to the catalytic activity [21] and the stability [13] of materials with the perovskite-type structure. Doping of elements by forming a solid solution or a nonintegral stoichiometry phase [24] has been one of the major methods to improve the chemical and physical properties and to develop new MIEC materials. One of the typical examples of forming solid solution is doping ZrO_2 with various rare-earth oxides [25]. ZrO_2 with fluorite-type structure can form extensive solid solutions with oxides of lower-valence cations such as CaO, Y_2O_3, and other rare-earth oxides (so-called stabilized ZrO_2). Doping with Y_2O_3, for example, results in the formation of mobile oxygen vacancies, and stabilizes the crystal structure of ZrO_2 by suppressing the phase transition to tetragonal-monoclinic at high temperatures. Apart from solid solution, a wide range of MIEC materials with ABO_3 perovskite-type structures has been developed with substitutions occurring on either the A-site atom, the B-site atom, or both, forming a structure of $A_xA'_{1-x}B_yB'_{1-y}O_{3-\delta}$ [26]. The symbol δ normally indicates the amount of oxygen vacancy (defect) in a unit cell. In

addition to the ABO_3 structure, two other types of perovskite-type structures, i.e. $A_2(B'B'')O_6$ and $A_3(B'B''_2)O_9$ can be obtained in the same way [27], although they are less popular in contrast to the $A_xA'_{1-x}B_yB'_{1-y}O_{3-\delta}$ counterparts.

Besides perovskite-type structures, a number of oxides with perovskite-related structures [16, 28] also exhibit mixed conducting property at elevated temperatures. Crystal structures of these materials are normally more complicated and the mechanisms of oxygen ion transport in bulk phase are also different from the perovskite-type counterparts.

2.2.4 Current status of MIEC materials

Due to the great interest in the MIEC materials, quite a number of useful reviews on the development of MIEC materials have been published [5-8, 11-14, 16, 29], giving elaborate details of almost every aspect of this area in the last 20 years. In order to avoid duplicating previous reviews, this section address mainly the MIEC materials covered by patents, which from another point of view presents the development of MIEC materials.

For most of the MIEC materials, electronic conductivity is lower than ionic conductivity, which restricts the transfer of more oxygen through the membranes. As a result, Ishihara and Takita [30] disclosed a Ga-based MIEC material with the general formula of $A_{1-x}Ca_xGa_{1-y}B_y$ (x and y were between 0.05-0.3). Compared with other similar materials, doping of Ga at B-site significantly increases the electronic conductivity over a wide range of

temperatures (600-1000 °C). Besides the great material stabilities, the ionic conductivity is comparable to the electronic conductivity, indicating a high total conductivity. Yang et al. [31] reported a series of materials with the general formula of $A_aB_bC_cD_dO_{3-\delta}$ ($0< \delta <1$, $0.7<a/(b+c+d)<1.3$). $BaCo_{0.4}Fe_{0.6-x}Zr_xO_{3-\delta}$ (BCFZ), as an example, exhibits both high oxygen permeation fluxes between 0.4-0.9 $ml \cdot cm^{-2} \cdot min^{-1}$ at 950 °C (feed side air of 150 ml/min, permeate side sweep gas of 30 ml/min), and great stability in reducing atmospheres. The membrane made of BCFZ was continuously operated over 1000h at 850 °C for the partial oxidation of methane (POM) to syngas. In addition, Yang et al. [32] observed that, besides the increasing oxygen permeation, the doping of Bi reduced the apparent activation energy of MIEC materials. The general formula of the materials of this type can be expressed as $A_aBi_xB_bO_{3-\delta}$ (b+x=1 if a=1; a+x=1 if b=1). It has been widely proved that, the doping of active Co at the B-site of the perovskite lattice significantly increases the oxygen permeation. However, materials with Co normally suffer from poor stabilities in reducing atmospheres. Focusing on this problem, Caro et al. [33] replaced Co with divalent cations with fixed oxidation states to improve the material stability. Although oxygen permeation flux is reduced at the expense, it can be made up by using membranes with higher surface area, which will be introduced in the following sections. Etchegoyen et al. [34] found that a simple change in chemical compositions did not fix the number of oxygen vacancies and that, consequently, was not a sufficient condition to ensure both good ionic conductivity and desirable stabilities of MIEC oxides under normal operating conditions, especially between 600 and 1000 °C. In order to develop a novel material displaying great ionic conductivity without

compromising stability over time, Etchegoyen et al. provided a method for screening material structures and disclosed some alternatives such as $La^{(III)}_{(1-x)}Sr^{(II)}_xAl^{(III)}_uFe^{(III)}_{(1-s-v)}Fe^{(IV)}_sTi_vO_{3-\delta}$, $La^{(III)}_{(1-x)}Sr^{(II)}_xAl^{(III)}_uFe^{(III)}_{(1-s-v)}Fe^{(IV)}_sGa_vO_{3-\delta}$ and $La^{(III)}_{(1-x)}Sr^{(II)}_xFe^{(III)}_{(1-s-v)}Fe^{(IV)}_sTi_vO_{3-\delta}$. For most of the MIEC materials, operating temperatures above 800 °C is required for a significant mixed conducting property, which is not favourable to membrane sealing and material stability. In order to lower the operating temperatures, Anderson et al. [35] disclosed a type of membrane materials possessing substantially cubic perovskite structure in air over a wide temperature range from 25 to 950 °C. Taking $La_{0.2}Sr_{0.8}Co_{0.9}Cu_{0.1}O_{3-\delta}$, the most preferred composition, as an example, reasonable oxygen permeation flux can be detected at 600 °C when 20 wt. % of 90%Ag/10%Pd alloy was employed to improve the mechanical property.

Apart from the ABO_3 perovskite structure, a number of oxides with perovskite-related structures exhibit great mixed conducting property as well. Vigeland et al. [36] invented a kind of "K_2NiF_4" materials consisting of a mixed metal oxide material with excess interstitial oxygen, the structure of which can be represented by the general formula of $A_yA'_{y'}A''_{y''}B_xB'_{x'}B''_{x''}B'''_{x'''}O_{4+\delta}$. A preferred example was $La_2Ni_{1-x}B_xO_{4+\delta}$, where x was between 0 and 1, and B site elements were selected from nickel, iron, cobalt and copper etc.. In contrast to the ABO_3 perovskite structure, the transport of oxygen ions takes place via both oxygen vacancies and interstitial sites in lattices, resulting in a significant reduction in apparent activation energy between 900-1000 °C. Oxygen permeation rate of approximately 1.0 $ml \cdot cm^{-2} \cdot min^{-1}$ was achieved over

a membrane of 0.5 mm at 975 °C, with an oxygen partial pressure difference of $\Delta\log(P_{O_2}/\text{bar})=2.3$. Another attractive feature of this type of materials over the ABO_3 perovskite structure is the smaller average "chemical expansion" due to the lost of lattice oxygen. Furthermore, materials of this type showed great chemical stability towards steam and CO_2 at elevated temperatures. Oxygen diffusion coefficient above 10^{-4} $cm^2 \cdot s^{-1}$ as well as great ionic conductivities were also observed between 800 and 1000 °C [37].

Besides doping at lattice sites, the formation of solid solution or dual-phase materials is also widely employed to tailor physical and chemical properties of MIEC materials. Maiya et al. [38] invented a kind of dual-phase MIEC materials by introducing a second metal phase (Ag, Co, Cr, Pt, Au etc.) or a metal alloy (Cu/Ag, Ag/Pd, Zr/Ni etc.) phase into $SrFeCo_{0.5}O_x$ (SCF). The modified SCF, surprisingly and unexpectedly, displayed superior properties. An increase in membrane density, fracture toughness were observed when approximately 2 wt.% of Ag was introduced, which is due to the possibility that metal phase melts and fills into the gaps between ceramic particles during the sintering. The electronic conductivity is also increased, especially at the edge of the gaps in ceramic phase. As a result, the oxygen permeation rate was approximately 25% higher than pure SCF under the same operating conditions. Moreover, significant microstructure stability was achieved by inhibiting the reduction of CoO to Co in strongly reducing environments.

In contrast to metals, ceramic is more preferred as a second phase due to the similar properties to the bulk phase, inducing less “inter-diffusion” between the two phases. Doping of alumina [39] and zirconium oxide [40] have been proved effective in improving the stabilities of Sr-Co-Fe based perovskite-type oxides, especially in strongly reducing atmospheres, without significantly sacrificing the oxygen permeation. Although a trace amount of a third phase was formed as a consequence of solid-state reactions between the doping phase and the bulk phase, stabilities of the composite materials of this type were still significantly improved. For example, a $SrCo_{0.8}Fe_{0.2}O_{3-\delta}$ disc-type membrane containing approximately 3wt. % of alumina was continuously operated at 850 °C for over 500 h in POM reaction [39], while the pure $SrCo_{0.8}Fe_{0.2}O_{3-\delta}$ counterpart can only last for several hours under similar operating conditions. The oxygen permeation rate of $La_{1-x'}Sr_{x'}Ga_{1-y'}Fe_{y'}O_{3-\delta}$ (LSGF), a very stable MIEC material, is approximately 0.05 $ml \cdot cm^{-2} \cdot min^{-1}$ at 900 °C due to the poor electronic conductivity. While $Ba_{1-x}Sr_xCo_{1-y}Fe_yO_{3-\delta}$ (BSCF) with high oxygen permeation fluxes suffers from stability issue in hydrogen atmosphere. Yang et al. [41] combined the two materials together and disclosed a new dual-phase oxygen permeable material in which the ratio of LSGF:BSCF was in the range of 5-50:1. The oxygen ion conductive phase (LSGF) was used as the skeleton of the membrane bulk, while the electron conductive phase (BSCF) acting as a continuous “conductor wire” passed through the skeleton. Besides the greatly improved stability in hydrogen, the oxygen permeation flux of LSGF-BSCF was increased to approximately 0.42 $ml \cdot cm^{-2} \cdot min^{-1}$ at 900 °C, which was about 8.4 times of LSGF. $La_{0.05}Sr_{0.95}CoO_{3-\delta}$ (LSC95, from Praxair Specialty Ceramics Inc.) possesses commendable

oxygen permeability at 900 °C, but reveals no oxygen flux below 850 °C due to the structure transformation from cubic to hexagonal. Chen et al. [42] employed $Ce_{0.8}Gd_{0.2}O_{2-\delta}$ (CGO, from Praxair Specialty Ceramics, Inc.) as a second phase to stabilize the cubic crystal structure of LSC95, and succeeded in detecting oxygen permeation fluxes between 400 and 800 °C . In another example, Sirman et al. [43] disclosed a composite membrane material consisting of $La_{0.6}Sr_{0.4}Co_{0.2}Fe_{0.8}O_{3-\delta}$ (LSCF) and $Ce_{0.9}Gd_{0.1}O_{2-\delta}$ (CGO). Commercially significant oxygen permeation fluxes were obtained at the temperatures as low as 600 °C in a 90%CO/10%CO_2 atmosphere. It should be noted here that the oxygen permeation measurement under the same operation conditions was not possible for LSCF as a consequence of the chemical instability of the material. Chen et al. [44] reported a type of reinforced oxygen permeable materials with the general formula of $(M_{1-y}M'_yCo_{1-x}Fe_xO_{3-\delta})_z(NBO_3)_{1-z}$, where N=Se, Ba, Ca and Mg, B=Sn and Zr, M=Sr, Ba, Ca and Mg, M'=rare earth elements. The highest oxygen permeation flux of the invented materials was approximately 3.1 $ml \cdot cm^{-2} \cdot min^{-1}$ at 1000 °C by using a 1.2mm thick membrane. Even at 560 °C, the oxygen permeation flux was about 0.07 $ml \cdot cm^{-2} \cdot min^{-1}$ and no permeation flux can be obtained by using the conventional counterpart. Besides the improved oxygen permeation performance, the inventors found that the use of NBO_3 simultaneously improves the thermal stability and the sintering property of the materials. Van et al. [45] invented a series of materials consisting of multiple crystalline phases, where the predominant phase was a brownmillerite-derived ceramics (80-99 wt.%). The materials contained one or more secondary crystalline phases (1-20 wt.%), including the AB_2O_4 structure, such as $SrAl_2O_4$, and the

A_2BO_4 structure, such as Sr_2AlO_4, which were distinct from the perovskite-type structure. Secondary phases did not significantly enhance ionic or electronic conductivity, but contributed to improve the mechanical property of the membrane, particularly under catalytic membrane reactor (CMR) operating conditions.

2.2.5 Summary of the development of MIEC materials

Up to now, a large amount of MIEC materials have been reported, greatly improving the development as well as the understanding of such materials for oxygen separation. Lower operating temperatures and better material stability in reducing atmosphere without significantly scarifying oxygen permeation are still of great concerns to the current research. Besides developing new materials, use of composite or dual-phase materials is quite efficient in further upgrading the material characteristics such as mixed conducting property and chemical and thermal stabilities at high temperatures.

2.3 Fundamentals of MIEC membranes for oxygen separation

Besides the nature of membrane materials, oxygen separation using MIEC membranes is largely dependent on the thickness, surface morphology and surface area per unit volume etc. of the membranes. As a result, the configurations of MIEC membranes, as well as the corresponding fabrication processes, are reviewed in this section.

2.3.1 Mechanism of oxygen permeation through MIEC membranes

Oxygen permeation through MIEC membranes undergoes a series of steps [15], which are schematically shown in Figure 2.3. As can be seen, 1) gaseous oxygen first transfers from gas stream to membrane surface (high pressure/feed side); 2) where oxygen molecules disassociate and diffuse into the membrane via oxygen vacancies (surface exchange); 3) oxygen ions migrate towards the other side of the membrane through bulk diffusion, while in the mean time electrons migrate in an opposite direction through electron-holes in crystal cells or electronic conducting phase, maintaining the electro-neutrality of the membrane; 4) lattice oxygen at the membrane surface (low pressure/permeate side) recombine into molecular oxygen; 5) and transfer to gas stream with lower oxygen partial pressure. Mass transfer resistances between membrane surfaces and gas streams (steps 1 and 5) are used to be small and negligible. As a result, the controlling steps for oxygen permeation is either bulk diffusion (step 3) or surface exchange processes (steps 2 and 4), and in most cases a coupling of both.

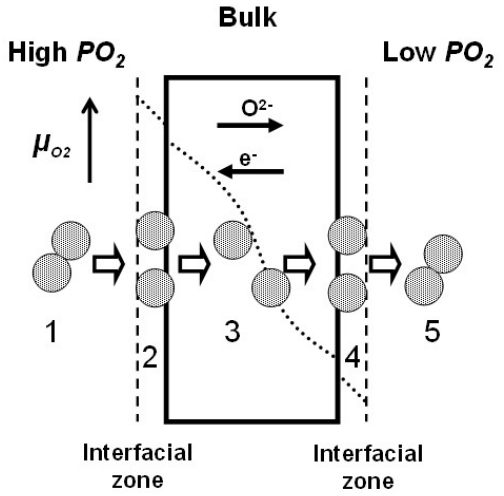


Figure 2.3 Schematic diagram of oxygen permeation through MIEC membranes

For the dual-phase membranes, the mechanism of oxygen permeation is slightly different, because the transfer of oxygen ions and electrons are carried out in a separate ionic conductive and electronic conductive phases.

2.3.2 Classification of MIEC membranes for oxygen separation

2.3.2.1 Membrane configurations

In most cases, 3 types of MIEC membranes, i.e. disk/flat sheet, tubular and hollow fibre, are studied for oxygen separation, in view of the geometrical configurations shown in Figure 2.4.

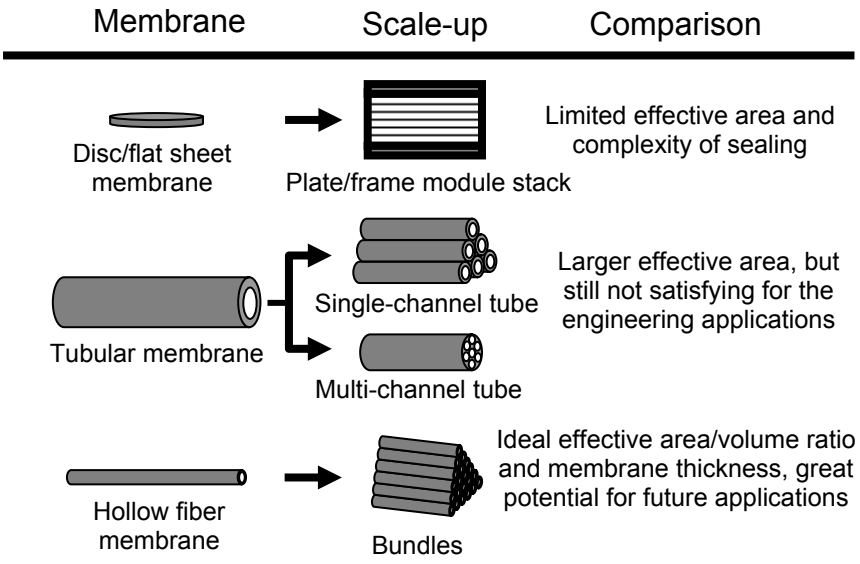


Figure 2.4 Classification of MIEC membranes in view of geometrical configurations

Although the surface area of disk-type membranes is very limited, they are the most frequently studied as a result of easy fabrication and quality control. In

addition, the membranes of this type are ideal for the investigation of oxygen permeation process because the parameters such as temperature, surface area and membrane thickness etc. can be easily determined. Besides the small surface area, membrane sealing at elevated temperatures has been a great challenge, which is more significant when disk-type membranes are converted into flat-sheet membranes with reduced membrane thickness and are integrated into a form of multiple planar stack with higher surface area/volume ratio.

In order to “compact” higher surface area into a unit with a certain volume for oxygen separation, and avert the challenge of membrane sealing at elevated temperatures, tubular membranes are developed by using an extrusion process followed with high temperature sintering. A module consisting of a number of single-channel tubes packed together or a one taking the form of a multi-channel tubular configuration contributes to increase the surface area/volume ratio to approximately 250 m^2/m^3. Membrane sealing can be achieved outside the high temperature zone and is much easier than the disk/flat sheet counterparts. However, the membranes of this type normally show a symmetric structure due to the membrane fabrication process. Membrane thickness is, in this case, equal to that of tube wall that has to be of a certain high level for a reasonable mechanical strength. In contrast, hollow fibre membranes with the highest surface area/volume ratio of up to 3000 m^2/m^3 show a number of advantages over the planar and tubular counterparts. Besides much higher surface area, easy membrane sealing and great membrane uniformity for large-scaled production, the effective membrane

thickness can be reduced to a much lower level of approximately 200 μm. Ceramic or MIEC membranes of this type can be fabricated by a combined phase-inversion/sintering process [46], which allows a more flexible control over the membrane macro/microstructures by adjusting fabricating parameters such as air gap, extrusion rate, internal coagulant composition and amount of non-solvent additive in the spinning suspensions etc. [47-50]. Such unique structural diversity delivers considerable possibilities of further improving oxygen separation performance, although the mechanical property of these membranes turns out to be the concern for promising engineering applications.

2.3.2.2 Membrane micro-structures

For MIEC membranes of the same geometrical configuration, there can still be a number of varieties in membrane micro-structures, as shown in Figure 2.5.

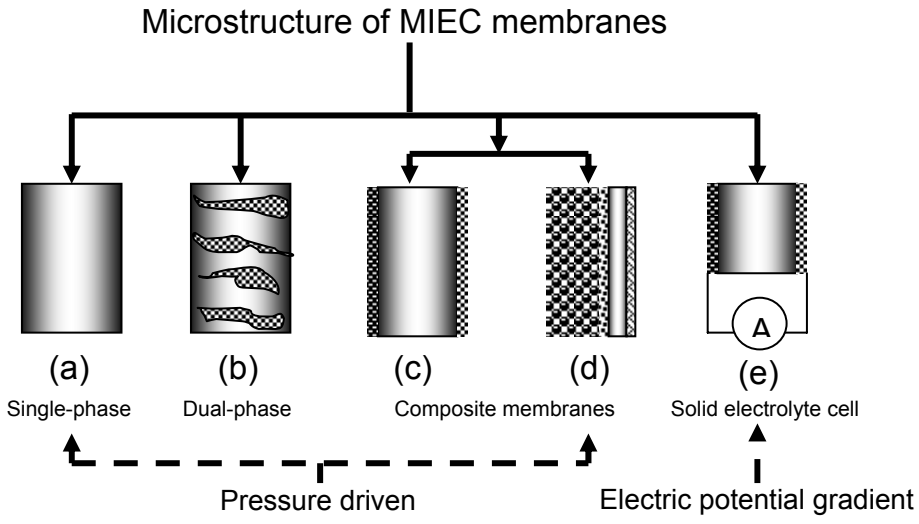


Figure 2.5 Classification of MIEC membranes in view of micro-structures

When the driving force of oxygen permeation is the oxygen partial pressure difference or chemical potential difference across membranes, namely without the use of electrodes and external circuitry, oxygen permeation through single-phase (Figure 2.5 (a)) and dual-phase MIEC membranes (Figure 2.5 (b)) are mainly determined by the properties of membrane materials and membrane thickness and surface property. For the dual-phase MIEC membranes, the use of a second phase (metal or oxide) continuously dispersed in another ceramic matrix contributes to improve electrical conductivity, mechanical strength, thermal stability and sintering property etc. of the membranes, which have been introduced in section 2.2.4. However, a careful selection and combination of membrane materials is required for the fabrication of the membranes of this type to minimize the differences in material properties such as thermal expansion coefficients (TEC), sintering behaviour and solid-state reaction between the two phases. If the TEC, a thermodynamic property of a solid [51], of one phase is too different from the other, cracks or defects may form during the sintering or high temperature operations. Solid state reaction between the two phases is the main reason for the formation of an impurity phase that prefers to congregate along the grain boundaries (the interface between two grains in a polycrystalline material). Besides changing the compositions of the membrane materials, the formation of the impurity phase functions as, in most cases, an insulating layer inhibiting the transfer of ions and electrons along or across grain boundaries, resulting in the degradation of oxygen permeation flux as a consequence [52, 53].

Besides promoting bulk diffusion by reducing membrane thickness and using membrane materials with better mixed conducting property, another way to improve oxygen permeation is to enhance surface exchange processes at the feed and/or permeate surfaces of MIEC membranes via surface modification, forming a kind of composite membranes (Figure 2.5 (c)). A thin porous layer made of materials active to oxygen reduction or combination can be coated on the feed side and/or the permeate side surface of the membrane, enlarging effective surface area where oxygen adsorption/reduction and desorption/combination occur. In most cases when oxygen permeation is affected or determined by surface exchange processes, surface modification has been proved efficiently in promoting oxygen permeation [54, 55]. In contrast to the design in Figure 2.5 (c) where the membrane supports the modification layer or layers, a lot of studies have been carried out to develop supported/asymmetric MIEC membranes [56-59] where a thin dense MIEC membrane is supported on a porous substrate, as shown in Figure 2.5 (d). The thickness of the oxygen separation layer, in this case, can be significantly reduced without scarifying mechanical property of the membrane, resulting in a substantial increase in oxygen permeation. In the mean time, the porous substrate can function as a modification layer promoting surface exchange process. However, the fabrication of such membranes is technically much more difficult and time-consuming multi-step fabrication processes have to be employed. The major technical challenges for the fabrication of such membranes are: 1) how to simultaneously form a thin fully gas-tight ceramic separation layer and a highly porous support layer, especially when the two layers are made of different materials; 2) how to achieve great adhesion

between the two layers; and 3) how to minimize crack/defect formation for membrane configurations with higher surface area/volume ratio, such as hollow fibre membranes. For the sake of completeness, a schematic representation of solid electrolyte cell is given in Figure 2.5 (e), in which a solid electrolyte is “sandwiched” between two gas-permeable electrically conductive electrodes. When the driving force of gas permeation is electric potential gradient (such as oxygen pump), oxygen can be selectively delivered without additional pressure difference.

2.3.3 Current status of MIEC membranes for oxygen separation

The fabrication and the use of disk and tubular MIEC membranes for oxygen separation have been well summarized in a number of reviews [5-8, 12-14]. In order to avoid repetition, this section mainly addresses the development of MIEC membranes in a hollow fibre configuration for oxygen separation, which is more correlated with the main research contents of this thesis, and has yet been systematically reviewed before.

2.3.3.1 A phase inversion process producing ceramic hollow fibres

To the best of our knowledge, the phase inversion process, which has been widely employed in fabricating polymer hollow fibre membranes, has been seldom used for the production of ceramic hollow fibre membranes until around 10 years ago [46, 60], possibly due to the lack of knowledge and understanding of the fabrication process. However, as a result of a number of advantages of such membrane configuration, a wide variety of researches has

been carried out in the last several years [61], stemming from a systematic study on the fabrication of alumina hollow fibre membranes [46, 47] by using a combined phase inversion/sintering method.

In a typical process of producing ceramic hollow fibres using the phase inversion process, more details of which will be introduced in Chapter 3, a uniform suspension comprised of well dispersed ceramic particles, dissolved polymer binders, solvents and sometime additives is extruded through a spinneret with a stream of internal coagulant in the lumen. After passing through an air gap (dry-wet spinning) or without the air gap (wet spinning), it goes into an external coagulation bath and forms precursor fibres. Both the internal and external coagulants are usually water, or a mixture of water and solvent. One of the main technical advantages of using the combined phase inversion/sintering method is that, by controlling the spinning parameters such as air gap, extrusion rate and types of internal/external coagulants etc., a variety of membrane morphologies, i.e. symmetric, asymmetric and highly asymmetric structures in which the thickness of a finger-like layer increases from zero to almost the whole fibre cross-section, can be obtained and used for different applications. This is also one of the major differences between the phase inversion process and the conventional extrusion process to fabricate ceramic membranes in a micro-tubular configuration.

The formation of finger-like voids at the inner/outer fibre surface is believed to be initiated by instabilities at the interface between the non-solvent and the

suspension [47, 62]. Finger-like void growth then proceeds as a result of non-solvent influx into the suspension due to the viscous fingering phenomenon. Because of the high concentration of non-solvent at the interface, polymer precipitation is instantaneous resulting in a rapid, large increase in the viscosity of the suspension in this region. Consequently, the suspension viscosity exceeds the critical value at which no further morphological change may take place and the size of the entrances to the finger-like voids is determined at this point. Non-solvent influx through these entrances into the suspension results in finger-like void growth. However, the polymer precipitation rate within the suspension is lower than that at the interface with non-solvent due to the lesser availability of non-solvent in this region. As a result the suspension viscosity remains below the critical value for a longer period of time and finger-like void growth may proceed, giving rise to the characteristic finger-like shape. Finger-like void growth cannot proceed above a critical suspension viscosity and consequently growth is halted when this value is exceeded. Exposure of the outer fibre surface to the atmosphere (dry-wet spinning) causes an increase in viscosity in this region due to simultaneous solvent evaporation and non-solvent condensation from the surrounding atmosphere, contributing to form an asymmetric structure consisting of an outer sponge-like layer and an inner finger-like layer.

2.3.3.2 MIEC hollow fibre membranes for oxygen separation

The first attempt to fabricate $LaSrCoFeO_{3-\delta}$-based MIEC hollow fibre membranes by a phase inversion process was carried out by Luyten et. al. in 2000 [60], in which no oxygen permeation result was given due to the poor

mechanical strength and the existence of macro defects in the developed membranes. Four years later, Tan et. al. [63] succeeded in fabricating a $La_{0.6}Sr_{0.4}Co_{0.2}Fe_{0.8}O_{3-\delta}$ (LSCF) hollow fibre membrane consisting of a central sponge-like layer "sandwiched" by two finger-like layers for oxygen separation using a combined phase inversion/sintering method. Oxygen permeation flux of more than 3 times of that of a tubular counterpart can be achieved under the same operating conditions, because of the greatly reduced effective membrane thickness. This shows the advantages of using ceramic membranes of this type for oxygen separation. From then on, 3 types of membrane materials, i.e. LSCF [48, 49, 63-66], $Ba_{0.5}Sr_{0.5}Co_{0.8}Fe_{0.2}O_{3-\delta}$ (BSCF) [67-70] and $BaCo_xFe_yZr_zO_{3-\delta}$ (BCFZ, x+y+z=1.0) [71-76], with great mixed ionic-electronic conductivity have been widely studied, further proving the advantages of the membrane fabrication process of this type in producing MIEC hollow fibre membranes.

Table 2.1 lists the oxygen permeation fluxes (under similar investigating conditions) of a number of hollow fibre membranes made of MIEC materials. As can be seen, although the oxygen permeation flux of LSCF is considerably lower than those of BSCF and BCFZ, it has been proved to be more stable in long term oxygen production tests of several months [64, 65]. Its oxygen permeation flux can be further improved by developing a highly asymmetric structure [48, 49], which has yet been done to BSCF and BCFZ probably due to the stability and mechanical property of the membrane materials.

Furthermore, ceramic materials such as $SrCo_{0.9}Sc_{0.1}O_{3-\delta}$ was employed for oxygen separation at intermediate temperatures [77]. Techniques such as surface modification was also used to increase the oxygen permeation flux [54, 55, 78-81], together with a number of studies simulating the oxygen permeation through the MIEC hollow fibre membranes [82-84].

Table 2.1 Oxygen permeation of MIEC hollow fibre membranes

Membrane	OD mm	ID mm	Oxygen permeation flux $ml \cdot cm^{-2} \cdot min^{-1}$	Reference
BSCF	1.15	0.71	5.1 (at 950 °C)	[67]
BSCF	1.4	0.4-1.0	4.2 (at 950 °C)	[68]
BSCF	1.36	0.86	3.9 (at 950 °C)	[69]
BSCF	1.27	0.87	3.9 (at 950 °C)	[70]
LSCF	1.56	1.12	0.8 (at 900 °C)	[63]
BCFZ	0.8-0.9	0.5-0.6	1.1 (at 850 °C)	[76]
BCFZ	0.88	0.53	6.0 (at 900 °C)	[74]
BCFZ	0.9	0.49	7.6 (at 900 °C)	[72]

In contrast to the hollow fibre membranes made of single-phase ceramics, Li et. al. [85, 86] developed a dual-phase hollow fibre membrane for oxygen separation, using yttrium-stabilized zirconia (YSZ) or $Ce_{0.8}Sm_{0.2}O_{2-\delta}$ (SDC) as oxygen ionic conducting phase and $La_{0.8}Sr_{0.2}MnO_{3-\delta}$ (LSM) as electronic conducting phase. Although the oxygen permeation fluxes of such dual-phase membranes are lower than that of the single-phase counterparts (for instance 0.28 and 0.43 $ml \cdot cm^{-2} \cdot min^{-1}$ for YSZ-LSM and SDC-LSM respectively at 950 °C), they are more promising to be used as a hollow fibre membrane reactor because of the excellent material stability in reducing atmosphere. Moreover,

the oxygen permeation flux would be further increased by a number of times at the presence of catalytic reactions on the permeate side of the membrane.

2.4 MIEC membrane reactors for methane conversion

2.4.1 Fundamentals of MIEC membrane reactors

Membrane reactor, a unit coupling membrane separation and catalytic reaction, can either be used to shift the equilibrium of a reversible reaction towards the product side by selectively removing one of the products, or to control the addition and distribution of a reactant, leading to higher reactant conversion, better product selectivity, improved efficiency and less operation cost etc. [16, 61]. Use of MIEC membranes as a separator and distributor to control the supply of oxygen to catalytic reactions of methane conversion, as shown in Figure 2.6, has been widely studied in the last several decades [12, 16, 29, 61, 87], because of the unique oxygen perm-selectivity of the MIEC membranes of this type.

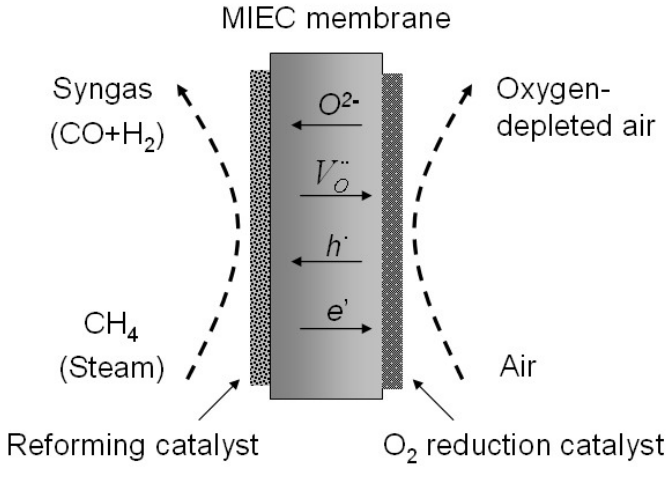


Figure 2.6 Operating principle of a MIEC membrane reactor for methane conversion

Oxygen permeating through the membrane is uniformly distributed along the reaction zone and is instantly consumed by the catalytic reaction, which creates a larger oxygen partial pressure differences across the membrane and results in a higher oxygen permeation flux when compared with non-reaction conditions where sweep gas or vacuum is normally employed to remove the permeated oxygen [88, 89]. In contrast to the use of MIEC membranes for oxygen production, membrane stability is of greater concern in MIEC membrane reactors due to the formation of reducing products such as H_2 and CO. As a consequence, MIEC membranes with greater oxygen permeation flux but suffering from material instability at high temperatures [12, 16, 29] can hardly be qualified for the use in membrane reactors.

Besides oxygen separation, another aspect of membrane reactor is how to integrate catalyst with MIEC membranes with various possible membrane configurations, such as disk, tubular and hollow fibre membranes. Normally, reforming catalyst is directly packed on MIEC membrane surface or inside tubular membranes, although there is a certain interaction between the catalyst and the membrane material especially during the long-term operation. The direct catalyst packing in a hollow fibre membrane reactor would result in a significant reduction in volume productivity of the membrane reactor design of this type, even if the MIEC hollow fibre membrane employed can be highly compact for oxygen separation. Although coating catalyst as a thin porous film on membrane surface contributes to solve this problem, there is still a concern over the active area accessible to the catalytic reaction.

2.4.2 MIEC hollow fibre membrane reactors

Similar to Section 2.3.3 (Current status in MIEC membranes for oxygen separation), in order to avoid duplicating the development of disk- and tubular-MIEC membrane reactors that have already been systematically summarized by a number of reviews [7, 12, 13, 29], this section focuses on the progress in MIEC hollow fibre membrane reactors.

To date, use of MIEC hollow fibre membranes for a catalytic membrane reactor has been mainly focused on two types of membranes, i.e. $BaCo_xFe_yZr_zO_{3-\delta}$ (BCFZ, x+y+z=1.0) and $La_{0.6}Sr_{0.4}Co_{0.2}Fe_{0.8}O_{3-\delta}$ (LSCF). Wang et. al. [90] studied the partial oxidation of methane (POM) to syngas using a BCFZ hollow fibre membrane reactor, in which Ni-based catalyst was packed in one of the 3 following ways: blank reaction (without catalyst), around membrane, around & behind membrane, as shown in Figure 2.7.

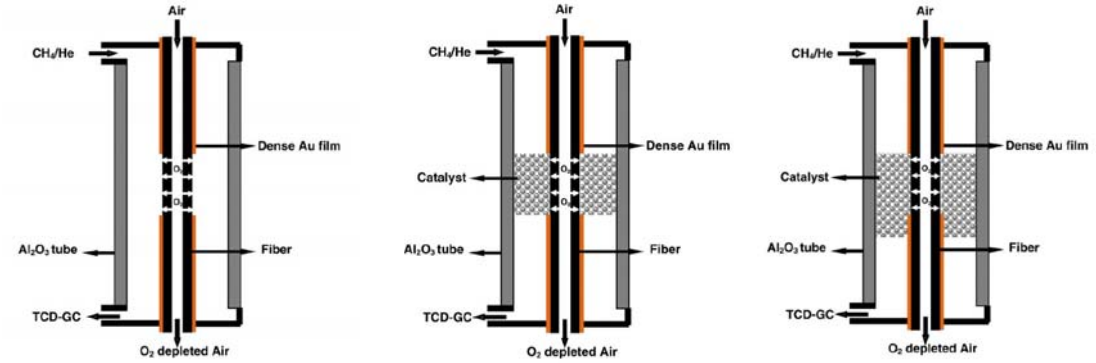


Figure 2.7 Schematic diagram of catalyst arrangement in a BCFZ hollow fibre membrane reactor for POM reaction: (a) blank reaction, (b) catalyst packed around membrane, (c) catalyst packed around & behind membrane [90]

BCFZ was found hardly active to POM reaction because the product gases of the configuration (a) in Figure 2.7 were mainly unreacted methane and oxygen, together with a very small amount of CO_2. Packing Ni-based catalyst around the membrane (Figure 2.7 (b)) resulted in a 70% of methane conversion and a 50% of CO selectivity at 925 °C. Although the methane conversion increased with the increasing operating temperatures (825-925 °C), CO selectivity dropped from 82% to 50% while in the mean time CO_2 selectivity increased from around 20% to 50%. This was due to the permeation of excessive amount of oxygen through the BCFZ membrane and more catalyst or catalyst with higher surface area was required in this case. By further packing catalyst behind the membrane, as shown in Figure 2.7 (c), CO selectivity over 97% and methane conversion of 96% with a H_2/CO ratio of around 2 were achieved at 925 °C. The reaction zone in this hollow fibre membrane reactor was proposed to consist of 3 parts, following a “oxidation-reforming process” [91].

Although the oxygen permeation flux of BCFZ is very high, which has been introduced in Section 2.3.3.2, this material is not stable in reducing atmosphere and the membrane reactor configuration (c) in Figure 2.7 broke after only 9 h of reaction at 875 °C due to the material decomposition [92]. As a consequence, catalyst was suggested to be packed only behind the membrane, which contributed to avoid the direct contact between the membrane and the catalyst [92], while great methane conversion and CO selectivity can still be maintained. Although the stability of BCFZ is of great concern at the presence of reducing products, its hollow fibre membrane

reactor is still studied for oxidative activation of ethane [93, 94], besides POM reaction [94-97], as a result of unique advantages of the hollow fibre membrane configuration.

For the same reason, LSCF hollow fibre membrane reactors have also been studied for oxyfuel combustion [98] or methane oxidation [99], oxidative coupling of methane [100, 101]. Normally catalyst is directly packed inside the reactor and better reactor performance over the disk- or tubular-counterparts can be achieved.

2.5 Summarization

First of all, the development of new membrane materials with both high mixed ionic-electronic conductivity and great stability is the key step of using MIEC ceramic membranes for oxygen separation and catalytic membrane reactor. Besides high operating temperatures, the trade-off between oxygen permeation and membrane stability currently challenges the MIEC materials with perovskite and perovskite-related structures. Although doping on lattice site or with a second metallic/ceramic phase is considered efficiently in improving some of material properties, the process of this type is always at the expense of other characters. In contrast to oxygen separation/production process, membrane stability in catalytic membrane reactor is of greater concern because membrane degradation is significantly intensified. As a result, most MIEC materials with promising oxygen permeation flux for practical oxygen production can hardly be employed in membrane reactor,

although the investigation of long-term oxygen production using these materials has been seldom systematically carried out.

Secondly, reducing membrane thickness and enlarging effective membrane surface area are both preferred for higher oxygen permeation flux, which can be achieved by developing supported/asymmetric membranes and surface modification, respectively. In terms of membrane configurations, ceramic hollow fibre membranes fabricated by a combined phase-inversion/sintering process have shown a number of advantages over the disk- and tubular-counterparts. However, the mechanical property of the membranes of this type may raise concerns over the practical applications, although they can be made into a bundle to improve the mechanical strength. Up to date, a number of typical MIEC materials have been used to prepare hollow fibre membranes, which has demonstrated the advantages of this membrane configuration, as well as the corresponding membrane fabrication process.

Finally, although the design of MIEC hollow fibre membrane reactor for methane conversion and other applications is currently basically same as the disk- and tubular-counterparts, in which catalyst is directly packed or coated on membrane surface, it is still a more advanced design because the reactor of this type can be more compact with higher surface area/volume ratio. As a relatively new MIEC membrane configuration and membrane fabrication process, there is still a lot of work to do for a hollow fibre membrane reactor design with higher oxygen permeation flux, better membrane stability, higher

volume productivity and greater efficiency etc., based on the achievements that have already been made.

References

1. W. Nernst, On the electrolytic conduction of solid bodies at high temperatures, Z. Electrochem., 6 (1899) 41.
2. T.E. T. Takahashi, H. Iwahara, Electrical conduction in the sintered oxides of the system Bi_2O_3–BaO, J. Solid State Chem., 16 (1976) 317.
3. Cales B., Baumard J.F. , Oxygen semipermeability and electronic conductivity in calcia-stabilized zirconia, J. Mater. Sci., 17 (1982) 3243.
4. Cales B., Baumard J.F.. Mixed conduction and defects structure of ZrO_2–Y_2O_3–CeO_2 solid solution, J. Electrochem. Soc., 131 (1984) 2407.
5. U. Balachandran, B. Ma, P.S. Maiya, R.L. Mieville, J.T. Dusek, J.J. Picciolo, J. Guan, S.E. Dorris, M. Liu, Development of mixed-conducting oxides for gas separation, Solid State Ionics, 108 (1998) 363-370.
6. P.N. Dyer, R.E. Richards, S.L. Russek, D.M. Taylor, Ion transport membrane technology for oxygen separation and syngas production, Solid State Ionics, 134 (2000) 21-33.
7. W.S. Yang, H.H. Wang, X.F. Zhu, L.W. Lin, Development and application of oxygen permeable membrane in selective oxidation of light alkanes, Topics in Catalysis, 35 (2005) 155-167.
8. J. Sunarso, S. Baumann, J.M. Serra, W.A. Meulenberg, S. Liu, Y.S. Lin, J.C.D. da Costa, Mixed ionic-electronic conducting (MIEC) ceramic-based

membranes for oxygen separation, Journal of Membrane Science, 320 (2008) 13-41.

9. H.U. Anderson, Review of P-Type Doped Perovskite Materials for Sofc and Other Applications, Solid State Ionics, 52 (1992) 33-41.
10. R.M. Ormerod, Solid oxide fuel cells, Chemical Society Reviews, 32 (2003) 17-28.
11. V.V. Kharton, F.M.B. Marques, A. Atkinson, Transport properties of solid oxide electrolyte ceramics: a brief review, Solid State Ionics, 174 (2004) 135-149.
12. H.J.M. Bouwmeester, Dense ceramic membranes for methane conversion, Catalysis Today, 82 (2003) 141-150.
13. A. Thursfield, I.S. Metcalfe, The use of dense mixed ionic and electronic conducting membranes for chemical production, Journal of Materials Chemistry, 14 (2004) 2475-2485.
14. K.R. Kendall, C. Navas, J.K. Thomas, H.C. zurLoye, Recent developments in perovskite-based oxide ion conductors, Solid State Ionics, 82 (1995) 215-223.
15. Bouwmeester H.J.M., Burggraaf A.J., *Dense ceramic membranes for oxygen separation*. Fundamentals of Inorganic Membrane Science and Technology, ed. Burggraaf A.J., Cot L. . 1996: Elsevier Science B.V., Amsterdam. 435–528.
16. Y.Y. Liu, X.Y. Tan, K. Li, Mixed conducting ceramics for catalytic membrane processing, Catalysis Reviews-Science and Engineering, 48 (2006) 145-198.

17. H. Hayashi, H. Inaba, M. Matsuyama, N.G. Lan, M. Dokiya, H. Tagawa, Structural consideration on the ionic conductivity of perovskite-type oxides, Solid State Ionics, 122 (1999) 1-15.

18. A.F. Sammells, R.L. Cook, J.H. White, J.J. Osborne, R.C. Macduff, Rational Selection of Advanced Solid Electrolytes for Intermediate Temperature Fuel-Cells, Solid State Ionics, 52 (1992) 111-123.

19. R.L. Cook, A.F. Sammells, On the Systematic Selection of Perovskite Solid Electrolytes for Intermediate Temperature Fuel-Cells, Solid State Ionics, 45 (1991) 311-321.

20. Y. Yamamura, C. Ihara, S. Kawasaki, H. Sakai, K. Suzuki, S. Takami, M. Kubo, A. Miyamoto, Materials design of perovskite-based oxygen ion conductor by molecular dynamics method, Solid State Ionics, 160 (2003) 93-101.

21. P.J. Gellings, H.J.M. Bouwmeester, Ion and Mixed Conducting Oxides as Catalysts, Catalysis Today, 12 (1992) 1-105.

22. B. Ma, U. Balachandran, J.H. Park, C.U. Segre, Electrical transport properties and defect structure of SrFeCo0.5Ox, Journal of the Electrochemical Society, 143 (1996) 1736-1744.

23. Y.S. Lin, Y. Zeng, Catalytic properties of oxygen semipermeable perovskite-type ceramic membrane materials for oxidative coupling of methane, Journal of Catalysis, 164 (1996) 220-231.

24. F.S. Galasso, *Structure, Properties and Preparation of Perovskite-Type Compounds*. 1969, London: Pergamon Press.

25. P. Knauth, H.L. Tuller, Solid-state ionics: Roots, status, and future prospects, Journal of the American Ceramic Society, 85 (2002) 1654-1680.

26. Y. Teraoka, H.M. Zhang, S. Furukawa, N. Yamazoe, Oxygen Permeation through Perovskite-Type Oxides, Chemistry Letters, (1985) 1743-1746.

27. A.S. Nowick, Y. Du, High-Temperature Protonic Conductors with Perovskite-Related Structures, Solid State Ionics, 77 (1995) 137-146.

28. R.E. Schaak, T.E. Mallouk, Perovskites by design: A toolbox of solid-state reactions, Chemistry of Materials, 14 (2002) 1455-1471.

29. U. Balachandran, J.T. Dusek, P.S. Maiya, B. Ma, R.L. Mieville, M.S. Kleefisch, C.A. Udovich, T.H. Fleisch, A.C. Bose, Development of dense ceramic membranes for methane conversion, Natural Gas Conversion Iv, 107 (1997) 409-414.

30. T. Ishihara, Y. Takita, *Conductive substance from mixed oxides and its application*. 1999, (Mitsubishi Materials Corp., Japan). DE. p. 18 pp.

31. W. Yang, J. Tong, R. Cai, B. Zhu, *Oxygen-permeable membrane materials*. 2002, (Dalian Inst. of Chemical Physics, Chinese Academy of Sciences, Peop. Rep. China). CN. p. 18 pp.

32. W. Yang, Z. Sho, C. You, G. Xiong, *Manufacture and uses of perovskite-type bismuth-containing mixed-conductor oxygen-penetrable membranes*. 2000, (Dalian Inst. of Chemical Physics, Chinese Academy of Sciences, Peop. Rep. China). CN. p. 17 pp.

33. J. Caro, H. Wang, C. Tablet, G. Grubert, *Oxygen transporting oxide ceramics and applications*. 2006, (Universitaet Hannover, Germany). EP. p. 17 pp.

34. G. Etchegoyen, T. Chartier, P. Del Gallo, *Perovskite material, preparation process, and use in a membrane catalytic reactor*. 2005, (L'Air Liquide

Societe Anonyme Pour l'Etude et l'Exploitation des Procedes Georges Claude, Fr.). FR. p. 34 pp.

35. H.U. Anderson, V. Sprenkle, I. Kaus, C.-C. Chen, *Oxygen separation method using a mixed conducting cubic perovskite ceramic ion transport membrane*. 2001, (Praxair Technology, Inc., USA). US. p. 14 pp.
36. B. Vigeland, R. Glenne, T. Breivik, S. Julsrud, *Ceramic membranes for oxygen separation*. 1999, (Norsk Hydro Asa, Norway). WO. p. 20 pp.
37. M. Al Daroukh, D. Stoever, F. Tietz, H. Ullmann, V. Vashuk, *Oxygen membrane for use at high temperatures*. 2003, (Forschungszentrum Juelich G.m.b.H., Germany; Kernforschungsanlage Juelich). WO. p. 13 pp.
38. P.S. Maiya, J.J. Picciolo, J.T. Dusek, *Dense ceramic membranes in conversion of methane to synthesis gas*. 2000, (The University of Chicago, USA). US. p. 7 pp.
39. N. Xu, W. Jin, Z. Wu, *Alumina-doped, conductive oxygen-permeable composite film material with high oxygen permeating efficiency and high chemical and structure stability*. 2005, (Nanjing University of Technology, Peop. Rep. China). CN. p. 8pp.
40. N. Xu, S. Li, W. Jin, J. Shi, *Conductive compact oxygen permeable composite membrane material*. 1999, (Nanjing University of Chemical Technology, Peop. Rep. China). CN. p. 10 pp.
41. W. Yang, H. Wang, C. You, *Two-phase mixed conductor oxygen-breathable film*. 2004, (Dalian Research Inst. of Chemical Physics, Chinese Academy of Sciences, Peop. Rep. China). CN. p. 15 pp.
42. C.-C. Chen, R. Prasad, *Stabilized perovskite for ceramic membranes*. 2000, (Praxair Technology, Inc., USA). US. p. 7 pp.

43. J.D. Sirman, J.C. Chen, *Dense layer-porous layer composite ceramic membranes for high-temperature oxygen separation, especially from air*. 2002, (Praxair Technology, Inc., USA). WO. p. 32 pp.

44. C. Chen, C. Fan, Z. Deng, *Oxygen permeable film enhanced by perovskite-type oxide and oxygen separator made with the film*. 2004, (Univ. of Sci-Tech of China, Peop. Rep. China). CN. p. No pp given.

45. C.P. Van, R. Mackay, A.F. Sammells, *Improved mixed ionic and electronic conducting ceramic membranes for hydrocarbon processing*. 2000, (Eltron Research, Inc., USA). WO. p. 41 pp.

46. X.Y. Tan, S.M. Liu, K. Li, Preparation and characterization of inorganic hollow fiber membranes, Journal of Membrane Science, 188 (2001) 87-95.

47. B.F.K. Kingsbury, K. Li, A morphological study of ceramic hollow fibre membranes, Journal of Membrane Science, 328 (2009) 134-140.

48. B. Zydorczak, Z.T. Wu, K. Li, Fabrication of ultrathin La0.6Sr0.4Co0.2Fe0.8O3-delta hollow fibre membranes for oxygen permeation, Chemical Engineering Science, 64 (2009) 4383-4388.

49. Z.G. Wang, N.T. Yang, B. Meng, X.Y. Tan, K. Li, Preparation and Oxygen Permeation Properties of Highly Asymmetric La0.6Sr0.4Co0.2Fe0.8O3-alpha Perovskite Hollow-Fiber Membranes, Industrial & Engineering Chemistry Research, 48 (2009) 510-516.

50. W.N. Yin, B. Meng, X.X. Meng, X.Y. Tan, Highly asymmetric yttria stabilized zirconia hollow fibre membranes, Journal of Alloys and Compounds, 476 (2009) 566-570.

51. D.L. Turcotte, G. Schubert, *Geodynamics*. 2nd Edition ed. ed. 2002: Cambridge.

52. A.L. Shaula, V.V. Kharton, F.M.B. Marques, A.V. Kovalevsky, A.P. Viskup, E.N. Naumovich, Oxygen permeability of mixed-conducting composite membranes: effects of phase interaction, Journal of Solid State Electrochemistry, 10 (2006) 28-40.

53. V.V. Kharton, A.V. Kovalevsky, A.P. Viskup, A.L. Shaula, F.M. Figueiredo, E.N. Naumovich, F.M.B. Marques, Oxygen transport in Ce0.8Gd0.2O2-delta-based composite membranes, Solid State Ionics, 160 (2003) 247-258.

54. Z.G. Wang, H. Liu, X.Y. Tan, Y.G. Jin, S.M. Liu, Improvement of the oxygen permeation through perovskite hollow fibre membranes by surface acid-modification, Journal of Membrane Science, 345 (2009) 65-73.

55. A. Leo, S. Liu, J.C.D. da Costa, Z. Shao, Oxygen permeation through perovskite membranes and the improvement of oxygen flux by surface modification, Science and Technology of Advanced Materials, 7 (2006) 819-825.

56. X.F. Chang, C. Zhang, Y.J. He, X.L. Dong, W.Q. Jin, N.P. Xu, A Comparative Study of the Performance of Symmetric and Asymmetric Mixed-conducting Membranes, Chinese Journal of Chemical Engineering, 17 (2009) 562-570.

57. X.F. Chang, C. Zhang, W.Q. Jin, N.P. Xu, Match of thermal performances between the membrane and the support for supported dense mixed-conducting membranes, Journal of Membrane Science, 285 (2006) 232-238.

58. W.Q. Jin, S.G. Li, P. Huang, N.P. Xu, J. Shi, Preparation of an asymmetric perovskite-type membrane and its oxygen permeability, Journal of Membrane Science, 185 (2001) 237-243.

59. X.L. Dong, C. Zhang, X.F. Chang, W.Q. Jin, N.P. Xu, A self-catalytic membrane reactor based on a supported mixed-conducting membrane, Aiche Journal, 54 (2008) 1678-1680.

60. J. Luyten, A. Buekenhoudt, W. Adriansens, J. Cooymans, H. Weyten, F. Servaes, R. Leysen, Preparation of LaSrCoFeO3-x membranes, Solid State Ionics, 135 (2000) 637-642.

61. K. Li, *Ceramic Membranes for Separation and Reaction*. 2007: Wiley.

62. Z.T. Wu, I.M.D. Hatim, B.F.K. Kingsbury, E. Gbenedio, K. Li, A Novel Inorganic Hollow Fiber Membrane Reactor for Catalytic Dehydrogenation of Propane, Aiche Journal, 55 (2009) 2389-2398.

63. X.Y. Tan, Y.T. Liu, K. Li, Preparation of LSCF ceramic hollow-fiber membranes for oxygen production by a phase-inversion/sintering technique, Industrial & Engineering Chemistry Research, 44 (2005) 61-66.

64. B. Wang, B. Zydorczak, Z.T. Wu, K. Li, Stabilities of La0.6Sr0.4Co0.2Fe0.8O3-delta oxygen separation membranes-Effects of kinetic demixing/decomposition and impurity segregation, Journal of Membrane Science, 344 (2009) 101-106.

65. X.Y. Tan, Z.B. Pang, K. Li, Oxygen production using La0.6Sr0.4Co0.2Fe0.8O3-alpha (LSCF) perovskite hollow fibre membrane modules, Journal of Membrane Science, 310 (2008) 550-556.

66. H. Liu, X.Y. Tan, Z.B. Pang, J.C.D. da Costa, G.Q. Lu, S.M. Liu, Novel dual structured mixed conducting ceramic hollow fibre membranes, Separation and Purification Technology, 63 (2008) 243-247.

67. S.M. Liu, G.R. Gavalas, Oxygen selective ceramic hollow fiber membranes, Journal of Membrane Science, 246 (2005) 103-108.

68. S. Liu, X. Tan, Z. Shao, J.C.D. da Costa, Ba0.5Sr0.5Co0.8Fe0.2O3-delta ceramic hollow-fiber membranes for oxygen permeation, Aiche Journal, 52 (2006) 3452-3461.

69. S.M. Liu, G.R. Gavalas, Preparation of oxygen ion conducting ceramic hollow-fiber membranes, Industrial & Engineering Chemistry Research, 44 (2005) 7633-7637.

70. S. Liu, M. Liu, Z. Shao, J.C.D. da Costa, Z.P. Xu, From chelating precursor to perovskite oxides and hollow fiber membranes, Journal of the American Ceramic Society, 90 (2007) 84-91.

71. H.H. Wang, C. Tablet, J. Caro, Oxygen production at low temperature using dense perovskite hollow fiber membranes, Journal of Membrane Science, 322 (2008) 214-217.

72. H. Wang, T. Schiestel, C. Tablet, M. Schroeder, J. Caro, Mixed oxygen ion and electron conducting hollow fiber membranes for oxygen separation, Solid State Ionics, 177 (2006) 2255-2259.

73. H.H. Wang, S. Werth, T. Schiestel, A. Caro, Perovskite hollow-fiber membranes for the production of oxygen-enriched air, Angewandte Chemie-International Edition, 44 (2005) 6906-6909.

74. J. Caro, H.H. Wang, C. Tablet, A. Kleinert, A. Feldhoff, T. Schiestel, M. Kilgus, P. Kolsch, S. Werth, Evaluation of perovskites in hollow fibre and disk geometry in catalytic membrane reactors and in oxygen separators, Catalysis Today, 118 (2006) 128-135.

75. H.H. Wang, P. Kolsch, T. Schiestel, C. Tablet, S. Werth, J. Caro, Production of high-purity oxygen by perovskite hollow fiber membranes swept with steam, Journal of Membrane Science, 284 (2006) 5-8.

76. C. Tablet, G. Grubert, H.H. Wang, T. Schiestel, M. Schroeder, B. Langanke, J. Caro, Oxygen permeation study of perovskite hollow fiber membranes, Catalysis Today, 104 (2005) 126-130.

77. B. Meng, Z.G. Wang, X.Y. Tan, S.M. Liu, SrCo0.9Sc0.1O3-delta perovskite hollow fibre membranes for air separation at intermediate temperatures, Journal of the European Ceramic Society, 29 (2009) 2815-2822.

78. A. Thursfield, I.S. Metcalfe, Air separation using a catalytically modified mixed conducting ceramic hollow fibre membrane module, Journal of Membrane Science, 288 (2007) 175-187.

79. A. Leo, S.M. Liu, J.C.D. da Costa, The enhancement of oxygen flux on Ba0.5Sr0.5Co0.8Fe0.2O3-delta (BSCF) hollow fibers using silver surface modification, Journal of Membrane Science, 340 (2009) 148-153.

80. X.Y. Tan, Z.G. Wang, H. Liu, S.M. Liu, Enhancement of oxygen permeation through La0.6Sr0.4Co0.2Fe0.8O3-delta hollow fibre membranes by surface modifications, Journal of Membrane Science, 324 (2008) 128-135.

81. H. Liu, Z.B. Pang, X.Y. Tan, Z. Shao, J. Sunarso, R. Ding, S. Liu, Enhanced oxygen permeation through perovskite hollow fibre membranes by methane activation, Ceramics International, 35 (2009) 1435-1439.

82. X.Y. Tan, K. Li, Oxygen production using dense ceramic hollow fiber membrane modules with different operating modes, Aiche Journal, 53 (2007) 838-845.

83. C. Hamel, A. Seidel-Morgenstern, T. Schiestel, S. Werth, H.H. Wang, C. Tablet, J. Caro, Experimental and modeling study of the O-2-enrichment by perovskite fibers, Aiche Journal, 52 (2006) 3118-3125.

84. X.Y. Tan, Y.T. Liu, K. Li, Mixed conducting ceramic hollow-fiber membranes for air separation, Aiche Journal, 51 (2005) 1991-2000.

85. W. Li, J.J. Liu, C.S. Chen, Hollow fiber membrane of yttrium-stabilized zirconia and strontium-doped lanthanum manganite dual-phase composite for oxygen separation, Journal of Membrane Science, 340 (2009) 266-271.

86. W. Li, T.F. Tian, F.Y. Shi, Y.S. Wang, C.S. Chen, Ce0.8Sm0.2O2-delta-La0.8Sr0.2MnO3-delta Dual-Phase Composite Hollow Fiber Membrane for Oxygen Separation, Industrial & Engineering Chemistry Research, 48 (2009) 5789-5793.

87. D. Eng, M. Stoukides, Catalytic and Electrocatalytic Methane Oxidation with Solid Oxide Membranes, Catalysis Reviews-Science and Engineering, 33 (1991) 375-412.

88. X.H. Gu, W.Q. Jin, C.L. Chen, N.P. Xu, J. Shi, Y.H. Ma, YSZ-SrCo0.4Fe0.6O3-delta membranes for the partial oxidation of methane to syngas, Aiche Journal, 48 (2002) 2051-2060.

89. C.Y. Tsai, A.G. Dixon, W.R. Moser, Y.H. Ma, Dense perovskite membrane reactors for partial oxidation of methane to syngas, Aiche Journal, 43 (1997) 2741-2750.

90. H.H. Wang, C. Tablet, T. Schiestel, S. Werth, J. Caro, Partial oxidation of methane to syngas in a perovskite hollow fiber membrane reactor, Catalysis Communications, 7 (2006) 907-912.

91. C.S. Chen, S.J. Feng, S. Ran, D.C. Zhu, W. Liu, H.J.M. Bouwmeester, Conversion of methane to syngas by a membrane-based oxidation-reforming process, Angewandte Chemie-International Edition, 42 (2003) 5196-5198.

92. H.H. Wang, A. Feldhoff, J. Caro, T. Schiestel, S. Werth, Oxygen Selective Ceramic Hollow Fiber Membranes for Partial Oxidation of Methane, Aiche Journal, 55 (2009) 2657-2664.

93. H.H. Wang, C. Tablet, T. Schiestel, J. Caro, Hollow fiber membrane reactors for the oxidative activation of ethane, Catalysis Today, 118 (2006) 98-103.

94. E.V. Kondratenko, H.H. Wang, V.A. Kondratenko, J. Caro, Selective oxidation of CH4 and C2H6 over a mixed oxygen ion and electron conducting perovskite-A TAP and membrane reactors study, Journal of Molecular Catalysis a-Chemical, 297 (2009) 142-149.

95. H.Q. Jiang, H.H. Wang, S. Werth, T. Schiestel, J. Caro, Simultaneous Production of Hydrogen and Synthesis Gas by Combining Water Splitting with Partial Oxidation of Methane in a Hollow-Fiber Membrane Reactor, Angewandte Chemie-International Edition, 47 (2008) 9341-9344.

96. J. Caro, K.J. Caspary, C. Hamel, B. Hoting, P. Kolsch, B. Langanke, K. Nassauer, T. Schiestel, A. Schmidt, R. Schomacker, A. Seidel-Morgenstern, E. Tsotsas, I. Voigt, H.H. Wang, R. Warsitz, S. Werth,A. Wolf, Catalytic membrane reactors for partial oxidation using perovskite hollow fiber membranes and for partial hydrogenation using a catalytic membrane contactor, Industrial & Engineering Chemistry Research, 46 (2007) 2286-2294.

97. A. Kleinert, A. Feldhoff, T. Schiestel, J.G. Caro, Novel hollow fibre membrane reactor for the partial oxidation of methane, Catalysis Today, 118 (2006) 44-51.

98. X.Y. Tan, K. Li, A. Thursfield, I.S. Metcalfe, Oxyfuel combustion using a catalytic ceramic membrane reactor, Catalysis Today, 131 (2008) 292-304.

99. A. Thursfield, I.S. Metcalfe, Methane oxidation in a mixed ionic-electronic conducting ceramic hollow fibre reactor module, Journal of Solid State Electrochemistry, 10 (2006) 604-616.

100. X.Y. Tan, K. Li, Oxidative coupling of methane in a perovskite hollow-fiber membrane reactor, Industrial & Engineering Chemistry Research, 45 (2006) 142-149.

101. X. Tan, Z. Pang, Z. Gu, S. Liu, Catalytic perovskite hollow fibre membrane reactors for methane oxidative coupling, Journal of Membrane Science, 302 (2007) 109-114.

Chapter 3

Single-Step Fabrication of Dual-Layer Ceramic Hollow Fibre Membranes

Abstract

Based on the combined phase-inversion/sintering technique to fabricate ceramic hollow fibre membranes [1], this chapter focuses on the development of a single-step membrane fabrication process, i.e. co-extrusion and co-sintering process, to fabricate dual-layer ceramic hollow fibre membranes. The resultant membranes are composed of a thin and dense outer oxygen separation layer supported on an inert inner substrate layer. Although such "dual-layer" membrane structure has been achieved on disc/flat-sheet and short tubular counterparts, using multi-step fabrication processes consisting of repeated coating and sintering steps, it is significantly more challenging if the membrane is in the form of hollow fibre, and if the two layers are going to be formed in a single-step fabrication process. As the surface area and the curvature of hollow fibre membranes are considerably higher than that of flat-sheet and tubular membranes, more efforts are going to be carried out on the membrane uniformity, integrity, adhesion between the layers and mechanical property, besides proper control over membrane morphology and micro-structures. Since this chapter addresses more on the membrane fabrication process, typical ceramic materials that have been well studied are used. Functionalization of the membranes with similar structure is going to be introduced in the following chapters.

Keywords: Single-step, co-extrusion and co-sintering, dual-layer, ceramic membrane, hollow fibre.

3.1 Introduction

As has been introduced in Chapter 2, in order for higher oxygen permeation flux of most mixed ionic-electronic conducting (MIEC) membranes, membrane thickness needs to be significantly decreased, while in the mean time membrane surface area in per unit volume should be considerably increased. This can be achieved and has been proved, respectively, by developing disc or short tubular supported/asymmetric MIEC membranes [2] and self-supported single-layer hollow fibre membranes [3]. The combination of the advantages of the two membrane configurations above would result in a dual-layer MIEC hollow fibre membrane, in which a thin and fully dense outer oxygen separation layer is supported on a porous inner substrate layer with great mechanical property. In order to achieve this, a number of technical challenges need to be addressed first:

1. How to uniformly coat a thin outer oxygen separation layer with consistent microstructure and uniformity onto a porous ceramic hollow fibre substrate with high surface area and curvature.
2. How to form great adhesion between the two layers to avoid delamination of separation layer from substrate layer, during high temperature sintering and operation.
3. How to simultaneously achieve a fully dense outer separation layer and a highly porous inner support layer.
4. How to guarantee great membrane uniformity and integrity in the membrane preparation process.

3.1.1 Objectives

The main objective of this chapter is to develop a single-step co-extrusion and co-sintering process to fabricate dual-layer MIEC hollow fibre membranes, and to evaluate the technical feasibility of such membrane fabrication process to control membrane morphology and microstructures, in order to provide guidance for the further fabrication of functional ceramic hollow fibre membranes for methane conversion. The specific objectives are listed as following:

1. Preparation of dual-layer MIEC hollow fibre membranes using the co-extrusion and co-sintering method.
2. Investigating the effects of fabrication parameters, such as membrane materials, spinning parameters and co-sintering temperatures etc., on the microstructures and the performances of the developed membranes.
3. Evaluation of the technical feasibility of using the co-extrusion and co-sintering method for the fabrication of high quality dual-layer ceramic hollow fibre membranes.

3.2 Background

3.2.1 Preparation of supported/asymmetric MIEC membrane

Supported/asymmetric MIEC membranes, which consist of a thin and dense oxygen separation layer supported on a porous disc-type [2, 4-8] or tubular-type [9-11] substrate, have been widely studied, because higher oxygen permeation fluxes can be obtained due to the significantly reduced membrane

thickness. Many methods, usually multi-step processes, have been developed for the fabrication of MIEC membranes of this type, such as sputtering, spray coating, dip coating, slurry casting and dry-pressing etc.. In principle, the membrane fabrication processes above can be classified into two types, regardless of what kind of membrane coating methods are employed: coating an oxygen separation layer (1) on a pre-sintered porous substrate or (2) on a green substrate with pore-formers, such as graphite, followed by another co-sintering process. In contrast, the second one is more efficient in avoiding cracking formation or delamination of separation layer, because both layers are sintered simultaneously. Furthermore, one of the typical common grounds of all these fabrication processes is that, substrate layer has to be prepared prior to the coating of oxygen separation layer.

As a consequence of the multi-step nature of the membrane fabrication processes above, only supported/asymmetric MIEC membranes with very limited surface area and surface curvature can be achieved. For hollow fibre membranes with a much larger surface area and higher curvature, there would be a significantly higher chance of delamination, crack or defect formation if the previous multi-step methods are employed. However, the development of supported/asymmetric MIEC membranes is still of great interest due to the higher oxygen permeation flux.

3.2.2 Preparation of self-supported single-layer MIEC hollow fibre membranes

In the last several years, the successful preparation of MIEC hollow fibre membranes for oxygen separation can be considered as a technical breakthrough in ceramic membrane fabrication. MIEC membranes of this type, which are prepared by a combined phase inversion/sintering technique [1, 3], have shown a number of advantages over the conventional disc or tubular counterparts, such as significantly reduced membrane thickness and considerably higher surface area/volume ratio. As a result, much higher oxygen permeation fluxes can be obtained. Moreover, this membrane fabrication technique enables the production of ceramic membranes with very uniform macrostructures, as such sponge-like/symmetric structure and asymmetric structures with finger-like voids from one side or both sides of membrane surfaces. The macrostructures of the membranes can be controlled by adjusting the spinning parameters, such as air gap, extrusion rate and flow rate of an internal coagulant etc., which is also one of the major differences from the conventional extrusion process for the fabrication of micro-tubular ceramic membranes.

A phase inversion/sintering process normally consists of three main steps, as shown in Figure 3.1. Typically, a certain amount of MIEC ceramic powder or its mixture is first mixed with solvent, polymer binder and additive, forming a uniform spinning suspension. The spinning suspension would be used for preparing precursor fibres by a phase inversion process, where different types of membrane macrostructures can be obtained. The precursor fibres are finally sintered using proper sintering profiles, forming resultant ceramic hollow fibre membranes with certain mechanical strength.

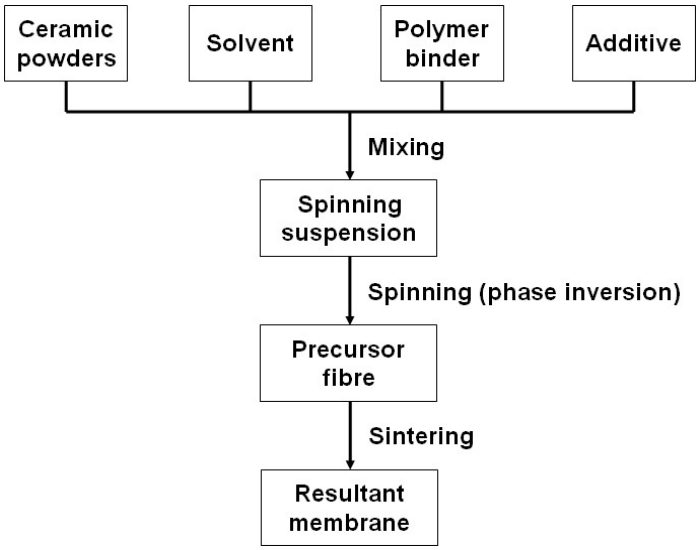


Figure 3.1 Schematic diagram of phase inversion/sintering process

The details of each step are introduced below:

1. Preparation of a spinning suspension

The preparation of a uniform spinning suspension consisting of ceramic particles, solvent, polymer binder and additives is one of the most critical steps in fabricating high quality hollow fibre membranes. The composition of the suspension may vary as a result of different size/surface area and surface property of ceramic particles, as well as the types of solvent and polymer binder to be used. The key factor of making a good spinning suspension is how to uniformly disperse ceramic particles inside the mixture free of agglomerations. The ceramic particle agglomeration will increase the actual particle size and significantly change the viscosity of resultant suspensions. This would further change spinning parameters and, even worse, affect the pore size, uniformity and mechanical strength of resultant hollow fibre membranes.

In contrast to polymer membranes, polymers such as polyethersulfone, acrylonitrile and vinyl acetate etc. act as a “binder”, instead of membrane materials, building up connections between ceramic particles in precursor fibres. These “binders” will be removed by high temperature sintering at the presence of oxygen after certain sort of “bonding” between ceramic particles is formed, which will be introduced in the following section. As a result, the amount of polymer binder in the spinning suspension, i.e. the ratio between ceramic powder and polymer binder, needs to be optimized first because too much polymer binder would increase the distance between ceramic particles, preventing proper sintering of ceramic particles. While an insufficient amount of polymer binder can not immobilize ceramic particles in precursor fibres. Furthermore, the amount of polymer binder used affects the viscosity of spinning suspensions, which contributes to change spinning parameters and macrostructures of resultant hollow fibre membranes.

The selection of solvent also affects the preparation of spinning suspensions as well as the macrostructure of resultant hollow fibre membranes. For example, use of solvent with higher freezing point would increase viscosity of the spinning suspension at room temperature. Moreover, the property of solvents will change the solvent-non-solvent exchange during phase inversion process, which affects the precipitation rate of polymer binder and subsequently affects length, width and shape of finger-like voids as well as macrostructure of the resultant hollow fibre membranes.

Additives functionalizing as dispersant, defoaming agent and plasticizer etc. are needed to improve the dispersion of ceramic particles in spinning suspensions, especially when ceramic powder employed is very small and is of different particle sizes. The dispersion is influenced by the interaction between particles which involves a number of surface forces such as electrostatic force, Van der Waals force and steric interaction [12].

2. Spinning ceramic hollow fibre membranes via phase inversion process

In the 1960s, Loeb and Sourirajan [13] first developed an immersion induced phase inversion method and produced an asymmetric polymeric membrane exhibiting high selectivity and high water flux. Since then, it has been one of the most useful methods for the fabrication of polymeric membranes. Conceptually, membrane formation via phase inversion can be described by a three component system: nonsolvent, solvent and polymer. After immersing a polymeric solution into a nonsolvent bath, solvent diffuses out of the polymer solution, while nonsolvent diffuses into the solution. This solvent-nonsolvent exchange in general leads to a change of polymer solution from a thermodynamically stable state to a metastable or unstable state. Then liquid-liquid demixing takes place in the solution. As has been introduced above, polymer in a ceramic spinning suspension is a “binder”, instead of membrane material, building up connection between ceramic particles in the precursor fibres. As a result, the knowledge of phase inversion, such as phase diagram, can be selectively used to direct the fabrication of ceramic hollow fibre membranes. Besides, in order to understand the formation of different membrane structures, such as sponge-like/symmetric structure, asymmetric

structures with finger-like voids developing from one side or both sides of membranes, another phenomenon named as viscous fingering needs to be introduced.

Hydrodynamically unstable viscous fingering is a well known phenomenon that occurs at the interface between fluids with different viscosities in the first moment of mixing. It has been used to explain the formation of finger-like voids in ceramic hollow fibre membranes [14]. When the spinning suspension is in contact with a non-solvent, a steep concentration gradient at the interface is formed and results in instant solvent/non-solvent exchange, which leads to a rapid increase in local viscosity and finally the precipitation of the polymer phase. Due to instabilities at the interface between the suspension and the coagulant (non-solvent), there is a tendency for viscous fingering to occur, initiating the formation of finger-like voids. And the morphologies of the resultant hollow fibre membranes, i.e. a sponge-like structure and a finger-like structure, can be adjusted by controlling the viscous fingering process. Although viscous fingering is considered as the reason for the formation of finger-like structures when combined with the theory of phase-inversion process, there are still a number of factors may affect the growth of these “fingers” in the resultant hollow fibre membranes, such as the density, shape, length/width and distribution etc. of the “fingers”. All these make a full control of the membrane structure into an extremely complex system, and as a result, the “macrostructure” of ceramic hollow fibre membranes in this thesis only indicates the relative thickness ratio between a sponge-like layer and a finger-like layer.

3. Sintering of ceramic hollow fibre membranes

Finally, the obtained precursor fibres are thermally treated in a tubular furnace in order for the desired microstructures (pore volume and average pore size) and mechanical property. The sintering of ceramic hollow fibre membranes normally experiences a number of steps, as shown in Figure 3.2, in which the heating rate is kept at a constant value.

In principle, the sintering process would not begin until the temperature exceeds one half to two thirds of the melting temperature of the ceramic material. As a result, only polymer binder and absorbed water would be removed from the precursor fibres in Step I of Figure 3.2, which also brings ceramic particles closer and in contact with each other. A further increase of temperature would cause a significant atomic diffusion for solid state sintering or significant diffusion and viscous flow when a liquid phase is presented or produced by a chemical reaction. This leads to the generation of a “neck” between particles to reduce the surface free energy. At the “neck”, the radius of curvature is negative and the vapour pressure is lower than the other parts, facilitating the transfer of materials to this part. Diffusion along the grain boundaries and diffusion through the lattices produce bigger and bigger “neck” with the increasing temperatures, and finally leads to grain growth. In the mean time, the membrane starts to shrink as a result of the reduction in pore volume and pore size.

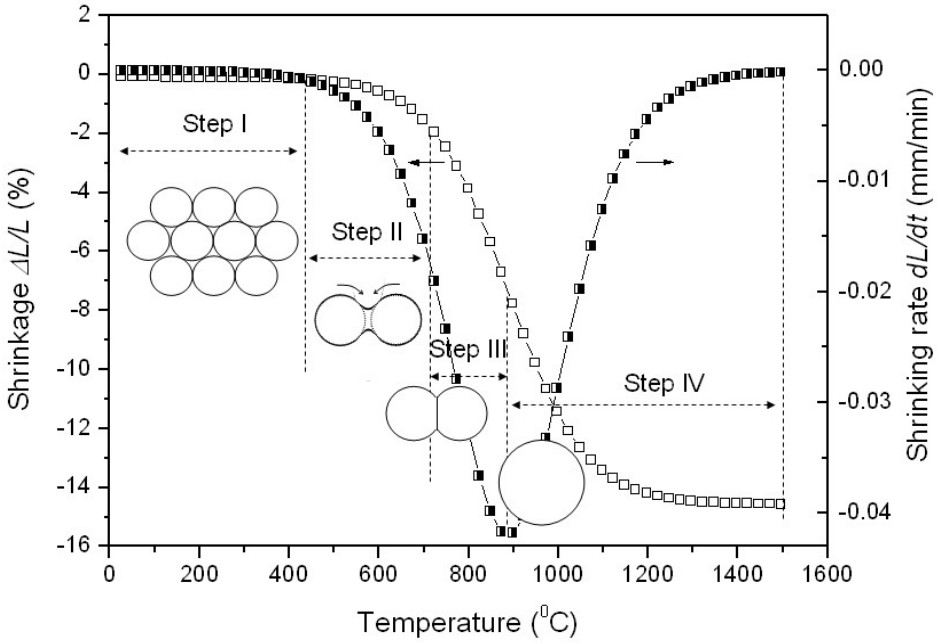


Figure 3.2 Schematic diagram of sintering ceramic hollow fibre membranes

As can also be seen in Figure 3.2, the membrane normally starts to shrink from a low rate (Step II) that increases significantly with the further increasing temperatures (Step III). The maximum shrinking rate can be obtained at a certain temperature, over which the shrinking rate dramatically decreases and finally gets to zero with the further increasing temperatures (Step IV). In the mean time, the change in shrinkage slows down and stabilizes at a certain value, indicating the stop of the sintering process. The density of the membrane can be very close to the theoretical density at this stage due to the elimination of pores. With the increasing sintering temperature, the amount of grain boundaries decreases as a result of increasing grain sizes. Mechanical strength of the membranes would also increase until they are “over-sintered”, which would cause a sudden loss of the mechanical property. Proper control over the sintering behaviour of ceramic materials by adjusting heating rate,

dwelling temperature, dwelling time and even the sintering atmosphere is always critical for the improved membrane performance with the controlled membrane microstructure.

3.3 Experimental

As the major objective of this chapter is to evaluate the feasibility of using a single-step co-extrusion and co-sintering method to prepare dual-layer ceramic hollow fibre membranes, more efforts are put on the technical aspects of the co-extrusion process. As a result, ceramic materials that have been widely studied are chosen as the membrane materials in this chapter. The selection of proper membrane materials for the co-sintering of functional dual-layer hollow fibre membranes will be introduced in the next chapter.

3.3.1 Materials

Commercially available $La_{0.6}Sr_{0.4}Co_{0.2}Fe_{0.8}O_{3-\delta}$ (LSCF) powders (d_{50} =0.6 μm, Praxair Surface Technologies), alumina (0.3 and 1.0 μm, Alfa Aesar) and YSZ-8 (6.7 m^2/g, FCM) were used as supplied. Polyethersulfone (PESf) (Radel A-300, Ameco Performance, Greenville, SC) and N-methyl-2-pyrrolidone (NMP, synthesis grade, Merck) were used as polymer binder and solvent respectively for the preparation of the spinning suspensions. Poly(vinylpyrrolidone) (PVP, K 30 from Acros Organics) was used as the additive. Deionized water and tap water were used as the internal and external coagulants, respectively.

3.3.2 Co-extrusion of dual-layer hollow fibre membranes

In a typical process of preparing the spinning suspensions, a certain amount of PESf with PVP is first fully dissolved in NMP under stirring (Heidolph RZR 2000) at room temperature, using a 250-mL wide-neck bottle. Ceramic powders or their mixtures are then gradually added into the bottle with a stirring rate of 300 rpm. After a 48 h of mixing, the formed suspensions are degassed at room temperature for 60 min, removing the air trapped inside. The spinning suspensions are then transferred to two stainless steel reservoirs of 250 ml, respectively, and pressurized by nitrogen. During the co-extrusion, the suspensions of the outer and inner layer are simultaneously extruded through the outer and inner orifices of a triple-orifice spinneret, respectively (Figure 3.3), while the internal coagulant is introduced through the tube at the centre of the spinneret.

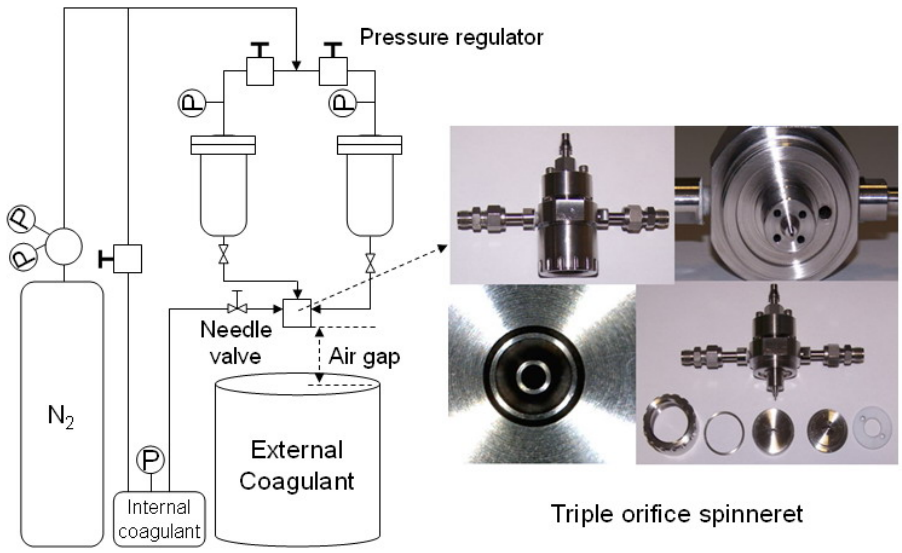


Figure 3.3 Co-extrusion of dual-layer hollow fibre membranes

The extrusion rates of spinning suspensions are controlled by adjusting nitrogen pressures through pressure regulators (PRG-101-60O, mega Engineering Ltd), while the flow rate of the internal coagulant is controlled by a needle valve and pre-calibrated prior to the co-extrusion. DI water and tap water are used as the internal and external coagulants, respectively. The formed hollow fibre precursors are immersed in a water bath for more than 24 h to complete the solidification process, and are heat treated in a CARBOLITE tubular furnace at 600 °C for 2 h to remove the organic polymer binder, followed by the sintering at target temperatures for 4 h to allow the fusion and bonding to occur, with heating and cooling rates of 5 °C/min, respectively.

3.3.3 Characterizations

The macrostructures of the dual-layer hollow fibres were visually observed by a scanning electron microscope (SEM, JEOL JSM-5610LV, Tokyo, Japan). Hollow fibres were snapped and sliced to obtain samples with clear cross-section, outer and inner surfaces. The samples were stuck to metal holders and gold-coated using sputter-coating under vacuum prior to the investigation of the microstructures.

3.4 Results and discussion

3.4.1 Preparation of LSCF/Al_2O_3 and LSCF/YSZ dual-layer hollow fibres

As the main objective of this chapter is to investigate the technical feasibility of using the single-step co-extrusion and co-sintering method to prepare dual-layer ceramic hollow fibre membranes, the membrane materials are selected

from those that have been widely studied. For example, the outer oxygen separation layer is made of $La_{0.6}Sr_{0.4}Co_{0.2}Fe_{0.8}O_{3-\delta}$ (LSCF) [3], while the inner support layer is made of Al_2O_3 or YSZ-8, both of which have great mechanical property and stability at high temperatures. The compositions of the spinning suspensions and corresponding spinning parameters are listed in Tables 3.1 and 3.2. Both LSCF/ Al_2O_3 and LSCF-YSZ-8 dual-layer hollow fibre membranes were co-sintered at 1280°C, which is high enough to densify LSCF single layer hollow fibre membranes [3].

Table 3.1 Compositions of LSCF/ Al_2O_3 spinning suspensions and co-extrusion parameters

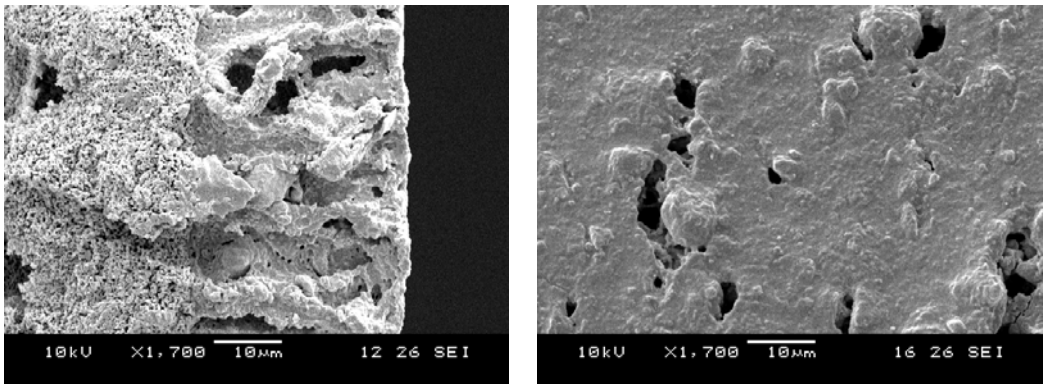
	Outer layer (wt. %)	Inner layer (wt. %)
LSCF	70.49	–
Al_2O_3	–	59.72
PESf	5.81	5.97
NMP	23.16	33.35
PVP K30	0.44	0.50
Additive	0.10	0.46
Extrusion pressure (psi)	8	14
Temperature (°C)	25	
Air gap (cm)	1	
Internal coagulant (ml/min)	15	

Table 3.2 Compositions of LSCF/ YSZ-8 spinning suspensions and co-extrusion parameters

	Outer layer (wt. %)	Inner layer (wt. %)
LSCF	70.49	–
YSZ-8	–	66.00
PESf	5.81	6.60

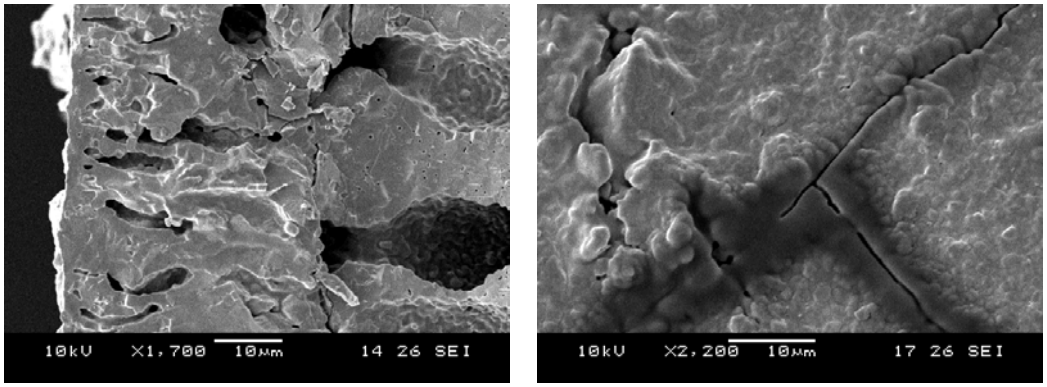
NMP	23.16	27.28
PVP K30	0.44	0
Additive	0.10	0.12
Extrusion pressure (psi)	10	14
Temperature (°C)	25	
Air gap (cm)	10	
Internal coagulant (ml/min)	18	

Figures 3.4 and 3.5 show the microstructures of the sintered dual-layer hollow fibre membranes. As can be seen, finger-like macro-voids are formed in the LSCF layers, due to the development of finger-like structures from the outer surface. The thicknesses of the LSCF layers of LSCF/ Al_2O_3 and LSCF-YSZ-8 dual-layer hollow fibre membranes are measured at approximately 33.6 and 38.6 μm, respectively. The sintered fibres show very poor mechanical strength due to the formation of cracks, which can be found on the outer surfaces of the membranes. The major reason for the crack formation is the different sintering behaviours of the membrane materials in each individual layer, which will be further investigated in the next chapter. Although a large amount of cracks were formed during the co-sintering, no delamination was observed in both membranes, which indicates an improved adhesion between the two layers when compared with the membranes prepared by the multi-step fabrication process. The improved adhesion is quite important for the fabrication of dual-layer hollow fibre membranes with higher surface area and curvature. This also partly demonstrates the feasibility of achieving the dual-layer membrane of this type by using the co-extrusion and co-sintering method.



(a) (b)

Figure 3.4 SEM images of LSCF/ Al_2O_3 sintered at 1280 °C for 4 h
(a) cross-section (b) separation layer surface



(a) (b)

Figure 3.5 SEM images of LSCF-YSZ-8 sintered at 1280 °C for 4 h
(a) cross-section (b) separation layer surface

3.4.2 Preparation of LSCF/LSCF-YSZ-8 dual-layer hollow fibres

If the different sintering behaviour of the two layers is the major reason for the crack formation, and as a consequence poor mechanical strength, measures have to be carried out to minimize such differences. And one of the most effective ways is to add a certain amount of LSCF into the inner layer to match the sintering behaviours of the two layers. As a result 15%, 30% and 50% of LSCF balanced with YSZ-8 were used for the preparation of LSCF/LSCF-

YSZ-8 dual-layer hollow fibres. 15% of LSCF in the inner layer turns out to be not enough to overcome the formation of surface cracks, resulting in the poor mechanical strength of the resultant membranes, while 50% of LSCF seems to be too much as the inner layer surface is densified together with the outer layer, which blocks the permeation of gas through this layer. As a result, only the experimental results of LSCF/LSCF(30%)-YSZ-8(70%) dual-layer hollow fibres are introduced in this section. The compositions of the spinning suspensions and the co-extrusion parameters are listed in Table 3.3

Table 3.3 Compositions of LSCF/ LSCF(30%)-YSZ-8(70%) spinning suspensions and co-extrusion parameters

	Outer layer (wt. %)	Inner layer (wt. %)
LSCF	70.49	19.50
YSZ-8	–	45.50
PESf	5.81	7.00
NMP	23.16	27.88
PVP K30	0.44	0
Additive	0.10	0.12
Extrusion pressure (psi)	9	14
Temperature (°C)	25	
Air gap (cm)	10	
Internal coagulant (ml/min)	12	

As can be seen in Figure 3.6, a thin and uniform LSCF outer layer is formed around and along a thicker LSCF(30%)-YSZ-8(70%) inner layer in a nice hollow fibre configuration, by using the single-step co-extrusion method. Finger-like structures are formed from both the outer and the inner surfaces, and the one from the outer surface penetrates through the interface between

two layers. No delamination occurred during the preparation of the precursor fibres of around 20 m in length (after co-sintering step), demonstrating the advantages of using the co-extrusion method for the production of ceramic hollow fibres with a dual-layer structure.

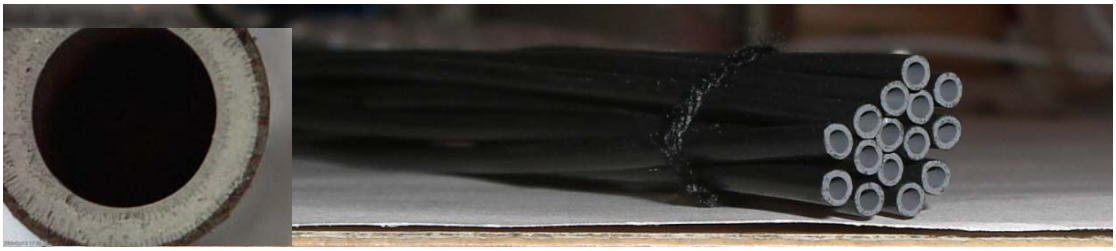


Figure 3.6 Photographic pictures of LSCF/LSCF(30%)-YSZ-8(70%) precursor dual-layer fibres

After the co-sintering at 1280°C for 4h, the OD of the fibres decreases from 1910 μm to 1190 μm, while the ID reduces from 1350 μm to 870 μm, as can be seen in Figure 3.7 (a) and (b). The inner surface is porous after co-sintering (Figure 3.7 (c)), while the outer surface is fully densified (Figure 3.7 (d)). No cracks were found either between the layers or on membrane surfaces, as a result of similar sintering behaviours between layers, leading to a significantly improved mechanical strength of the resultant membranes. This also indicates that, the use of dual-phase membrane materials in one or both layers of the dual-layer ceramic hollow fibre membranes is efficient in matching the sintering behaviours, although the possible solid state reaction between different membrane materials may be an issue and will be discussed in the following chapters.

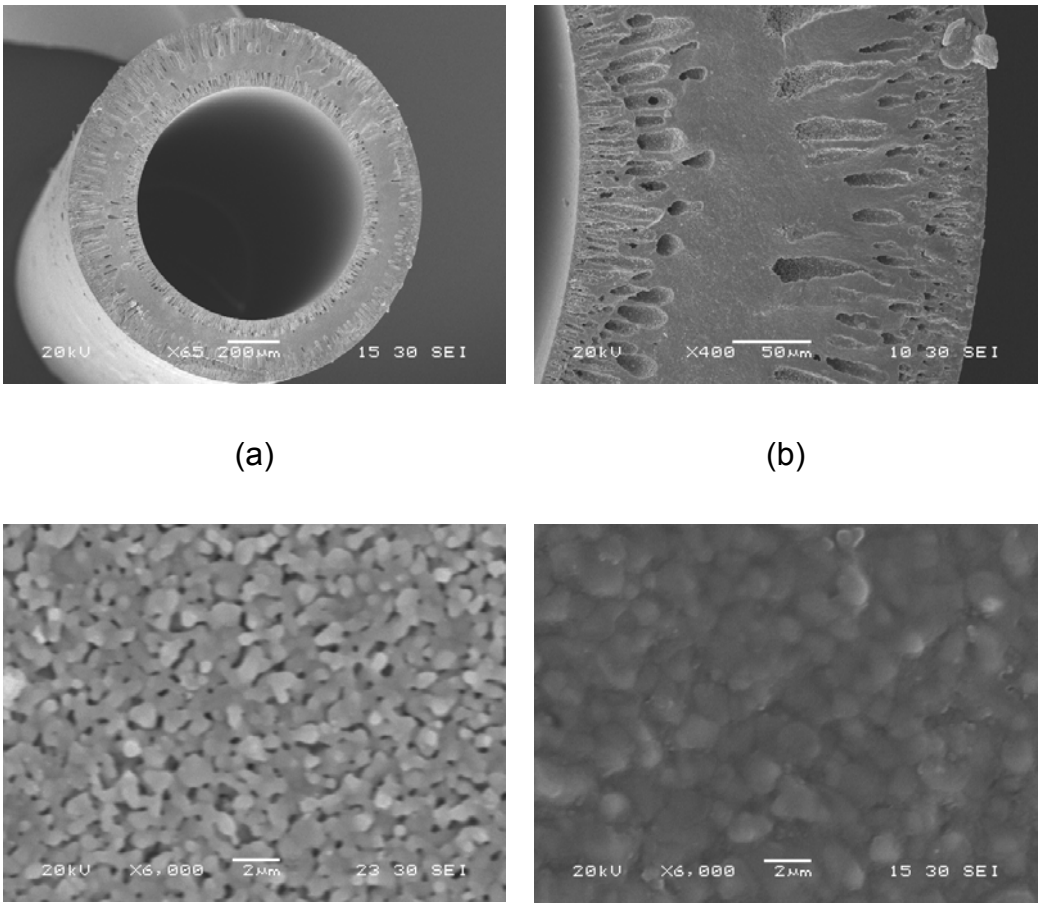


Figure 3.7 SEM images of LSCF/LSCF-YSZ-8 dual-layer fibres co-sintered at 1280 °C for 4h (a) whole cross section (b) cross section (c) inner surface (d) outer surface

However, a further investigation on the microstructure shows that, a sponge-like layer at the central of the inner layer is also nearly densified, as shown in Figure 3.8. This layer produces the major resistance for oxygen permeation, which can be proved by comparing the oxygen permeation flux between the dual-layer membrane and a LSCF single layer fibre under the same operating conditions.

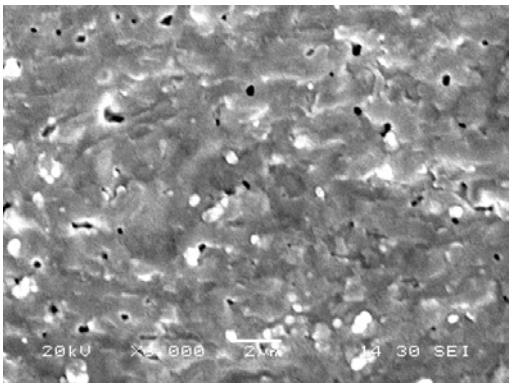


Figure 3.8 SEM image of the sponge-like layer in the inner layer

As can be seen in Figure 3.9, although the LSCF oxygen separation layer of the dual-layer hollow fibre membrane (30-40 microns in thickness) is much thinner than that of the LSCF single layer counterpart, the oxygen permeation flux is dramatically lower due to the nearly densified sponge-like layer in the inner layer. However, only a trace amount of leaking was detected by GC, indicating a great integrity of the developed dual-layer hollow fibre membranes.

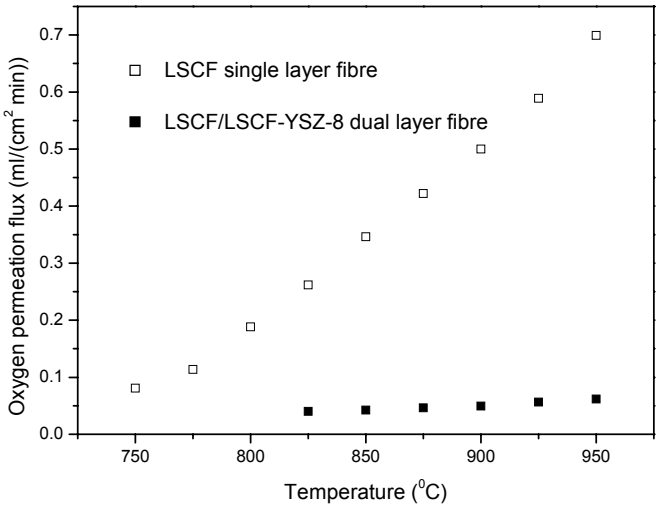


Figure 3.9 Temperature dependent oxygen permeation fluxes of LSCF and LSCF/LSCF-YSZ-8 hollow fibre membranes

The average particle sizes of LSCF and YSZ-8 used for the preparation of LSCF/LSCF (30%)-YSZ-8(70%) dual-layer hollow fibres are 0.34 and 0.3 μm, respectively. In order to increase the porosity of the inner layer, two methods can be used: 1) use of a certain amount of pore formers such as carbon and 2) use of bigger YSZ-8 particles. If pore formers are employed, they need to form a continuous phase to achieve a highly inter-connected pore structure after high temperature sintering. As a result, the amount of pore formers needed could significantly change the rheology of the spinning suspension, which may turn into a paste that is not spinnable. Moreover, NMP is a very strong solvent and most of the organic pore formers dissolve in it, and as a consequence can hardly function as a pore former. In contrast with small particles, bigger YSZ-8 particles may not be fully sintered, and the pore structure formed as a result of particle packing can be continuous and highly inter-connected.

However, the use of bigger YSZ particles in the inner layer enlarges the differences of sintering behaviours between the two layers, when the LSCF powder of 0.34 μm is employed. For example, the oxygen separation layer of a dual-layer hollow fibre membrane consists of LSCF/LSCF(30 wt.%)-YSZ (63% 3 micron & 7% 0.3 micron) can not be densified at 1280 °C, although the inner support layer is still porous after co-sintering (Figure 3.10). A further increase of the co-sintering temperature to 1380 °C results in a fully densified inner layer (Figure 3.11). The efforts of adjusting membrane microstructure by controlling co-sintering temperature or dwelling time would not be productive because too many conditions have to be tested for a single combination of membrane materials. It should be noted that, similar to the dual-layer fibres

introduced above, no delamination occurred after the co-sintering, indicating great adhesion between the two layers.

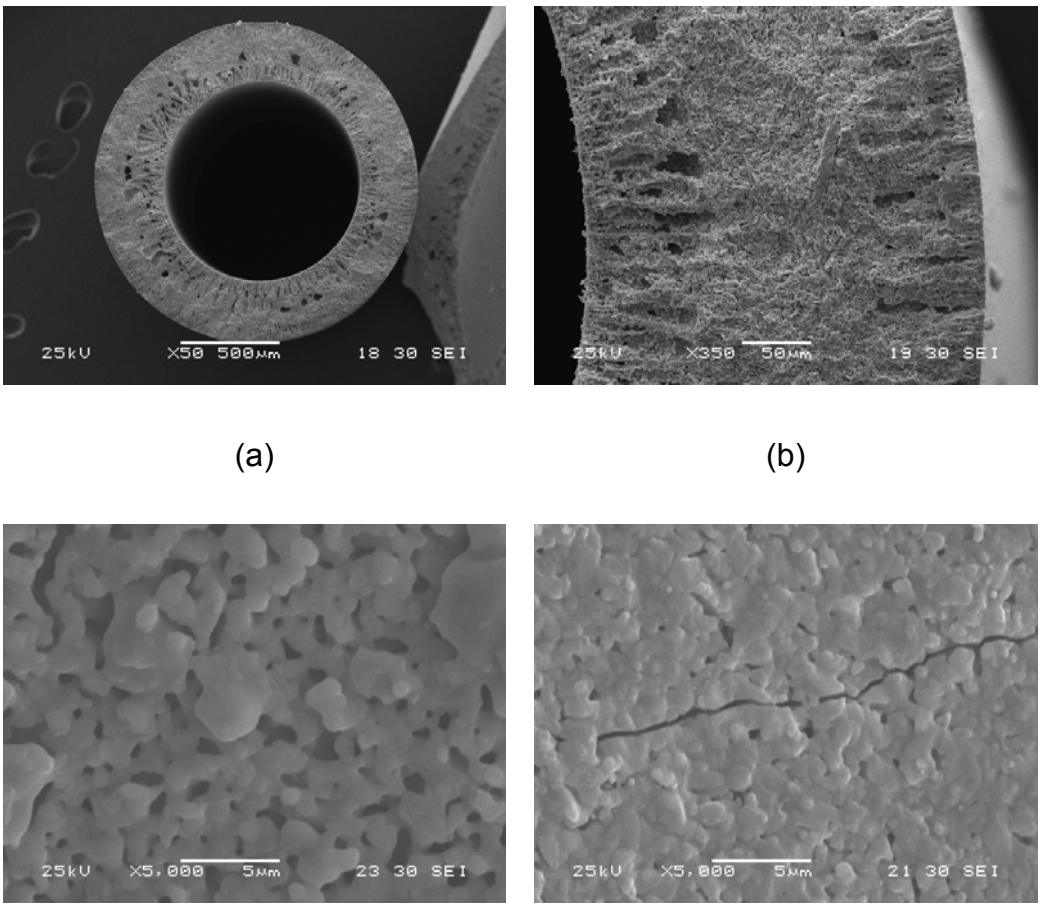


Figure 3.10 SEM images of LSCF/LSCF-YSZ (63% 3 micron & 7% 0.3 micron) dual-layer hollow fibres sintered at 1280 °C for 4 h

(a) whole view (b) cross-section (c) inner surface (d) outer surface

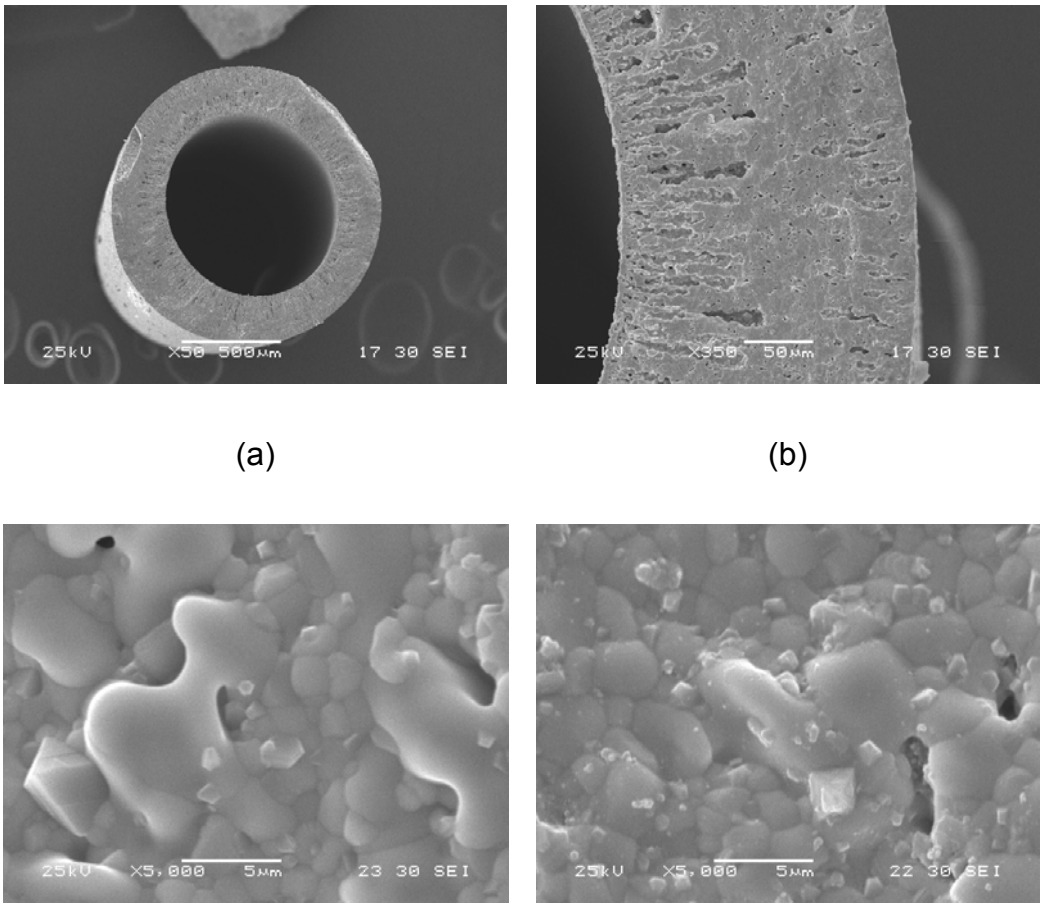


Figure 3.11 SEM images of LSCF/LSCF-YSZ (63% 3 micron & 7% 0.3 micron) dual-layer hollow fibres sintered at 1380 °C for 4 h

(a) whole view (b) cross-section (c) inner surface (d) outer surface

Table 3.4 summarises the shrinkages of the developed dual-layer hollow fibre membranes, based on the changes in the OD and ID before and after high temperature sintering, and compared them with a single-layer LSCF hollow fibre membrane prepared separately. As can be seen, the shrinkage of a dense single-layer LSCF hollow fibre membrane sintered at 1280 °C is about 35 %. As a result, the shrinkage of the inner support layer of the dual-layer

fibres should be as close as possible to this value in order to survive the co-sintering and obtain reasonable mechanical strengths. However, the inner support layer turns into a dense structure under these co-sintering temperatures, although reasonable mechanic strength can be obtained. This makes it unsuitable as the inner layer of a dual-layer hollow fibre membrane because it creates high resistance for gas permeation. As a consequence, selection of proper membrane materials is critically important and will be introduced in the next chapter. However, the co-extrusion and co-sintering process has been proved technically feasible in fabricating dual-layer ceramic hollow fibre membranes.

Table 3.4 Summarization of the shrinkages of the hollow fibres membranes

	OD mm*	ID mm*	OD shrinkage	ID shrinkage
LSCF single layer fibre (1280 °C)	2.47/1.56	1.72/1.12	36.84%	34.88%
LSCF/LSCF(30%)-YSZ(70% 0.3μm) (1280 °C)	1.91/1.35	1.19/0.87	29.4%	27.1%
LSCF/LSCF (30%)- LSCF(30%)-YSZ(63% 3 μm & 7% 0.3 μm) (1280 °C)	1.9/1.35	1.17/0.86	14.7%	13.68%
LSCF/LSCF (30%)- LSCF(30%)-YSZ(63% 3 μm & 7% 0.3 μm) (1380 °C)	1.9/1.35	1.17/0.86	28.95%	26.5%

* The values are shown as precursor fibre/sintered fibre

3.5 Conclusion

Ceramic dual-layer hollow fibre membranes consisting of an outer oxygen separation layer supported by an inner inert layer have been fabricated using

a single-step co-extrusion and co-sintering method. Benefiting from the similar nature of the spinning suspensions, as well as the fact that the two layers are simultaneously formed during the membrane preparation process, great adhesion between the layers can be achieved without delamination after high temperature sintering. In addition, consistent microstructures of the developed dual-layer fibres can be achieved although the surface area and the curvature of hollow fibre configuration are considerably higher than those of the disc/flat sheet and tubular counterparts, which further proves the feasibility of using such membrane preparation process to produce high quality ceramic dual-layer hollow fibre membranes.

However, it is still challenging to simultaneously obtain a fully dense outer oxygen separation and a highly porous inner support layer without pore formers during the co-sintering process. The major concern is the different sintering behaviours of each layer, which is closely dependent on the nature of membrane materials. As a result, a re-selection of membrane materials is necessary prior to the use of such dual-layer hollow fibre membranes for oxygen separation and membrane reactor.

Reference

1. X.Y. Tan, S.M. Liu, K. Li, Preparation and characterization of inorganic hollow fiber membranes, Journal of Membrane Science, 188 (2001) 87-95.

2. W.Q. Jin, S.G. Li, P. Huang, N.P. Xu, J. Shi, Preparation of an asymmetric perovskite-type membrane and its oxygen permeability, Journal of Membrane Science, 185 (2001) 237-243.

3. X.Y. Tan, Y.T. Liu, K. Li, Preparation of LSCF ceramic hollow-fiber membranes for oxygen production by a phase-inversion/sintering technique, Industrial & Engineering Chemistry Research, 44 (2005) 61-66.

4. X.F. Chang, C. Zhang, W.Q. Jin, N.P. Xu, Match of thermal performances between the membrane and the support for supported dense mixed-conducting membranes, Journal of Membrane Science, 285 (2006) 232-238.

5. Z.H. Chen, Z.P. Shao, R. Ran, W. Zhou, P.Y. Zeng, S.M. Liu, A dense oxygen separation membrane with a layered morphologic structure, Journal of Membrane Science, 300 (2007) 182-190.

6. X.L. Dong, Z.K. Liu, W.Q. Jin, N.P. Xu, A self-catalytic mixed-conducting membrane reactor for effective production of hydrogen from methane, Journal of Power Sources, 185 (2008) 1340-1347.

7. X.L. Dong, C. Zhang, X.F. Chang, W.Q. Jin, N.P. Xu, A self-catalytic membrane reactor based on a supported mixed-conducting membrane, Aiche Journal, 54 (2008) 1678-1680.

8. M. Ikeguchi, K. Ishii, Y. Sekine, E. Kikuchi, M. Matsukata, Improving oxygen permeability in SrFeCo0.5Ox asymmetric membranes by modifying support-layer porous structure, Materials Letters, 59 (2005) 1356-1360.

9. X. Yin, C. Choong, L. Hong, Z.L. Liu, Crafting La0.2Sr0.8MnO3-delta membrane with dense surface from porous YSZ tube, Journal of Solid State Electrochemistry, 10 (2006) 643-650.

10. X. Yin, L. Hong, Z.L. Liu, Development of oxygen transport membrane La0.2Sr0.8CoO3-delta/Ce0.8Gd0.2O2-delta on the tubular CeO2 support, Applied Catalysis a-General, 300 (2006) 75-84.

11. X. Yin, L. Hong, Z.L. Liu, Oxygen permeation through the LSCO-80/CeO2 asymmetric tubular membrane reactor, Journal of Membrane Science, 268 (2006) 2-12.

12. J.A. Casey, *Theoretical basic for control of suspension properties, in Dispersion and aggregation: Fundamentals and applications*, ed. RM Moudgil, P Somasandaran. 1992, New York: The Engineering Foundation.

13. S. Loeb, S. Sourirajan, *Sea water demineralization by means of an osmotic membrane, in Saline Water Conversion–II, Advances in Chemistry*. 1963, Washington DC: American Chemical Society. 117–132.

14. B.F.K. Kingsbury, K. Li, A morphological study of ceramic hollow fibre membranes, Journal of Membrane Science, 328 (2009) 134-140.

Chapter 4

A Novel Dual-Layer Ceramic Hollow Fibre Membrane Reactor for POM

Abstract

In Chapter 3, the technical feasibility and advantages of using the single-step co-extrusion and co-sintering method to fabricate ceramic dual-layer hollow fibre membranes consisting of a thin dense outer oxygen separation layer supported on an inert inner substrate layer have been investigated and demonstrated. However, it is still challenging to simultaneously obtain a dense outer layer and a very porous inner support layer without pore formers. In this chapter, the same membrane fabrication process is employed to develop ceramic hollow fibre membranes of similar dual-layer structure but used as a membrane reactor for methane conversion. The resultant dual-layer hollow fibre membrane reactor (DL-HFMR) consists of a dense outer oxygen separation layer supported on a highly porous inner Ni-based catalytic substrate layer. Oxygen in ambient air permeates through the outer layer and reacts with CH_4 (introduced through the lumen) on the inner catalytic support layer at elevated temperatures. Such membrane reactor design is of extremely high surface area/volume ratio by avoiding extra packing of catalysts.

Keywords: Dual-layer hollow fibre, co-extrusion and co-sintering, membrane reactor, partial oxidation of methane (POM)

4.1. Introduction

Pore formers such as carbon and polymers have been widely used in the preparation of asymmetric/supported mixed ionic-electronic conducting (MIEC) membranes for oxygen separation [1-3]. However, use of conventional pore formers for a highly porous inner support layer of ceramic dual-layer hollow fibres would raise a number of problems in the co-extrusion process: 1) most of polymers partly or fully dissolve in strong solvents such as N-methyl-2-pyrrolidone (NMP) and Dimethyl Sulfoxide (DMSO) that are employed for the preparation of spinning suspensions. As a consequence, they can hardly function as a pore former occupying a space among ceramic particles to form an inter-connected pore structure in ceramic membranes; 2) even if some conventional pore formers manage to withstand aggressive solvents, a considerable amount, for example 30 vol. % in a mixture of ceramic powders and pore formers, is necessary for a continuous porous structure in ceramic membranes. Use of such amount of pore formers would significantly change the viscosity of the spinning suspensions, and sometimes turn them into a paste that is not spinnable. As a result, use of conventional pore formers is not recommended in the co-extrusion process, unless they can be chemically treated to withstand the aggressive solvents.

NiO has been widely used for preparing a highly porous composite/dual-phase anode of solid oxide fuel cell (SOFC), because a approximately 40 % of volume reduction can be achieved when NiO (density: 6.67 g/cm^3, melting point: 1955 °C) is reduced into Ni (density: 8.9 g/cm^3, melting point: 1453 °C).

In this case, NiO functions as both the electronic conductive phase (after reduction) and an inorganic pore former. When combined with ceramic materials such as YSZ with good ionic conductivity, it also shows great catalytic activity to methane conversion, such as partial oxidation of methane (POM) to syngas and steam reforming reaction [4, 5]. Such knowledge can be transferred to meet the challenge in Chapter 3. Moreover, the porous inner layer of this type is not only a support of the outer oxygen separation layer, but also a catalytic layer for methane conversion, forming a highly compact multifunctional hollow fibre membrane reactor. Similarly, instead of using single-phase MIEC materials for oxygen separation, the materials of the outer oxygen separation layer can be selected from composite/dual-phase cathodes of SOFC with great compatibility and stability, in order to match the sintering behaviours with the inner layer. As a result, the developed dual-layer ceramic hollow fibres can be functionalized by changing the membrane materials, which also contribute to match the sintering behaviours of the two layers during the co-sintering process.

4.1.1 Objectives

The main objective of this chapter is to develop a dual-layer hollow fibre membrane reactor (DL-HFMR) for methane conversion by using the single-step co-extrusion and co-sintering process. The specific objectives are listed below:

1. Selection of membrane materials with great mechanical property, compatibility and stability under reducing atmosphere.

2. Investigation on the sintering behaviours of the membrane materials.
3. Preparation of DL-HFMR using the co-extrusion and co-sintering method.
4. Use of the developed DL-HFMR for methane conversion

4.2 Background

Membrane reactor is a device coupling membrane separation and catalytic chemical reaction in one unit [6]. Benefiting from the advantages of such reactor design, much lower operating cost can be achieved as a result of coupling reaction with separation together. Use of dense ceramic membranes to control the addition and distribution of oxygen from ambient air to chemical reactions, such as partial oxidation of methane (POM) to syngas, has been widely studied in the last several decades [7-9], stemming from a number of technological advantages over the conventional techniques. Great progress has been achieved, particularly in the light of the development of membrane materials with higher oxygen permeation flux and better high temperature stabilities in reducing atmospheres [10, 11], as well as the technical breakthrough in fabricating dense ceramic hollow fibre membranes with much higher surface area/volume ratio and significantly reduced membrane thickness [12-14] over most of the disk/tubular counterparts. However, there are still several fundamental concerns over the designs of dense ceramic membrane reactors: 1) trade-off between oxygen permeation and life-time of the ceramic membranes, which is more significant in POM reaction due to the formation of reducing products such as H_2 and CO; 2) because of direct

catalyst packing on membrane surface, the surface area per unit volume and the volume productivity of current membrane reactor designs are still small, limiting the scale-up process for industrial applications.

In order to meet these challenges, various studies have been carried out, mainly focusing on the improvement in one aspect/characteristic of the membrane reactors. Up to date, use of stable membrane materials prepared by doping [11] is one of the major ways to extend the life-time of dense ceramic membranes, usually at the expense of oxygen permeation flux. Membrane configurations such as supported/asymmetric membranes [2, 15] with reduced membrane thickness and tubular or hollow fibre membranes with greater surface area are widely studied, aiming for higher oxygen permeation flux. Techniques such as surface modification are also considered efficient in improving oxygen permeation through the membranes. Coupling of membrane with catalyst in a dense catalytic membrane reactor can be achieved basically in two ways [16]: 1) directly packing catalyst pellets or coating a catalyst in the form of paste on membrane; 2) membrane itself is catalytically active. The first arrangement, especially the one of catalyst packing, has been widely employed in the dense ceramic membrane reactor designs although the reactor volume is considerably increased as a consequence. While the major concern over the second arrangement is how to achieve a sufficient effective catalytic area on a dense membrane. More detailed information on dense ceramic membrane reactor can be found in Chapter 2.

In contrast, a novel design of dense ceramic hollow fibre membrane reactor with a dual-layer structure (DL-HFMR) for methane conversion is developed in this chapter. The membrane in hollow fibre configuration consists of an outer oxygen separation layer and another inner layer made of NiO and yttria-stabilized zirconia (YSZ). The outer layer is made of a mixture of $La_{0.8}Sr_{0.2}MnO_{3-\delta}$ (LSM, 40 vol.%)-yttria-stabilized zirconia (YSZ, 60 vol.%), which has been widely used as a composite cathode material in SOFC with great compatibility and stability in reducing atmosphere [17], and similar sintering temperature as well as thermal expansion coefficients [18, 19]. The inner layer changes into a highly porous structure without using any additional pore formers when NiO is reduced into Ni, which is catalytic active to POM reaction when combined with YSZ [4, 5, 20]. As a result, the inner layer functions not only as the support of the membrane, but also the catalyst of the DL-HFMR, substantially increasing the surface area/volume ratio of the membrane reactor design of this type by avoiding the extra packing of catalyst. A single-step co-extrusion and co-sintering technique is used to fabricate the DL-HFMR, which results in a great adhesion between the separation and the catalytic support layers during the hollow fibre fabrication process. In addition, the YSZ forms, somewhat, a sort of structural matrix in both layers and acts as a bridge for a strong connection between the two layers at high temperatures. One of the additional advantages of using dual-phase membrane materials is that, by adjusting the materials compositions, the sintering behaviours of the two layers can be well matched in order to minimize crack formation during the co-sintering process. Furthermore, the generic advantages of the single-step co-extrusion and co-sintering technique

and the DL-HFMR design of this type can be applied to other applications of great importance, such as micro-tubular solid oxide fuel cell (SOFC) [21] and chemical productions.

4.3. Experimental

4.3.1 Materials

$La_{0.8}Sr_{0.2}MnO_{3-\delta}$ (LSM, NexTech Materials Ltd, 5.8 m^2/g), NiO (NexTech Materials Ltd, 5.2 m^2/g) and yttria-stabilized zirconia 8 mole% (YSZ, NexTech Materials Ltd, 12.4 m^2/g) were used as supplied. Polyethersulfone, (PESf, Radel A-300, Ameco Performance, USA), Dimethyl Sulfoxide (DMSO, Sigma, >99.5%) and Arlacel P135 (Uniqema, UK) were used as polymer binder, solvent and additive functioning as dispersant respectively. DI water and tap water were used as the internal and the external coagulants, respectively, when fabricating the dual-layer hollow fibres.

4.3.2 Fabrication of LSM-YSZ/NiO-YSZ dual-layer hollow fibres

Compositions of the spinning suspensions of the outer oxygen separation layer and the inner catalytic support layer are listed in Table 4.1. In a typical process of preparing the suspensions, the right amounts of the ceramic powders, the solvent and the additive were pre-mixed and ball-milled in a high speed shimmy ball mill (MTI Corporation, SFM-1 (QM-3SP2)) for 48 h. After adding of the polymer binder, a further ball milling of 48 h was required to obtain homogeneous spinning suspensions. The resultant spinning

suspensions were then degassed with stirring under vacuum for about 2 h to remove air bubbles trapped inside.

Table 4.1 Compositions of the spinning suspensions and co-extrusion parameters

	Outer oxygen separation layer (wt. %)	Inner support /catalytic layer (wt. %)
LSM	27.4	–
YSZ	37.6	45.6
NiO	–	22.4
DMSO	28.0	25.1
PESf	6.5	6.8
Additive	0.5	0.1
Extrusion rate (ml/min)	4.5-6.5	8
Temperature (°C)	25	
Air gap (cm)	25	
Internal coagulant (ml/min)	10	

After degassing, the suspensions of the outer layer and the inner layer were transferred to stainless steel syringes with a maximum volume of 100 ml and 200 ml, respectively, and were simultaneously extruded through a triple-orifice spinneret (Figure 4.1) into an external coagulation bath containing around 120 litres of tap water with an air-gap of 25 cm. The extrusion rates of the spinning suspensions as well as the flow rate of the internal coagulant were accurately controlled and monitored by a KDS410 and two Harvard PHD 22/2000 Hpsi syringe pumps, ensuring the uniformity of the prepared fibres. The formed precursor fibres were cut into the required length, heated in an Elite tubular furnace at 600 °C for 2 h to remove the organic polymer binder and were

finally sintered at 1400 °C for 5 h with heating and cooling rates of 5 and 3 °C /min, respectively.

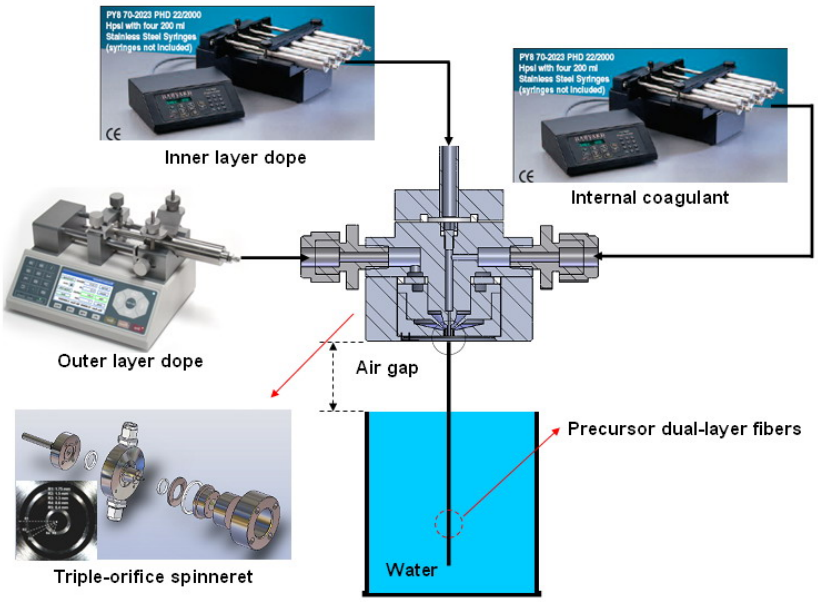


Figure 4.1 Schematic diagram of preparing dual-layer hollow fibres using the co-extrusion process

4.3.3 Characterizations of the dual-layer hollow fibres

The sintering behaviours of the membrane materials were investigated using a dilatometer (ZRPY-1600, Xiangtan Instrument and Apparatus Co., Ltd). Ceramic powder mixtures were well pre-mixed in ethanol using ball-milling. After drying, the powders were pressed into a rectangular bar with the dimensions of 6mm×6mm×20mm for testing. The measurements were carried out under static air atmosphere, using a heating rate of 5 °C /min from room temperature to 1500 °C. The microstructures of the dual-layer fibres were visually observed using a scanning electron microscope (SEM, JEOL JSM-5610LV, Tokyo, Japan). The mechanical strength of the fibres was examined

by three points bending test (Instron Model 5544) using a load cell of 1 kN. Samples of around 5 cm in length were fixed on the sample holder with a 3 cm distance. The bending strength (σ_F, MPa) is calculated using the following equation[22]:

$$\sigma_F = \frac{8 \cdot F \cdot L \cdot D}{\pi (D^4 - d_i{}^4)} \tag{4-1}$$

where F is the measured load at which fracture occurred (N); L, D, d_i are the length (m), the outer diameter and the inner diameter of the hollow fibres (m), respectively.

4.3.4 Methane conversion using the DL-HFMR

The developed LSM-YSZ/NiO-YSZ dual-layer hollow fibres were used for methane conversion by using an experimental set-up shown in Figure 4.2.

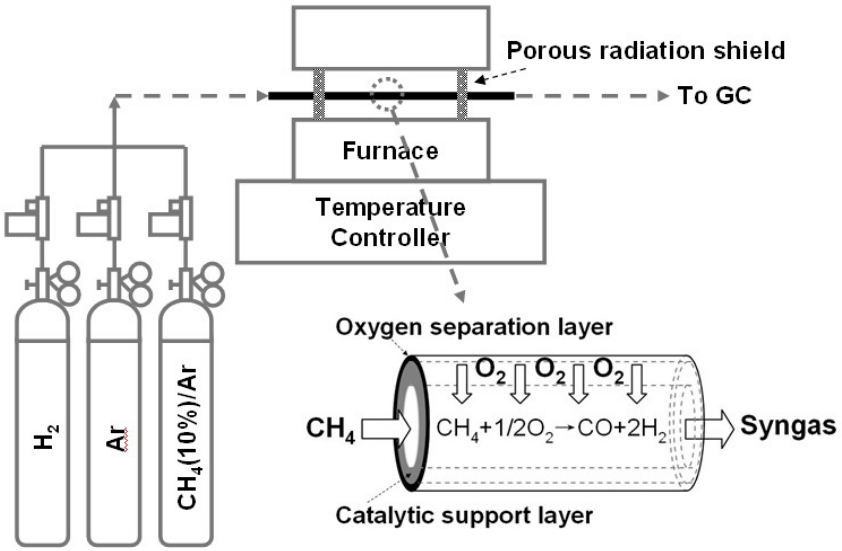


Figure 4.2 Schematic diagram of experimental setting-up for POM reaction

Before the reaction, NiO in the inner layer was reduced into Ni using pure H_2 at 550 °C for 30 min. Ambient air was used directly as the source of oxygen and the flow rate of the reactant (10% CH_4/Ar) was controlled by a mass flow controller. Methane reacted with permeated oxygen on the highly porous inner layer, and was converted into syngas (H_2+CO). The product stream was on-line analysed by GC (Unicam 610 and Varian 3900). Methane conversion (X_{CH4}) and CO selectivity (S_{CO}) were calculated using the following equations:

$$X_{CH4} = \frac{F_{CH4inlet} - F_{CH4outlet}}{F_{CH4inlet}} \times 100\% \quad (4\text{-}2)$$

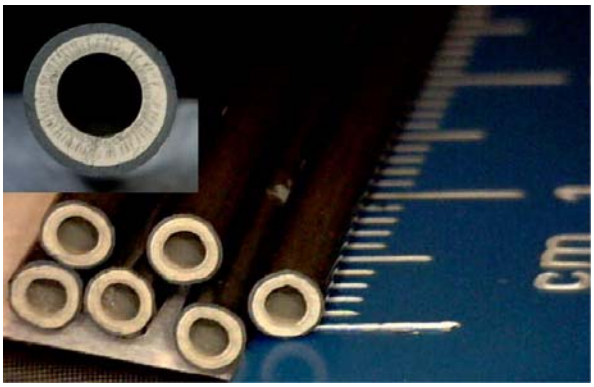
$$S_{CO}^{'} = \frac{F_{CO}}{F_{CH4inlet} - F_{CH4ioutlet}} \times 100\% \quad (4\text{-}3)$$

4.4. Results and discussion

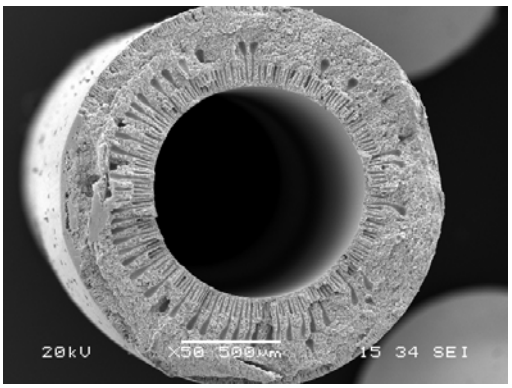
4.4.1 Co-extrusion of the dual-layer precursor hollow fibres

A photographic picture of the precursor fibres (before co-sintering) is shown in Figure 4.3 (a). As can be seen, a thin outer layer has been uniformly coated around an inner layer with a clear interface between them. Benefiting from the accurate control over the extrusion rates of the two layers, as well as similar spinning suspension properties such as the compositions of the suspensions, the types of ceramic powder, the polymer binder and the solvent used, the outer layer is able to be firmly attached to the inner layer with consistent thickness and uniform microstructure for the whole batch of the prepared fibres. The OD and ID of the dual-layer precursor fibres are measured at

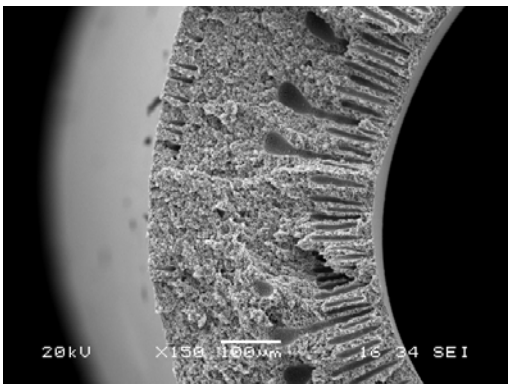
1935.9 and 1064.1 μm, respectively, according to the SEM images shown in Figure 4.3 (b). The interface between the layers is not observable in Figure 4.3 (c) because of the polymer binder in the precursor fibres. Tiny finger-like voids are found in the outer layer, while the inner layer is composed of a sponge-like layer and a finger-like layer. The finger-like structure, which is formed as a result of viscous fingering phenomena during the phase-inversion process [23], contributes to reduce the resistance of gas permeation through the inner layer, but at the cost of mechanical property of the hollow fibres. It should be noted here that, the finger-like structure of this type can be eliminated by further optimizing the spinning parameters, such as the viscosity of the spinning suspension [23].



(a)



(b)



(c)

Figure 4.3 Photographic and SEM images of the precursor dual-layer hollow fibres (a) photograph, (b) whole view (SEM), (c) cross section (SEM)

4.4.2 Sintering behaviours of LSM-YSZ and NiO-YSZ

During the co-sintering of a ceramic membrane with a dual-layer structure, which is also named as a supported or asymmetric structure for disk-type membranes [1, 3], matching the sintering behaviours of the two layers made of different materials is critically important for simultaneously achieving a dense oxygen separation layer and a porous support layer free of defects. In contrast to supported/asymmetric disk-type membranes with limited surface area, which are prepared by conventional multi-step fabrication processes, there is a considerably higher chance of crack formation during the co-sintering of dual-layer hollow fibre membranes due to a much higher surface area and curvature. As a result, sintering behaviours of the membrane materials need to be investigated in order to determine the right composition of membrane materials.

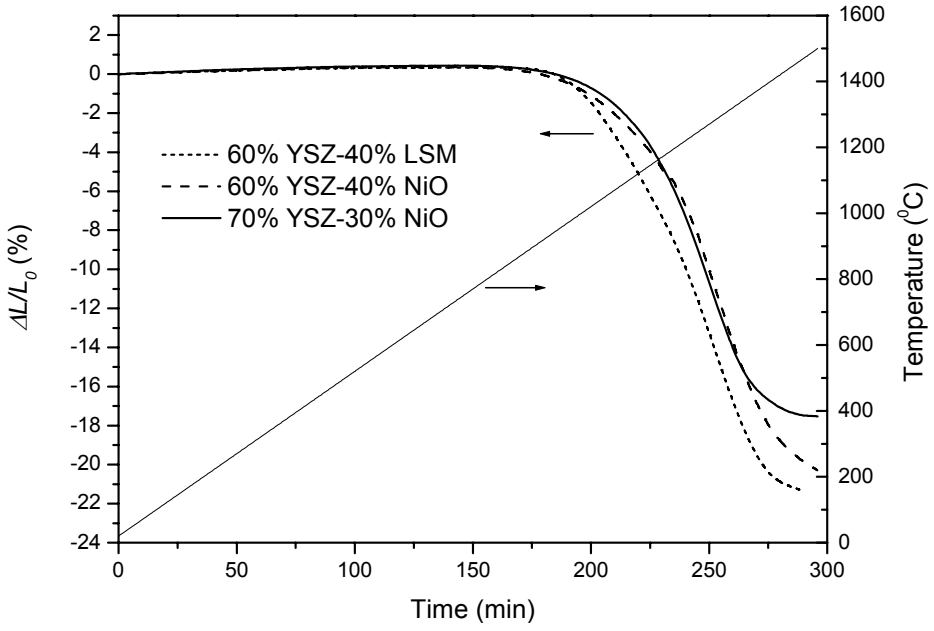
Benefiting from the advantages of the co-extrusion process, great adhesion between the two layers of the precursor dual-layer hollow fibres can be achieved, which has been discussed above. This also indicates that the interaction between the two layers during the co-sintering may be significant. Dual-phase materials are employed in the inner and the outer layer, in both of which a large amount of YSZ is used. YSZ with great mechanical property can be, in this case, considered as a matrix of the hollow fibres dominating the co-sintering process, which contributes to match the sintering behaviours of the two layers. Figure 4.4 shows the sintering curves as well as sintering rate curves of the outer layer (LSM (40 vol.%)-YSZ (60 vol.%)) and the inner layer (NiO-YSZ) materials. In order to highlight the importance of material

composition on the sintering behaviours, two types of NiO-YSZ inner layer materials with different NiO concentration, i.e. 30 vol.% and 40 vol.%, were tested for comparison.

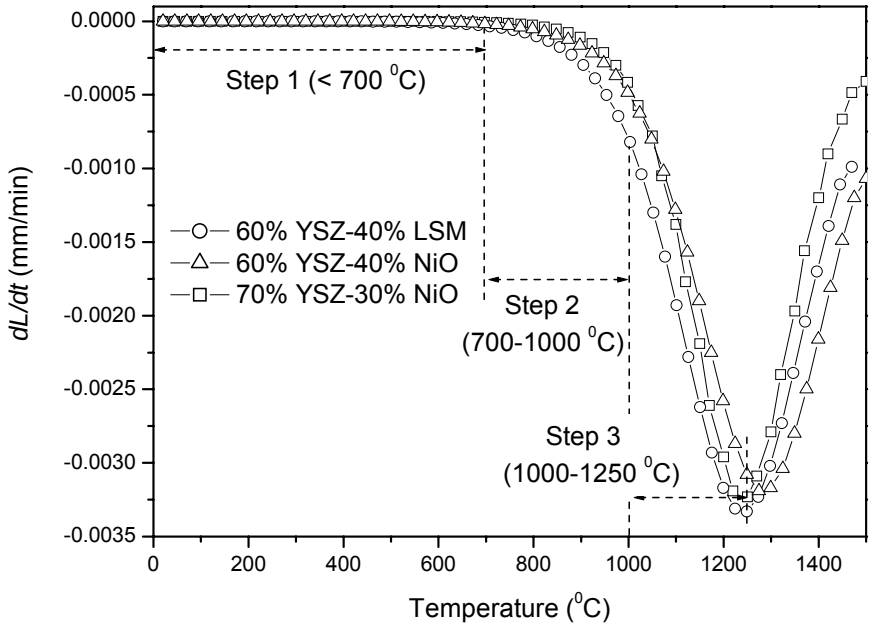
As can be seen in Figure 4.4 (a), LSM-YSZ starts to shrink at a lower temperature and shows a higher final shrinkage over NiO-YSZ. When more YSZ is used in the inner layer, the final shrinkages reduce from 20.31% to 17.53%, which is further less than that of LSM-YSZ of 21.41%. Besides the nature of materials, the final shrinkages of the membrane materials are considerably dependent on green packing density that can be affected by a number of factors such as particle size, particle shape and distance between particles. As the particle size of YSZ is about half of that of NiO, use of more YSZ would reduce the distance between particles, increase the green packing density of the corresponding sample and result in a lower final shrinkage. The values of final shrinkages from the sintering curves are still not enough to determine the co-sintering process because they are not able to reflect how the materials change during the high temperature sintering, especially when there is an interaction between the two layers.

Based on the sintering curves in Figure 4.4 (a), the sintering rate curves revealing the most critically important and useful information of the sintering process can be obtained and are shown in Figure 4.4 (b). As can be seen, there is little sintering below 700 °C, at which temperature the polymers in the precursor fibres have been removed. With the increasing temperatures, ceramic membrane materials start to be sintered from a very low sintering rate

and then slowly increase with the increasing temperatures up to about 1000 °C. When the sintering temperature is above 1000 °C, there is a significant increase in the sintering rate which gets to the maximum value at about 1250 °C.



(a)



(b)

Figure 4.4 Sintering curves and sintering rates curves of the dual-layer hollow fibre materials, (a) sintering curves and (b) sintering rates

As a result, step 3 is the most important stage in the co-sintering process because the difference in sintering rates at this stage is the one of the main reasons for the formation of cracks or defects resulting in poor integrity and mechanical strength of the resultant membranes. If the difference in the sintering rate is too big, the membrane cannot even survive the co-sintering. For example, although the final shrinkage of 60 vol.%YSZ-40 vol.%NiO is closer to that of LSM-YSZ, when compared with 70 vol.%YSZ-30 vol.% NiO (Figure 4.4 (a)), its sintering rate curve is quite different from that of LSM-YSZ, and as a consequence the corresponding dual-layer hollow fibres break into several parts with very poor mechanical property when the heating rate of the co-sintering is 5 °C/min. Although the fibres can survive the co-sintering when the heating rate is increased to 10 °C/min, the stress formed results in a sudden break of the fibres during the POM reaction. In contrast, 70 vol.%YSZ-30 vol.%NiO is more suitable as the inner layer material. Moreover, use of higher amount of YSZ in the inner layer improves the mechanical property of the resultant hollow fibre membranes.

4.4.3 Mechanical property and microstructure of dual-layer hollow fibres

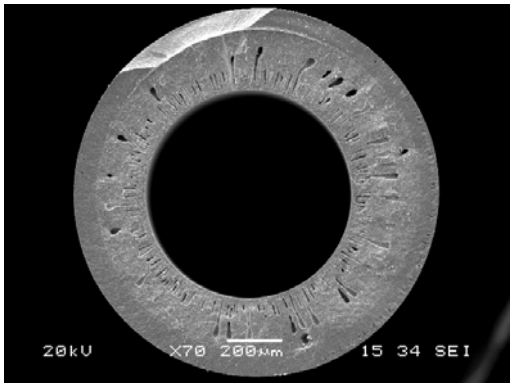
The precursor fibres of 40 cm in length, which are composed of a 40 vol.% LSM-60 vol.% YSZ outer oxygen separation layer supported on a 30 vol.% NiO-70 vol.% YSZ inner catalytic support layer are then co-sintered at 1400 °C for 5 h. The mechanical property of the developed dual-layer hollow fibres were investigated and compared with an inner single-layer fibre prepared separately under the identical conditions. As can be seen in Table 4.2, the dual-layer fibres are stronger than the inner single-layer counterparts in terms

of the higher loading needed to break the samples, as a result of the additional outer oxygen separation layer. However, the bending strengths of the two types of the samples are quite similar to each other, because the OD of the dual-layer fibres is bigger than that of the inner single-layer fibres, while the IDs of both fibres are same. These bending strength values are slightly higher than a YSZ hollow fibre with a similar asymmetric structure [24] due to the thicker hollow fibre wall. The comparable bending strengths between the dual-layer and the inner single-layer fibres in Table 4.2 further indicate that, benefiting from the well matched sintering behaviours of the outer oxygen separation layer and the inner support layer materials (Figure 4.4), the formation of structural defects or cracks during the co-sintering process can be eliminated, further proving the great integrity of the developed dual-layer hollow fibres.

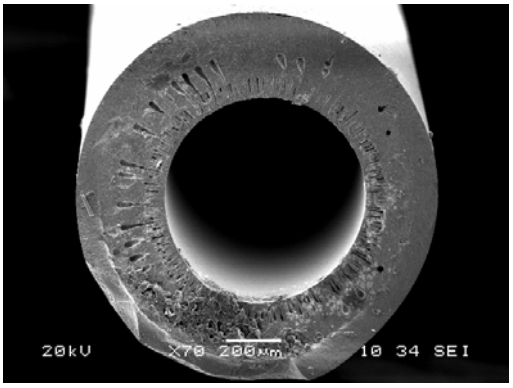
Table 4.2 Three-point bending of single-layer and dual-layer hollow fibres

	Inner single-layer fibres (YSZ-NiO)		Dual-layer fibres (LSM-YSZ/YSZ-NiO)	
	Load (N)	Bending strength (MPa)	Load (N)	Bending strength (MPa)
Sample 1	5.61	298.80	8.24	311.91
Sample 2	5.07	270.04	7.33	277.47
Sample 3	5.26	280.15	7.49	283.52
Average	5.31	283.00	7.69	290.97

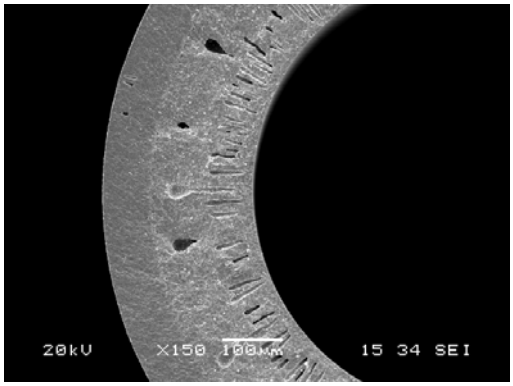
After co-sintering, the average length of the fibres is reduced to 28.7 cm, while the OD and ID of the resultant dual-layer fibres decrease to approximately 1309.1 and 736.4 μm, respectively (Figure 4.5 a-I), resulting in a surface area/volume ratio up to 2769.7 m^2/m^3. The thickness of the outer oxygen separation layer is measured to be 75.0 μm (Figure 4.5 b-I). No cracks are found after the co-sintering and there is a clear interface between the two layers. The cross sections of the outer (Figure 4.5 c-I) and the inner (Figure 4.5 d-I) layers, as well as the inner surface (Figure 4.5 f-I), are densified, although dead-end pores are observed on the outer surface (Figure 4.5 e-I). No obvious micro-structural changes in the outer layer are found when NiO in the inner layer was reduced into Ni (Figure 4.5 a, b, c-II and e-II), indicating great material stability in reducing atmosphere. While the cross-section (Figure 4.5 d-II) and the inner surface (Figure 4.5 f-II) of the inner layer turn into a highly porous structure after reduction. In addition, the porous structure formed as a result of the reduction is highly inter-connected in the inner layer, which provides a high catalytic surface area in the resultant DL-HFMR for methane conversion.



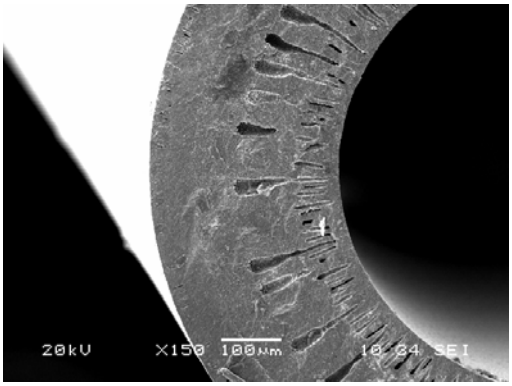
(a-I)



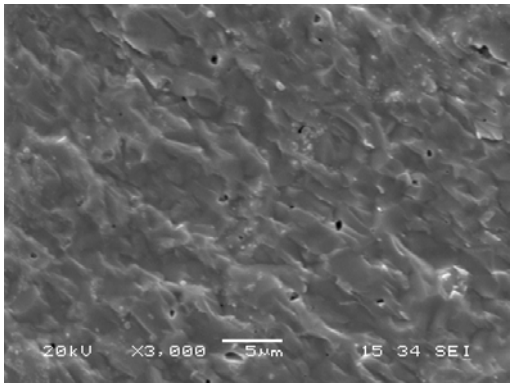
(a-II)



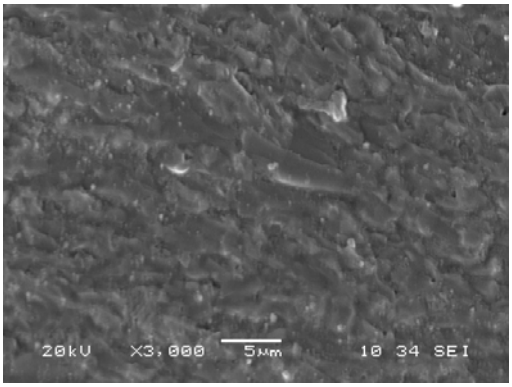
(b-I)



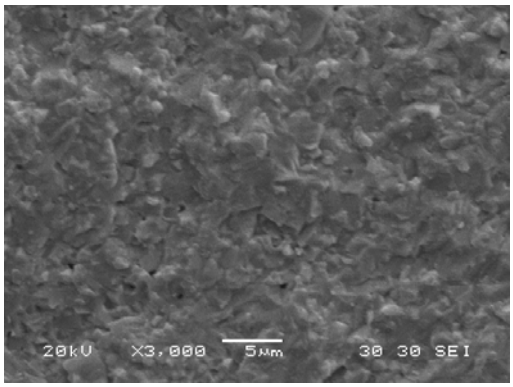
(b-II)



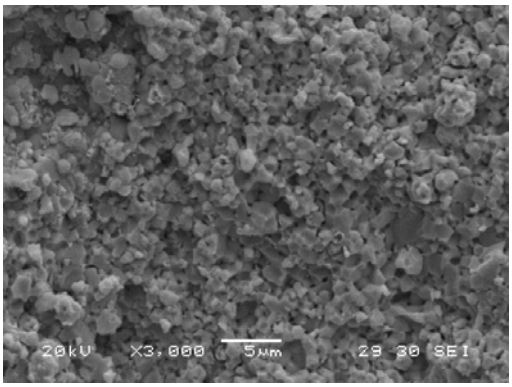
(c-I)



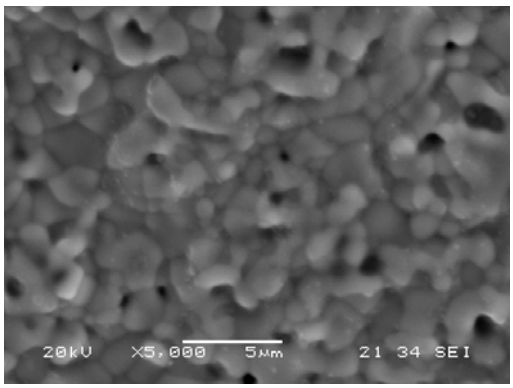
(c-II)



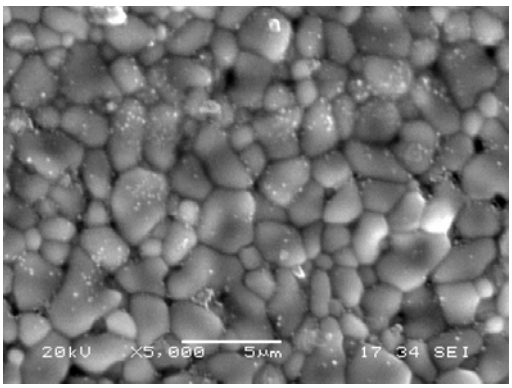
(d-I)



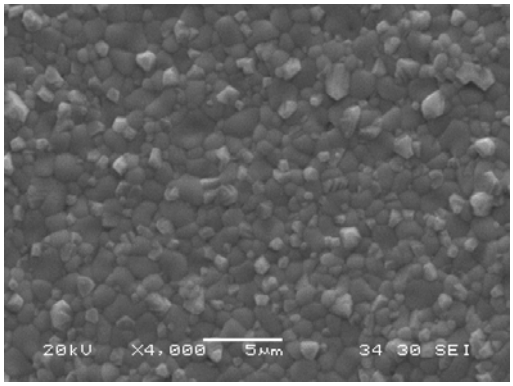
(d-II)



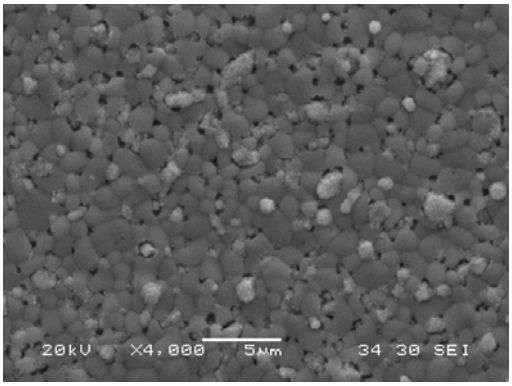
(e-I)



(e-II)



(f-I)



(f-II)

Figure 4.5 SEM images of dual-layer hollow fibres after co-sintering (I) and after reduction (II), (a) whole view, (b) cross section, (c) outer layer cross section, (d) inner layer cross section, (e) outer layer surface, (f) inner layer surface

4.4.4 DL-HFMR for methane conversion

The developed dual-layer hollow fibre membranes are then directly used as a membrane reactor for methane conversion using the experimental setting-up shown in Figure 4.2. Prior to the reaction, NiO in the inner layer was reduced into Ni at 550 °C for 30 min using a hydrogen stream of 20ml/min. The reduced inner layer shows great catalytic activity to methane conversion. As shown in Figure 4.6, an initial methane conversion of around 78.94% can be achieved at 750 °C after 10 min of the reaction. However, methane conversion drops to 12.75% within one hour of operation. This is in good agreement with the report of Yin et. al. [5], in which a mixture of NiO and YSZ-8 (1:1 by weight) was used as the catalyst for POM reaction. The reason for the drop of methane conversion was considered as a consequence of coke accumulation on Ni(0) grain surface, which hindered the access of methane to catalyst [5], and this explanation was proved by XRD analysis [4]. Figure 4.6

further indicates that, after 20 min of reaction at 750 °C, CO selectivity increases with the reaction time while the value of H_2/CO ratio is slightly affected and is stabilized at about 3.5.

After one hour of reaction at 750 °C, the reactant stream was switched to argon of 20 ml·min^{-1} for 30 min, after which the argon was switched back to the reactant stream. In the mean time, the operating temperature was increased to 800, 850, 900 and 950 °C, respectively with a heating rate of 5 °C/min. Only CO is detectable in the product stream when the stream of methane is switched to argon, which indicates the removal of coke by the permeated oxygen, agreeing well with the work of Yin et. al. [4, 5]. In addition, only trace amount of nitrogen of approximately 1.4×10^{-4} ml·cm^{-2}·s^{-1} can be detected in the product stream of the DL-HFMR during the reaction, further proving the great membrane integrity at high temperatures.

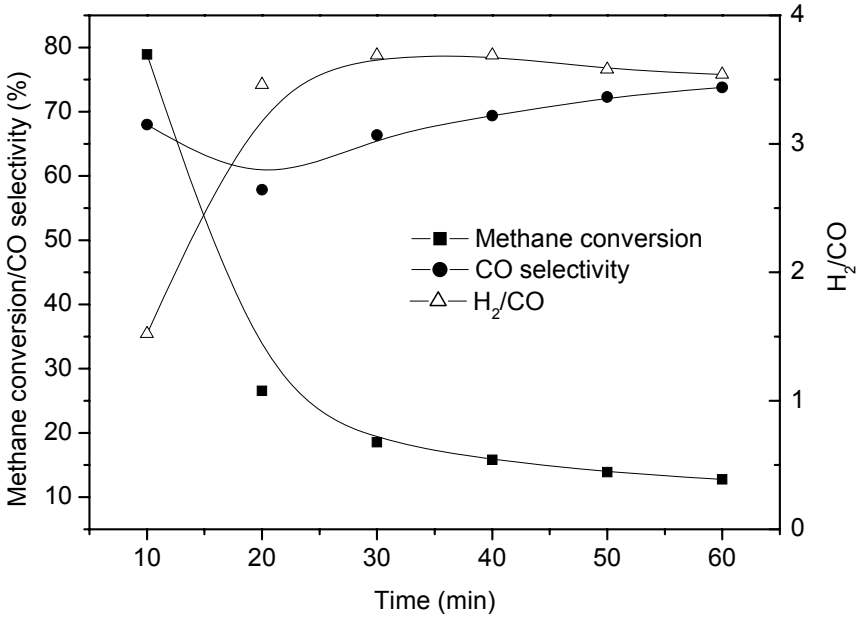


Figure 4.6 The time dependent performance of DL-HFMR at 750°C

As can be seen in Figure 4.7, methane conversion and CO selectivity increase with increasing temperatures between 800 °C and 950 °C. At the same temperature, methane conversion drops sharply from a high initial value and stabilizes within 1 hour of reaction, while CO selectivity increases with the reaction time, which is similar to the trend at 750 °C. A sudden increase in CO selectivity is observed at 40 min of reaction when the temperature is above 850 °C, the reason of which is still under investigation and may be related to the consuming of coke accumulated on the inner layer during the reaction. At 950 °C, the stabilized methane conversion and CO selectivity are 35.54% and 91.98%, respectively.

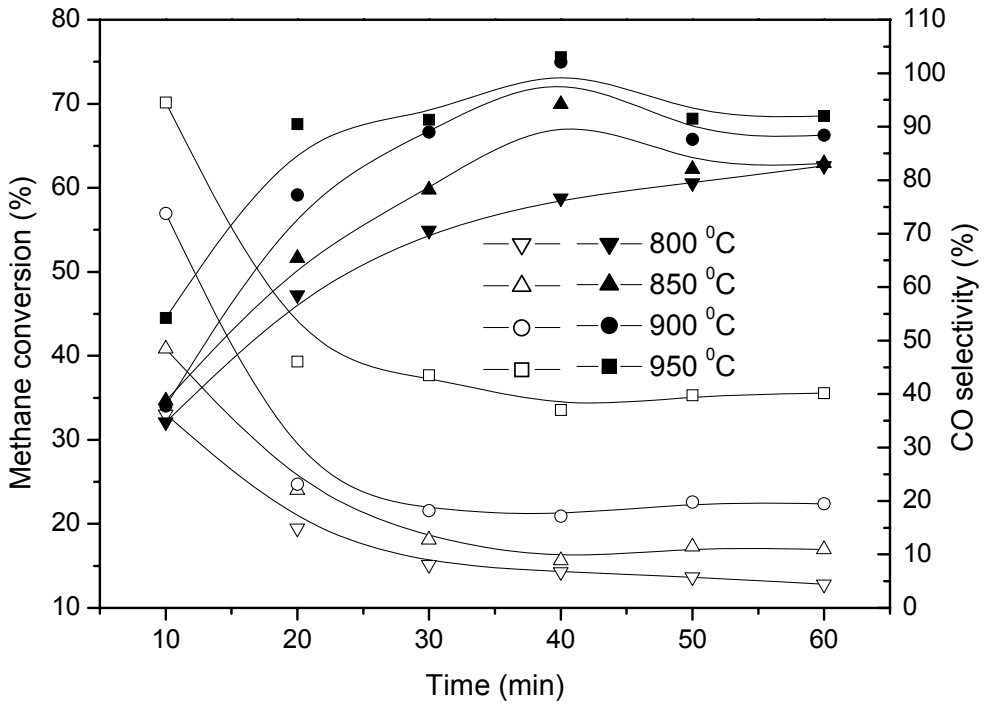


Figure 4.7 The time dependent methane conversion (open symbols) and CO selectivity (solid symbols) of DL-HFMR between 800-950°C

With the increasing temperatures, as can be seen in Figure 4.8, the oxygen permeation rate increases while H_2/CO ratio decreases. At the same temperature, the oxygen permeation rate slightly changes with the reaction time while H_2/CO ratio decreases and is finally stable at a certain value in 1 hour of operation between 800 °C and 900 °C. In contrast, the value of H_2/CO ratio at 950 °C is less dependent on the reaction time and is stable at around 2, although there is a sharp drop of methane conversion after 10 min of reaction at this temperature as well (Figure 4.7).

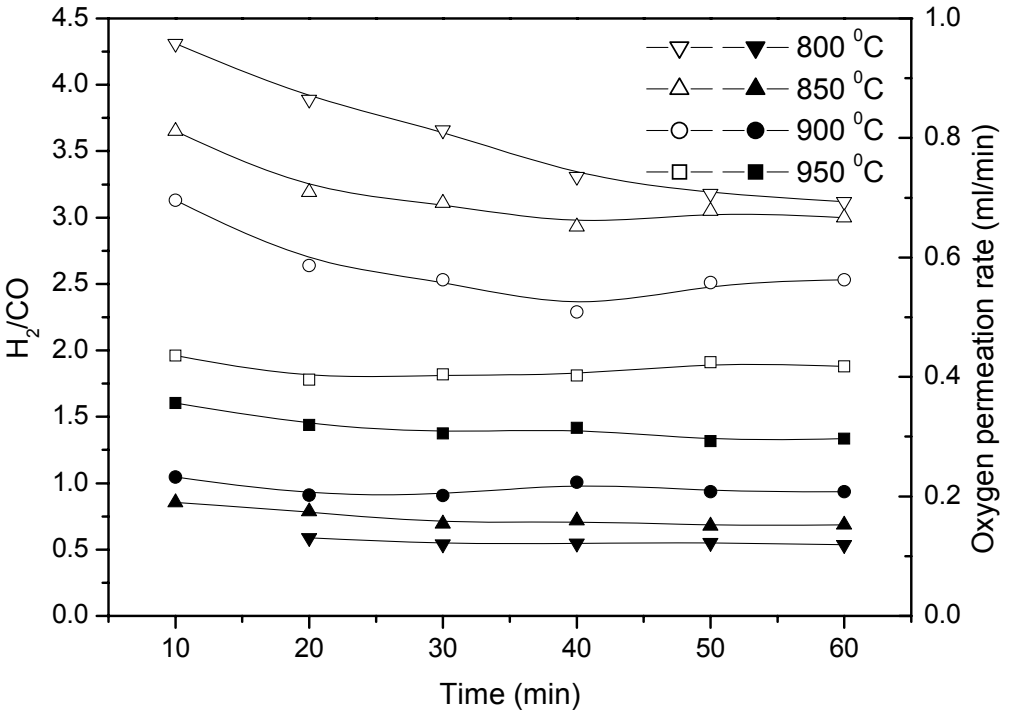


Figure 4.8 The time dependent H_2/CO (open symbols) and oxygen permeation rate (solid symbols) of DL-HFMR between 800-950°C

It has been reported that the coke deposition rate on Ni-YSZ increases with the increasing temperatures [25], which is in line with the bigger drop of methane conversion at higher temperatures shown in Figure 4.7. However,

higher oxygen permeation rate through the LSM-YSZ outer layer at elevated temperatures contributes to increase the methane conversion, CO selectivity and result in a H_2/CO ratio closer to the value of 2. As a result, less coking on the inner catalytic support layer and higher oxygen permeation rate of the outer oxygen separation layer are helpful in further improving the performance of the DL-HFMR for methane conversion, which can be achieved by replacing Ni-YSZ with more coking-resistant materials and further reducing the thickness of the outer layer by using the same membrane fabrication process, respectively. Moreover, the generic advantages of the single-step co-extrusion and co-sintering technique and the design of the DL-HFMR have been proved and can be applied to the fabrication of micro-tubular solid oxide fuel cell (SOFC) and chemical productions.

4.5 Conclusions

A highly compact multifunctional ceramic hollow fibre membrane reactor with a unique dual-layer structure (DL-HFMR) has been developed for partial oxidation of methane (POM), using a single-step co-extrusion and co-sintering technique. The developed DL-HFMR with great mechanical strength of 291 MPa is composed of two layers. The outer oxygen separation layer of approximately 75.0 μm is made of 40 vol% $La_{0.8}Sr_{0.2}MnO_{3-\delta}$ (LSM) and 60 vol% yttria-stabilized zirconia (YSZ), while the inner support layer consists of NiO (30 vol.%) and YSZ (70 vol.%). After reducing NiO into Ni, the inner layer turns into a highly porous structure and is catalytic active to the reactions for methane conversions, such as partial oxidation of methane (POM) to syngas. Benefiting from this membrane reactor design as well as the single-step

membrane fabrication technique, a surface area/volume ratio of approximately 2769.7 m^2/m^3 can be achieved with a great adhesion between the separation and catalytic support layers. With the increasing operating temperatures, methane conversion and CO selectivity increase while H_2/CO ratio decreases, as a result of increased oxygen permeation rate. CO selectivity over 90% with a H_2/CO ratio of about 2 can be obtained at 950 °C. Although coke formation during the reaction greatly affects methane conversion, the catalytic activity of the inner layer can be easily recovered by periodically switching between the reaction stream and the sweep gas. And the performance of the DL-HFMR can be further improved by reducing the thickness of the oxygen separation layer and using more coking-resistant materials for the inner layer.

Reference

1. X.F. Chang, C. Zhang, W.Q. Jin, N.P. Xu, Match of thermal performances between the membrane and the support for supported dense mixed-conducting membranes, Journal of Membrane Science, 285 (2006) 232-238.
2. X.L. Dong, C. Zhang, X.F. Chang, W.Q. Jin, N.P. Xu, A self-catalytic membrane reactor based on a supported mixed-conducting membrane, Aiche Journal, 54 (2008) 1678-1680.

3. W.Q. Jin, S.G. Li, P. Huang, N.P. Xu, J. Shi, Preparation of an asymmetric perovskite-type membrane and its oxygen permeability, Journal of Membrane Science, 185 (2001) 237-243.
4. X. Yin, L. Hong, Z.L. Liu, Asymmetric tubular oxygen-permeable ceramic membrane reactor for partial oxidation of methane, Journal of Physical Chemistry C, 111 (2007) 9194-9202.
5. X. Yin, L. Hong, Z.L. Liu, Integrating air separation with partial oxidation of methane - A novel configuration of asymmetric tubular ceramic membrane reactor, Journal of Membrane Science, 311 (2008) 89-97.
6. K. Li, *Ceramic Membranes for Separation and Reaction*. 2007: Wiley.
7. H.J.M. Bouwmeester, Dense ceramic membranes for methane conversion, Catalysis Today, 82 (2003) 141-150.
8. U. Balachandran, J.T. Dusek, P.S. Maiya, B. Ma, R.L. Mieville, M.S. Kleefisch, C.A. Udovich, T.H. Fleisch, A.C. Bose, Development of dense ceramic membranes for methane conversion, Natural Gas Conversion Iv, 107 (1997) 409-414.
9. Y.Y. Liu, X.Y. Tan, K. Li, Mixed conducting ceramics for catalytic membrane processing, Catalysis Reviews-Science and Engineering, 48 (2006) 145-198.
10. A. Thursfield, I.S. Metcalfe, The use of dense mixed ionic and electronic conducting membranes for chemical production, Journal of Materials Chemistry, 14 (2004) 2475-2485.
11. J. Sunarso, S. Baumann, J.M. Serra, W.A. Meulenberg, S. Liu, Y.S. Lin, J.C.D. da Costa, Mixed ionic-electronic conducting (MIEC) ceramic-based

membranes for oxygen separation, Journal of Membrane Science, 320 (2008) 13-41.

12. X.Y. Tan, S.M. Liu, K. Li, Preparation and characterization of inorganic hollow fiber membranes, Journal of Membrane Science, 188 (2001) 87-95.
13. X.Y. Tan, K. Li, Oxygen production using dense ceramic hollow fiber membrane modules with different operating modes, Aiche Journal, 53 (2007) 838-845.
14. X.Y. Tan, Z.B. Pang, K. Li, Oxygen production using La0.6Sr0.4Co0.2Fe0.8O3-alpha (LSCF) perovskite hollow fibre membrane modules, Journal of Membrane Science, 310 (2008) 550-556.
15. Z.H. Chen, Z.P. Shao, R. Ran, W. Zhou, P.Y. Zeng, S.M. Liu, A dense oxygen separation membrane with a layered morphologic structure, Journal of Membrane Science, 300 (2007) 182-190.
16. K. Scott, R. Hughes, *Industrial membrane separation technology*. 1st edn. ed. 1996: Blackie Academic and Professional, Chapman and Hall.
17. B.C.H. Steele, A. Heinzel, Materials for fuel-cell technologies, Nature, 414 (2001) 345-352.
18. N.Q. Minh, Ceramic Fuel-Cells, Journal of the American Ceramic Society, 76 (1993) 563-588.
19. W. Li, J.J. Liu, C.S. Chen, Hollow fiber membrane of yttrium-stabilized zirconia and strontium-doped lanthanum manganite dual-phase composite for oxygen separation, Journal of Membrane Science, 340 (2009) 266-271.
20. H.X. You, A. Abuliti, X.W. Ding, Y.H. Zhou, Reactions of low and middle concentration dry methane over Ni/YSZ anode of solid oxide fuel cell, Journal of Power Sources, 165 (2007) 722-727.

21. N. Droushiotis, M.H.D. Othman, U. Doraswami, Z.T. Wu, G. Kelsall, K. Li, Novel co-extruded electrolyte-anode hollow fibres for solid oxide fuel cells, Electrochemistry Communications, 11 (2009) 1799-1802.

22. S.M. Liu, X.Y. Tan, K. Li, R. Hughes, Preparation and characterisation of SrCe0.95Yb0.05O2.975 hollow fibre membranes, Journal of Membrane Science, 193 (2001) 249-260.

23. B.F.K. Kingsbury, K. Li, A morphological study of ceramic hollow fibre membranes, Journal of Membrane Science, 328 (2009) 134-140.

24. C.C. Wei, K. Li, Yttria-stabilized zirconia (YSZ)-based hollow fiber solid oxide fuel cells, Industrial & Engineering Chemistry Research, 47 (2008) 1506-1512.

25. K. Ke, A. Gunji, H. Mori, S. Tsuchida, H. Takahashi, K. Ukai, Y. Mizutani, H. Sumi, M. Yokoyama, K. Waki, Effect of oxide on carbon deposition behavior of CH4 fuel on Ni/ScSZ cermet anode in hihh temperature SOFCs, Solid State Ionics, 177 (2006) 541-547.

Chapter 5

Functional LSM-ScSZ/NiO-ScSZ Dual-Layer Hollow Fibres for Partial Oxidation of Methane

Abstract

It has been proved in Chapter 4 that higher oxygen permeation is critically important to a better dual-layer hollow fibre membrane reactor (DL-HFMR) for methane conversion, although coke formation on the Ni-based inner catalytic substrate layer leads to the degradation of catalytic activity and stability. As a result, in this chapter, Scandia -Stabilized-Zirconia (ScSZ) is employed to replace YSZ to develop another functional $La_{0.80}Sr_{0.20}MnO_{3-\delta}$ (LSM)-ScSZ/NiO-ScSZ dual-layer hollow fibre for methane conversion, by using the same single-step co-extrusion and co-sintering process. In contrast to YSZ, the ionic conductivity of ScSZ is higher, which not only contributes to increase oxygen permeation of the outer oxygen separation layer, but also improve catalytic activity and stability of the inner substrate layer. Moreover, ScSZ is stronger than YSZ, which improves the mechanical strength of the membrane reactor. And by comparing with the DL-HFMR-YSZ in Chapter 4, the controlling step of such membrane reactor design is also outlined.

Key words: Dual-layer hollow fibre, co-extrusion and co-sintering, membrane reactor, POM

5.1 Introduction

Use of membrane reactor for partial oxidation of methane (POM) is of great importance, and has been widely studied in respect of catalysis [1, 2], membrane separation [3] and simulation [4, 5] etc.. Based on Chapter 3 and Chapter 4, a clearer picture of ceramic dual-layer hollow fibre membrane reactor (DL-HFMR) for methane conversion can be generated and is shown in Figure 5.1.

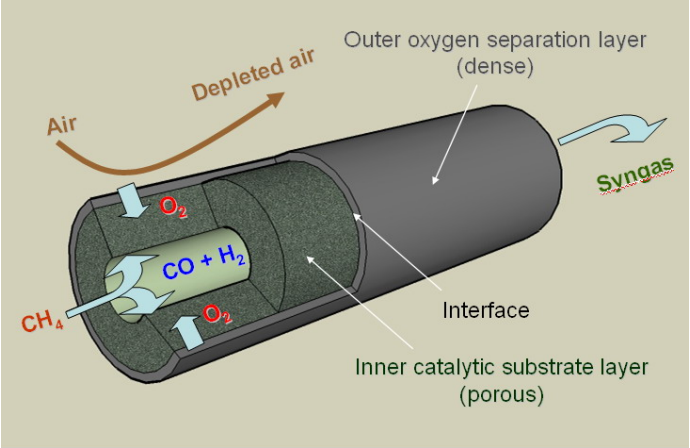


Figure 5.1 Schematic diagram of a dual-layer membrane reactor for methane conversion

Oxygen in ambient air permeates through a fully densified outer separation layer and reacts with methane on another highly porous inner catalytic substrate layer, forming syngas as the product. The reactor design of this type shows a number of advantages, such as (1) high surface area/volume ratio when compared to a conventional flat sheet/tubular reactor design, in which additional catalyst has to be packed, (2) less challenges in high temperature sealing and (3) adjustable membrane morphologies. Chapter 3 and Chapter 4

also answer two questions about DL-HFMR, which are how to fabricate high quality dual-layer ceramic hollow fibres and how to functionalize each layer for a simultaneous oxygen separation and partial oxidation of methane, respectively. Based on the results in Chapter 4, the use of dual-phase membrane materials can easily functionalize each membrane layer, and higher oxygen permeation and less coke formation are critically important to a better membrane reactor performance. Higher oxygen permeation through the outer layer, which is made of separate ionic conducting and electronic conducting phases, can be achieved by increasing the conductivity. As can be seen in Figure 5.2, Scandia -Stabilized-Zirconia (ScSZ) is of higher ionic conductivity than YSZ [6], as well as better mechanical property, and can thus be used to replace YSZ in order for higher oxygen permeation of the outer oxygen separation layer and better coking-resistance of the inner catalytic substrate layer [7, 8].

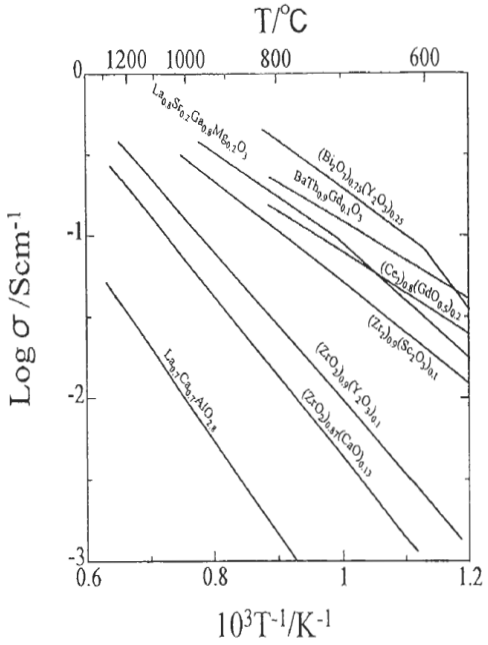


Figure 5.2 Temperature dependence of electrical conductivity for selected oxide ion conductors [6]

5.1.1 Objectives

As a result, this chapter mainly focuses on the optimization of membrane materials, i.e. replacing YSZ by ScSZ with better ionic conductivity and coking resistance to methane conversion [7, 8], and its effects on the membrane fabrication and reactor performance. The specific objectives are listed below:

1. Optimizing the membrane material compositions of both outer and inner layers, in order for a successful co-sintering of the dual-layer hollow fibre membranes.
2. Fabricating the dual-layer hollow fibre membranes and investigating the key factors that affect the adhesion between the two layers at high operating temperatures.
3. Investigating the performance of the DL-HFMR for methane conversion, including reactant conversion, product selectivity and coke formation.
4. Comparing with the reactor in Chapter 4, in order to outline the controlling step of the DL-HFMR of this type.

5.2 Background

For the functional ceramic dual-layer hollow fibre membranes to be used as a compact membrane reactor design for methane conversion, membrane material and membrane fabrication are the two highly interactive factors that co-determine the performance of the resultant membrane reactor. Due to the use of dual-phase materials to functionalize dual-layer fibres, the selection and composition of membrane materials greatly affects the co-sintering behaviour as well as performances of the developed membranes. Taking the

dual-layer hollow fibre of LSM-ScSZ/NiO-ScSZ to be prepared in this chapter as an example, as illustrated in Figure 5.3, the ratio between LSM, an electronic conducting phase, and ScSZ, an ionic conducting phase, determines oxygen permeation as well as sintering behavior of the outer layer, while the ratio between NiO and ScSZ in the inner catalytic substrate layer determines, not only the sintering behavior that has to be matched with the outer layer, but also its catalytic activity and stability, porosity and coking resistance during the actual reactions, when NiO is reduced to Ni.

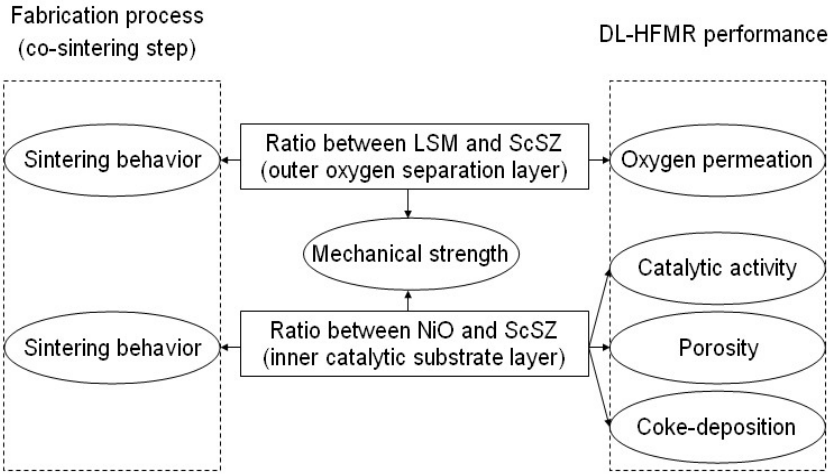


Figure 5.3 Effects of membrane material on fabrication process and reactor performance

Generally, use of more NiO increases porosity of the inner layer after the reduction of NiO, which facilitates the mass transfer of reactants and products but at the cost of mechanical strength as well as coking resistance of the inner layer [8]. Also, for this type of membrane reactor design in which the oxygen separation layer acts as a “distributor” supplying permeated oxygen to the reaction zone, reactor performance is affected by the “balance” between the

oxygen permeation/distribution and the catalytic reaction. Insufficient oxygen permeation would limit methane conversion, while excessive supply of oxygen would lead to a deeper oxidation of methane and even re-oxidization of Ni to NiO that changes catalytic activity of the catalyst layer. All these indicate the importance of membrane materials to the development of the dual-layer hollow fibre membranes made of dual-phase materials, such as LSM-ScSZ/NiO-ScSZ.

5.3 Experimental

5.3.1 Materials

$La_{0.80}Sr_{0.20}MnO_{3-\delta}$ (LSM, 5.8 m^2/g), NiO (5.2 m^2/g) and scandia(10%)-stabilized-zirconia (ScSZ, 9.4 m^2/g) were used as supplied (NexTech Materials Ltd). Polyethersulfone, (PESf, Radel A-300, Ameco Performance, USA), Dimethyl Sulfoxide (DMSO, Sigma, >99.5%) and Arlacel P135 (Uniqema, UK) were used as polymer binder, solvent and additive, respectively. DI water and tap water were used as the internal and the external coagulants, respectively, when fabricating the dual-layer hollow fibres.

5.3.2 Determination of membrane material compositions

The outer oxygen permeation layer consisted of 40 vol. % of LSM as an electronic conducting phase and 60 vol. % of ScSZ as an ionic conducting phase, while the inner catalytic substrate was made of a mixture of NiO and ScSZ. Besides catalytic activity/stability, porosity and mechanical strength, the ratio between NiO and ScSZ is the determining factor for the successful co-

sintering of the dual-layer hollow fibres. As a result, dilatometer (Netzsch, model DIL 402C) was employed to investigate the effects of material composition on its sintering behaviour that has to be matched with the outer counterpart.

5.3.3 Fabrication of LSM-ScSZ/NiO-ScSZ dual-layer hollow fibres

The preparation of spinning suspensions, the co-extrusion process and the triple-orifice spinneret used to fabricate dual-layer hollow fibre precursors have been described elsewhere [9]. The spinning parameters are listed in Table 5.1.

Table 5.1 Compositions of spinning suspensions and co-extrusion parameters

	Suspension compositions	
	Outer oxygen separation layer (wt.%)	Inner catalytic substrate layer (wt.%)
Ceramics	65.0	68.0
DMSO	28.0	24.7
PESf	6.5	6.8
Additive	0.5	0.5
	Co-extrusion parameters	
	Outer layer suspension	Inner layer suspension
Extrusion rate (ml/min)	5.0	8.0
Temperature (°C)	20	
Air gap (cm)	26	
Internal coagulant (ml/min)	10	

The formed precursor fibres were cut into the required length, dried and straightened, and finally co-sintered at 1400 °C for 5 h, with heating rates of 5-10 °C/min and cooling rate of,. 3 °C/min.

5.3.4 Characterizations of dual-layer hollow fibres

X-ray diffraction (XRD) was used to investigate the compatibility between membrane materials. Morphology and microstructure of the developed dual-layer hollow fibres were visually observed using a scanning electron microscope (SEM, JEOL JSM-5610LV, Tokyo, Japan). Sintering behaviours of inner and outer layer materials were investigated by using a dilatometer (Netzsch, model DIL 402C) from room temperature to 1400-1450 °C, with a heating rate of 5 °C/min.

5.3.5 Partial oxidation of methane

The developed LSM-ScSZ/NiO-ScSZ dual-layer hollow fibres were directly used as a membrane reactor for methane conversion, by using an experimental set-up described elsewhere [9]. Before the reaction, the furnace was heated up from room temperature to 800 °C at a heating rate of 5 °C/min, with a continuous flow of Ar (20 ml/min) in the lumen. NiO in the inner layer was then reduced into Ni by a H_2/Ar (1:1) stream of 20 ml/min for 30 min, after which the reactant stream was introduced into the reactor. Ambient air was used as the source of oxygen. The flow rate of the reactant (10% CH_4/Ar, 20 ml/min) was controlled by a mass flow controller. As shown in Figure 5.1, methane reacts with the permeated oxygen on the highly porous inner layer,

and is converted into syngas (H_2 + CO) as the product. The product stream was on-line analysed by GC (Unicam 610 and Varian 3900). Methane conversion (X_{CH4}, %), CO selectivity ($S_{CO,}$ %) and S_C (%) indicating the methane converted into coke and possibly tiny amounts of C2 products were calculated by the following equations, while oxygen permeation rate (F_{O2}, ml/min) was calculated based on the mass balances of oxygen.

$$X_{CH_4} = \frac{F_{CH_4 inlet} - F_{CH_4 outlet}}{F_{CH_4 inlet}} \times 100\% \quad (5\text{-}1)$$

$$S_{CO} = \frac{F_{CO}}{F_{CO} + F_{CO_2}} \times 100\% \quad (5\text{-}2)$$

$$S_c = (1 - \frac{F_{CO} + F_{CO_2}}{F_{CH_4 inlet} - F_{CH_4 outlet}}) \times 100\% \quad (5\text{-}3)$$

5.4 Results and discussion

5.4.1 Compatibility of membrane materials

Since the functionalized dual-layer ceramic hollow fibres are achieved by using dual-phase membrane materials, good material compatibility is the prerequisite for both successful membrane functionalization and great membrane integrity. Although LSM, NiO and ScSZ are stable individually, corresponding mixtures may lead to the formation of impurity phases at high temperatures due to solid state reactions, and consequently affect membrane functions.

Figure 5.4 shows XRD results of LSM-ScSZ and NiO-ScSZ (1:1 by weight ratio) sintered at 1450 °C for 6 h in static air. In accordance with Hagiwara's report [10], a very small amount of $La_2Zr_2O_7$ impurity phase identified by the tiny peaks at 2θ = 28.6° and 47.5° was found in LSM-ScSZ. Although it seems to be unavoidable for the formation of this $La_2Zr_2O_7$ phase in presence of La and Zr [10], such a low level of impurity phase would not significantly affect material functions, as suggested by Hagiwara etc. [10]. In contrast, the mixture of NiO-ScSZ shows a better material compatibility as no detectable impurity phase was observed.

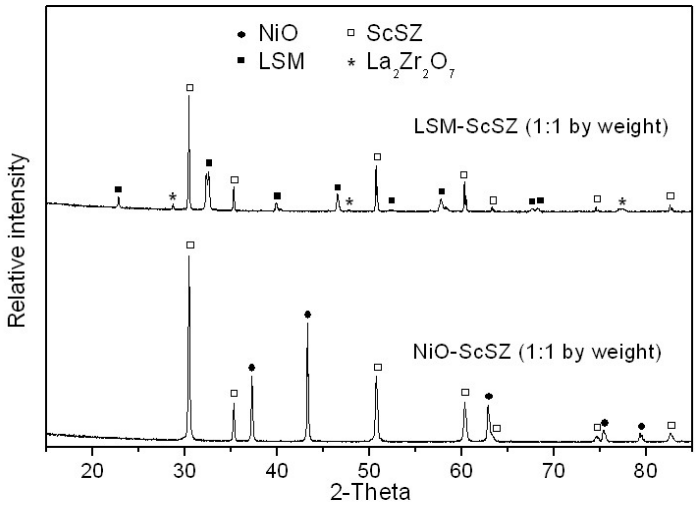


Figure 5.4 XRD patterns of LSM-ScSZ and NiO-ScSZ (1:1 by weight ratio) sintered at 1450 °C for 6 h

5.4.2 Adhesion between the separation and the catalytic layers

For a composite ceramic membrane where a thin top layer for separation is supported on a porous substrate, great adhesion between the two layers is critically important to membrane performance, especially when the two layers

are made of different ceramic materials and operated at high temperatures [11, 12].

With regards to the single-step co-extrusion and co-sintering fabrication process, ceramic particles of the two different layers are first dispersed separately in a mixture containing solvent, additive and polymer binder to form two uniform spinning suspensions [13]. The two suspensions are then co-extruded through a triple-orifice spinneret into an external coagulation bath (non-solvent), with a stream of internal coagulant (non-solvent) flowing through the central bore at the same time [9, 14-16]. The solvent-non-solvent exchange results in the precipitation of polymer binder [17], which not only forms an organic matrix holding ceramic particles in the precursor fibres, but also tightly binds the two layers together, as shown in Figure 5.5. As long as the spinning suspensions are made of same or similar solvent, additive and polymer binder, and possess comparable properties such as viscosity and how viscosity changes during the phase inversion process, this organic matrix should be a uniform and continuous phase throughout the fibre. This indicates that the contact between ScSZ particles packed in the inner and outer layers of precursor fibres are same as the one at the boundary. As a result, when the polymer binder is removed due to the high temperature co-sintering, a continuous ScSZ phase for high temperature applications can be formed throughout the fibre, forming a strong inorganic matrix binding the two layers together. Moreover, this continuous inorganic matrix helps to buffer the impacts of different thermal expansions when the two layers are made of different materials. The reduction of NiO in the inner layer into Ni would not

affect the integrity of the ScSZ phase, and turns the inner layer into a highly porous structure that facilitates the access of the reactant and diffusion of the products.

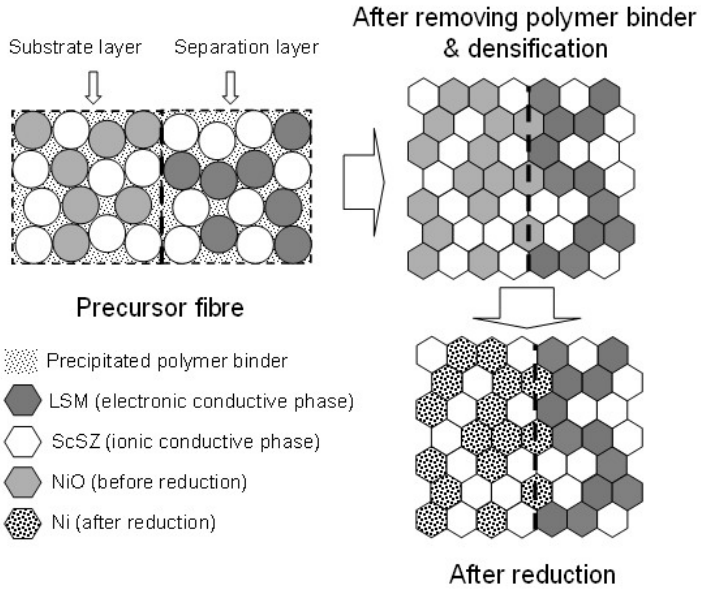
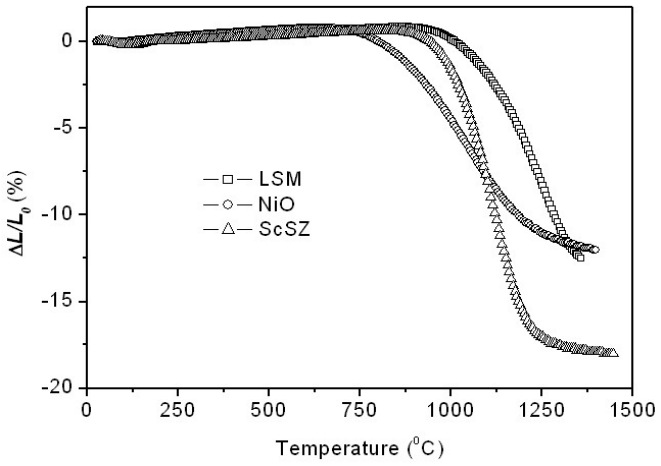


Figure 5.5 Schematic diagram of forming great adhesion between the two layers of LSM-ScSZ/NiO-ScSZ

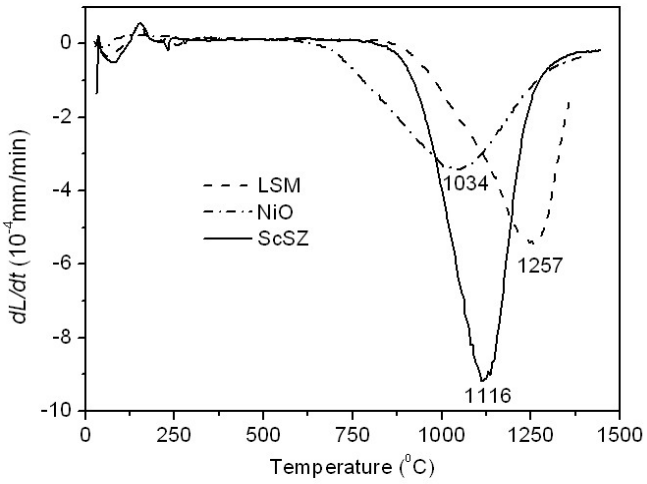
5.4.3 Sintering behaviour of membrane materials

In order to deliver a clearer picture of sintering behaviours of dual-phase membrane materials, the one of LSM, NiO and ScSZ was investigated first and is shown in Figure 5.6. As can be seen in Figure 5.6 (a), final shrinkages of these ceramics at around 1400 °C decreases in the order of ScSZ, LSM and NiO, while the temperature for the initial shrinking to occur increases in the order of NiO, ScSZ and LSM. Moreover, the temperature for the highest sintering rates of these ceramics increases in the order of NiO (1034 °C),

ScSZ (1116 °C) and LSM (1257 °C), as shown in Figure 5.6 (b), while the highest sintering rate decreases in the order of ScSZ, LSM and NiO.



(a)



(b)

Figure 5.6 Dilatometric curves of LSM, NiO and ScSZ (a) sintering curves and (b) sintering rate curves

As can also be seen in Figure 5.6, the sintering behaviours of each membrane material is quite different from each other, which is actually the case for most

of the single-phase MIEC materials with perovskite or perovskite-related structures. This is also one of the major reasons that little successful fabrications of dual-layer ceramic membranes by using the single-phase ceramics in each layer have been achieved.

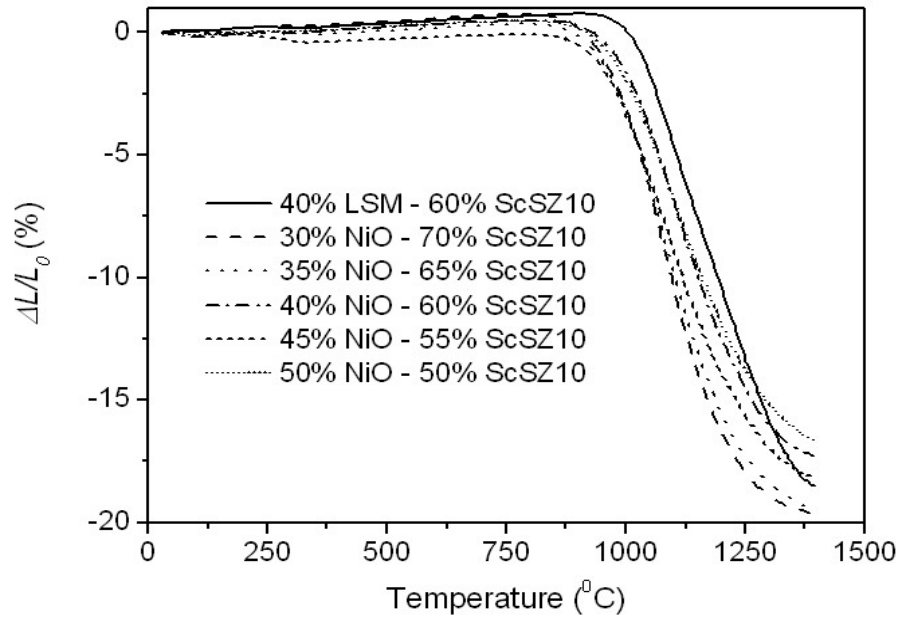
However, the sintering behaviours of dual-phase materials are not a simple sum of each individual phase, because grain boundaries are also formed between different phases. This changes the way that the overall dual-phase materials shrinks and indicates that there is an interaction between different phases during high temperature sintering that can be dependent on a number of factors such as the ratio between different phases, particles size and particle shape, etc.. The overall sintering process of dual-phase materials can be quite complex and is beyond the scope of this chapter. Therefore, dilatometric curves of dual-phase membrane materials, i.e. a mixture of 40 vol. % LSM and 60 vol. % ScSZ for the outer layer and the mixtures made of NiO and ScSZ with volumetric ratios varied from 30/70 to 50/50 for the inner layer are presented in Figure 5.7, mainly for the purpose of selecting a suitable inner layer material composition that can match with the sintering behaviour of the outer layer, in order for a successful co-sintering.

As can be seen in Figure 5.7 (a), LSM-ScSZ starts to shrink at a temperature higher than that of NiO-ScSZ. Final shrinkage of NiO-ScSZ decreases with the increasing amounts of NiO, in agreement with the trend shown in Figure 5.6 (a), except for the sample with 45 vol. % of NiO. LSM-ScSZ shows two

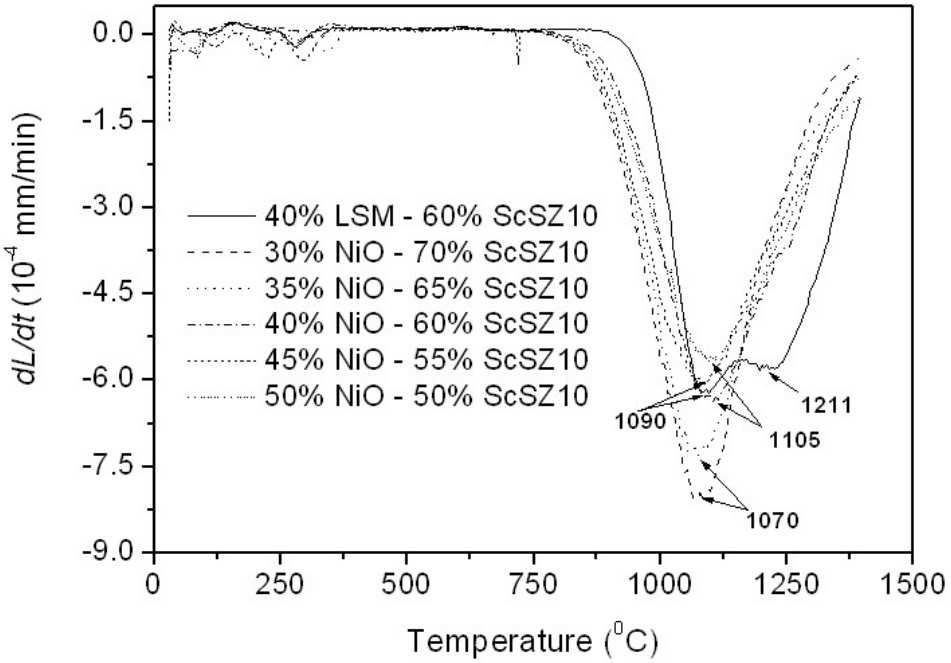
sintering rate peaks at 1090 and 1211 °C, respectively, as shown in Figure 5.7 (b), which may indicate a “separate” sintering of ScSZ and LSM phases possibly due to the big gap between the corresponding temperatures where the highest sintering rates occur for ScSZ and LSM (Figure 5.6 (b)). In contrast, NiO-ScSZ shows only one sintering rate peak, maybe due to the wide sintering rate peak of NiO (Figure 5.6 (b)), that gradually shifts towards higher temperatures with the increasing amounts of NiO, except for the 45 vol. % of NiO. Moreover, the maximum sintering rate decreases with the increasing amounts of NiO, which is also in agreement with Figure 5.6 (b).

Although the reason for the special sintering behaviour of 45 vol. % NiO - 55 vol. % ScSZ, which was repeated several times, is yet clear, it should be considered as the composition of inner layer material because the final shrinkage, the maximum sintering rate and the temperature of the highest sintering rate are almost same as the 40% LSM - 60 % ScSZ outer layer (Figure 5.7). And all these parameters are critically important in avoiding or minimizing crack formation during the co-sintering of dual-layer fibres with quite high surface curvature. However, the fibres of such inner layer material composition can hardly survive the operation conditions of the reaction, due to crack formation near to the edge of the heating zone where insulator (quartz wool) is positioned, even if such membrane material composition guarantees great membrane integrity after co-sintering. The reason for such crack formation is considered as the substantial temperature gradient across the insulation, as well as the different thermal conductivities between the two

layers when there is a high concentration of NiO in the inner layer, leading to a significant temperature difference within the fibres.



(a)



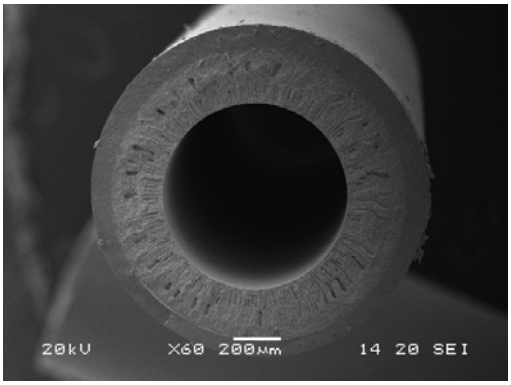
(b)

Figure 5.7 Dilatometric curves of LSM-ScSZ and NiO-ScSZ (a) sintering curves and (b) sintering rate curves

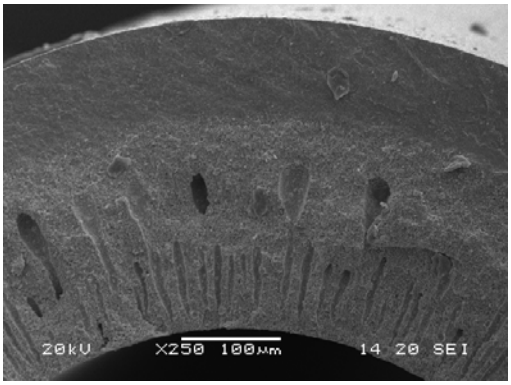
As the result, 35% vol. NiO - 65% vol. ScSZ was used as the inner layer material. And in order to overcome the possible impacts of the different sintering behaviour to 40% LSM - 60 % ScSZ outer layer during the co-sintering step, a fast heating rate of 10 °C /min was used between 600 °C and 1400 °C. Below 600 °C, when no obvious sintering occurs to both the inner and the outer layer materials, lower heating rates of 1 to 2 °C/min can be used for a full removal of organic phases in precursor fibres in a slower way, in order to avoid additional structural defects.

5.4.4 Morphology and microstructure of LSM-ScSZ/Ni-ScSZ

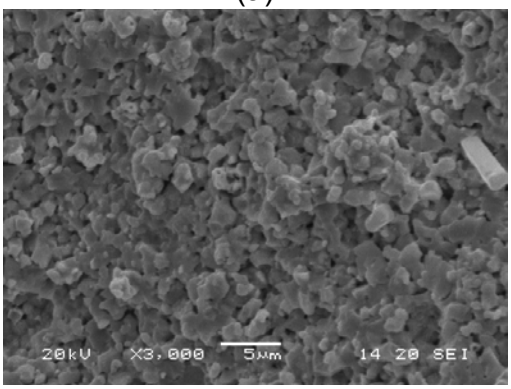
After co-sintering and reduction, LSM-ScSZ/Ni-ScSZ consists of a dense oxygen separation layer of approximately 109.2 μm supported on an asymmetric porous catalytic substrate, as shown in Figures 5.8 (a) and (b). OD and ID of the fibre were measured to be 1419.4 and 780.6 μm, respectively. Finger-like voids in the inner layer are formed during the co-extrusion step as the result of viscous fingering phenomena [17] and are conserved after co-sintering and reduction. The inner layer shows a highly porous structure when NiO is reduced into Ni (Figure 5.8 (c)), while the outer layer remains a fully dense structure (Figure 5.8 (d)). The two layers are tightly bound together without noticeable gaps in between (Figure 5.8 (e)), indicating great adhesion between the two layers. A clear porous structure can also be observed on the inner surface (Figure 5.8 (f)), while the outer counterpart is fully dense except for a number of small non-permeable cavities (Figure 5.8 (g)).



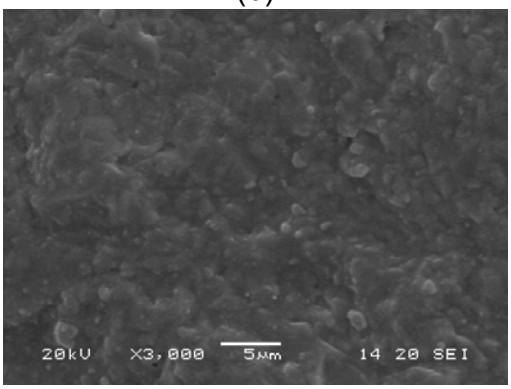
(a)



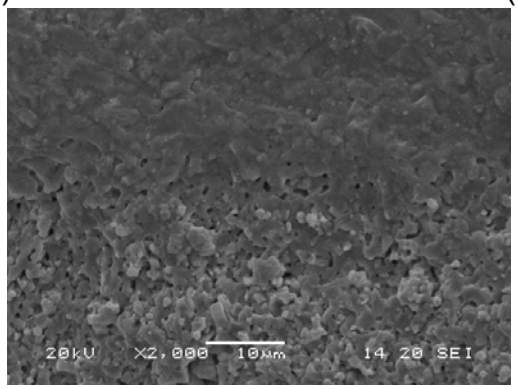
(b)



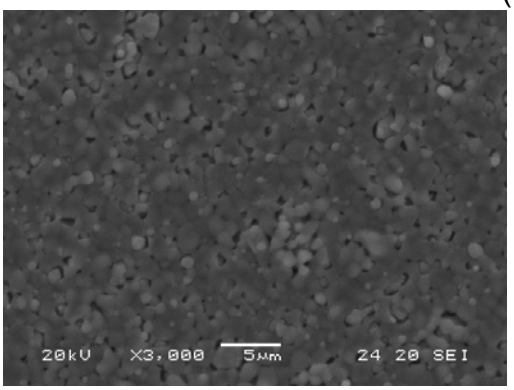
(c)



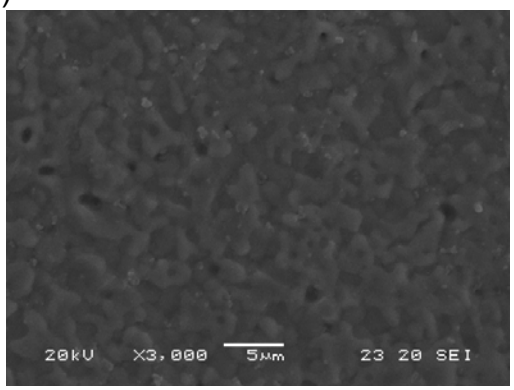
(d)



(e)



(f)



(g)

Figure 5.8 SEM images of LSM-ScSZ/Ni-ScSZ (a) whole view (b) cross section (c) inner layer cross section (d) outer layer cross section (e) boundary between the two layers (f) inner surface (g) outer surface

5.4.5 Partial oxidation of methane

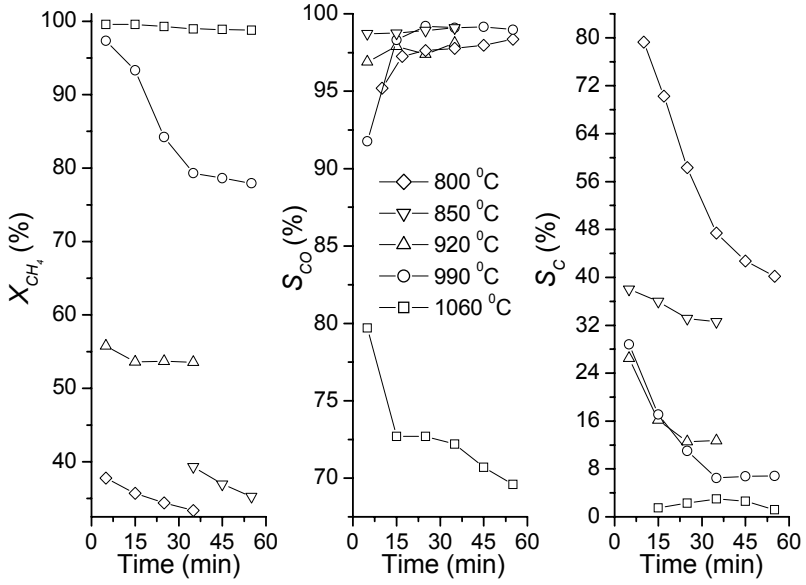
Prior to the reaction, the LSM-ScSZ/NiO-ScSZ fibre was reduced at 800 °C for 30 min. A mixture of CH_4 (10%)/Ar of 20 ml/min was used as the reactant stream in the lumen of the fibre. A trace amount of N_2 of approximately 1.2×10^{-3} ml/s can be detected by GC before and after reduction, which did not change during the reaction. This indicates that the slight leak is probably from the joints of the experimental set-up, instead of from the membrane.

As can be seen in Figure 5.9 (a), X_{CH4} increases from approximately 33.4 % to 98.8 % when the operating temperature is elevated from 800 to 1060 °C. In most cases, there is a drop in methane conversion (due to the coke formation) that tends to stabilize within 1 h of operation, except for the one at 1060 °C. CO selectivity higher than 95 % can be maintained when the temperatures are below 990 °C, which indicates an efficient utilization of the permeated oxygen for syngas production. While the relatively lower CO selectivity of approximately 70 % at 1060 °C indicates the excessive permeation of oxygen from the oxygen separation layer, resulting in the formation of more CO_2 and H_2O as by-products, and catalytic reaction subsequently turns into the controlling step. S_C, which is mainly the result of coke-deposition during methane conversion, decreases with the increasing temperatures, agreeing well with previous studies [7, 18] that coke-deposition on the mixture of Ni and ScSZ is alleviated with elevated temperatures.

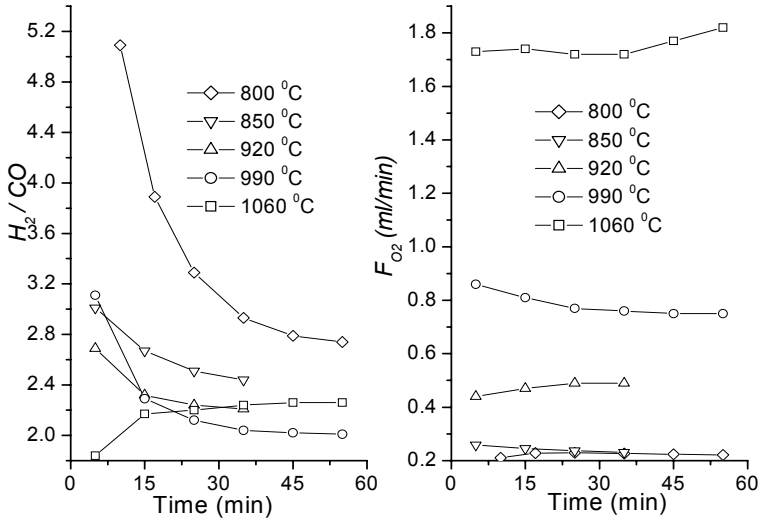
Figure 5.9 (b) shows that the ratio between H_2 and CO in the product stream decreases and gets closer to the value of 2 with the elevated temperatures to 990 °C, where the oxygen permeation is still the controlling step. However, at 1060 °C, the value of H_2/CO is slightly higher than that at lower temperatures, agreeing well with the change in S_{CO} at this temperature (Figure 5.9 (a)), and is considered as the result of excessive oxygen permeation. The oxygen permeation rate, F_{O2} increases as operating temperature is increased and the F_{O2} of approximately 0.49 ml/min can be achieved at 920 °C, which is 58% higher than that obtained in our previous study operated at 950 °C and with thinner outer oxygen separation layer (75 μm) [1], demonstrating the advantages of new material selected which improves the oxygen permeation as well as the performance of the partial oxidation of methane. At 990 °C, the value of H_2/CO is 2, which indicates that there is just a sufficient amount of oxygen permeated through the outer separation layer that takes part into the partial oxidation of methane (POM), matching well with the catalytic activity of the inner layer. This also indicates that, for the current DL-HFMR design, an oxygen permeation rate of approximately 0.8 ml/min is high enough to convert approximately 80 % of 2 ml/min of methane into syngas. And a further enhancement of the oxygen permeation at lower operating temperatures would help to improve the reactor performance.

Furthermore, the results in Figure 5.9 highlight the importance of oxygen permeation in improving the performance for methane conversion, such as better X_{CH4} , CO selectivity and less coke formation. Oxygen permeation rate should match with the reaction rate at a certain operating temperature to avoid

deep oxidation. The compatible reaction and permeation rates can be achieved by developing dual-layer ceramic hollow fibres with adjustable thickness of the separation layer, which has been proved to be achievable by using the single-step co-extrusion and co-sintering process [14].



(a)



(b)

Figure 5.9 Time dependent (a) X_{CH4}, S_{CO} and S_C, (b) H_2/CO and F_{O2} between 920 and 1060 °C

5.4.6 Comparison between DL-HFMR-YSZ and DL-HFMR-ScSZ

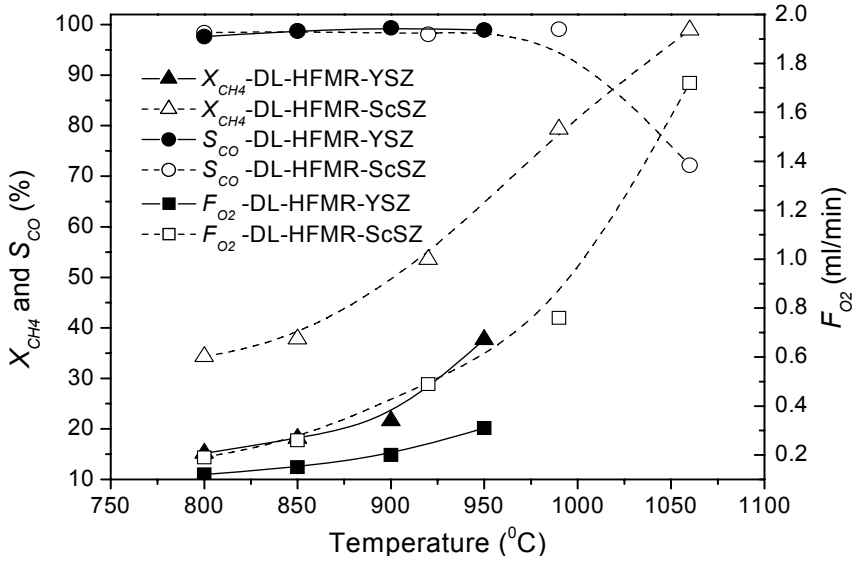
This section compares the performance of DL-HFMR-YSZ developed in Chapter 4 and the DL-HFMR-ScSZ in this chapter, in order to determine the key factors of using DL-HFMR design for methane conversion. Table 5.2 lists the operating conditions and the differences in the membrane reactor structures. Both DL-HFMR designs were achieved by using the single-step co-extrusion and co-sintering process. While due to the different sintering behaviours of the membrane materials, the volume percentages of NiO in DL-HFMR-YSZ and DL-HFMR-ScSZ were 30 % and 35 %, respectively.

Table 5.2 Operating conditions and the differences in membrane reactor structure

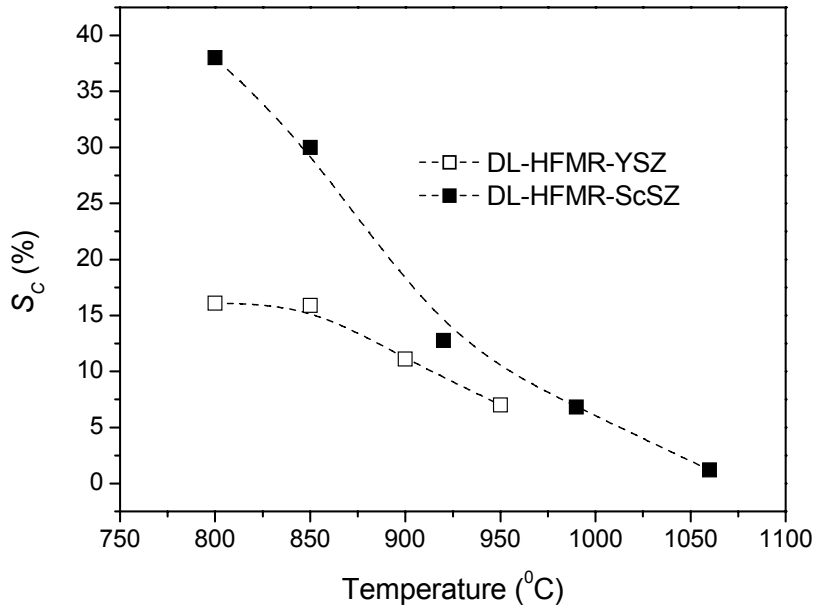
	DL-HFMR-YSZ	DL-HFMR-ScSZ
Outer layer composition	LSM/YSZ (40/60 vol. %)	LSM/ScSZ (40/60 vol. %)
Inner layer composition	YSZ/NiO (70/30 vol. %)	ScSZ/NiO (65/35 vol. %)
Outer layer thickness (μm)	75	109
Inner layer thickness (μm)	170	226
Reactant flow rate (10%CH_4/Ar, ml/min)	20	20
Temperature (°C)	800-950	800-1060

As can be seen in Figure 5.10 (a), the oxygen permeation of both DL-HFMR-YSZ and DL-HFMR-ScSZ increases with the elevated temperatures, and the replacement of YSZ by ScSZ increases oxygen permeation although its oxygen separation layer is thicker (Table 5.2). The higher oxygen permeation rate subsequently increases the methane conversion that also increases with

the elevated temperatures, while the CO selectivity is always maintained at a high level (above 95 %), until excess oxygen permeation at 1060 °C turns the catalytic reaction into the controlling step.



(a)



(b)

Figure 5.10 Comparison between DL-HFMR-YSZ and DL-HFMR-ScSZ (a) X_{CH4}, S_{CO} and F_{O2} and (b) S_C

With regards to the coke-formation, although the replacement of YSZ by ScSZ with higher ionic conductivity should decrease the coke deposited on the inner catalytic layer that reduces the catalytic activity, more NiO was employed in the inner layer of DL-HFMR-ScSZ in order to match the sintering behaviour with the outer layer. This results in more coke formation of DL-HFMR-ScSZ especially at lower operating temperatures (Figure 5.10 (b)). But the coke formation drops in a faster way when compared with DL-HFMR-YSZ, and reaches to a very low level at higher temperatures due to the higher oxygen permeation. This also proves that oxygen permeation is still the key factor in order for higher methane conversion and less coke formation (or catalyst deactivation).

Although the replacement of YSZ by ScSZ contributes to improve the membrane reactor performance for methane conversion, higher operating temperature of around 990 °C has to be used in order for a proper methane conversion and product selectivity. This means that further measures for higher oxygen permeation at possibly lower operating temperatures should be carried out to improve the performance of the reactor design of this type.

5.5 Conclusions

Functional LSM-ScSZ/NiO-ScSZ dual-layer hollow fibres have been developed in this chapter by a single-step co-extrusion and co-sintering process, and used as a highly compact hollow fibre membrane reactor for partial oxidation of methane. Dual-phase membrane materials, i.e. LSM-ScSZ

for the oxygen separation layer and NiO-ScSZ for the catalytic substrate layer, are used to functionalize the fibres, and contribute to form a great adhesion between the two layers for high temperature applications. Oxygen permeation is the key factor in efficiently improving methane conversion. Higher oxygen permeation rate of 1.8 ml/min at 1060 °C results in a methane conversion of 98.8% and suppresses the coke formation to a very low level. However, the drop in CO selectivity from approximately 99% at 990 °C to 70% at 1060 °C indicates the oversupply of oxygen. NiO acted as a “pore former” and catalytic active phase in the inner catalytic substrate should be adjusted according to a number of factors, such as porosity, catalytic activity, coke-deposition and mechanical property etc., in addition to the sintering behaviour that has to be matched with the outer layer.

References

1. Wang Y, Wang W, Hong X, Li Y, Zhang Z. Yttrium-stabilized zirconia-promoted metallic nickel catalysts for the partial oxidation of methane to hydrogen. Int. J. Hydrogen Energy 2009; 34 (5): 2252-2259.

2. Corbo P, Migliardini F. Hydrogen production by catalytic partial oxidation of methane and propane on Ni and Pt catalysts. Int. J. Hydrogen Energy 2007; 32 (1): 55-66.

3. Sunarso J, Baumann S, Serra JM, Meulenberg WA, Liu S, Lin YS, Diniz da Costa JC. Mixed ionic-electronic conducting (MIEC) ceramic-based membranes for oxygen separation. J. Membr. Sci. 2008; 320 (1-2): 13-41.

4. Rui Z, Zhang K, Li Y, Lin YS. Simulation of methane conversion to syngas in a membrane reactor. Part II: Model predictions. Int. J. Hydrogen Energy 2008; 33 (10): 2501-2506.

5. Rui Z, Zhang K, Li Y, Lin YS. Simulation of methane conversion to syngas in a membrane reactor: Part I A model including product oxidation. Int. J. Hydrogen Energy 2008; 33 (9): 2246-2253.

6. Singhal SC, Kendall K (2003),*High-temperature Solid Oxide Fuel Cells: Fundamentals, Design and Applications*, Oxford, Elsevier Ltd, The Boulevard, LangfordLane, Kidlington, Oxford OX5 IGB, UK.

7. Ke K, Gunji A, Mori H, Tsuchida S, Takahashi H, Ukai K, Mizutani Y, Sumi H, Yokoyama M, Waki K. Effect of oxide on carbon deposition behavior of CH4 fuel on Ni/ScSZ cermet anode in hihh temperature SOFCs. Solid State Ionics 2006; 177 (5-6): 541-547.

8. Eguchi K, Tanaka K, Matsui T, Kikuchi R. Reforming activity and carbon deposition on cermet catalysts for fuel electrodes of solid oxide fuel cells. Catal. Today 2009; 146 (1-2): 154-159.

9. Wu ZT, Wang B, Li K. A novel dual-layer ceramic hollow fibre membrane reactor for methane conversion. J. Membr. Sci. 2010; 352 (1-2): 63-70.

10. Hagiwara A, Hobara N, Takizawa K, Sato K, Abe H, Naito M. Preparation of LSM/ScSZ composite powder materials by spray pyrolysis for the pre-

fabrication of SOFC cathodes. Solid State Ionics 2007; 178 (27-28): 1552-1562.

11. Chang X, Zhang C, Jin W, Xu N. Match of thermal performances between the membrane and the support for supported dense mixed-conducting membranes. J. Membr. Sci. 2006; 285 (1-2): 232-238.

12. Jin W, Li S, Huang P, Xu N, Shi J. Preparation of an asymmetric perovskite-type membrane and its oxygen permeability. J. Membr. Sci. 2001; 185 (2): 237-243.

13. Tan XY, Liu SM, Li K. Preparation and characterization of inorganic hollow fiber membranes. J. Membr. Sci. 2001; 188 (1): 87-95.

14. Othman MHD, Droushiotis N, Wu Z, Kanawka K, Kelsall G, Li K. Electrolyte Thickness Control and Its Effect on Electrolyte/Anode Dual-Layer Hollow Fibres for Micro-Tubular Solid Oxide Fuel Cells. J. Membr. Sci. 2010; In Press, Accepted Manuscript.

15. Othman MHD, Wu ZT, Droushiotis N, Doraswami U, Kelsall G, Li K. Single-step fabrication and characterisations of electrolyte/anode dual-layer hollow fibres for micro-tubular solid oxide fuel cells. J. Membr. Sci. 2010; 351 (1-2): 196-204.

16. Droushiotis N, Othman MHD, Doraswami U, Wu ZT, Kelsall G, Li K. Novel co-extruded electrolyte-anode hollow fibres for solid oxide fuel cells. Electrochemistry Communications 2009; 11 (9): 1799-1802.

17. Kingsbury BFK, Li K. A morphological study of ceramic hollow fibre membranes. J. Membr. Sci. 2009; 328 (1-2): 134-140.

18. Gunji A, Wen C, Otomo J, Kobayashi T, Ukai K, Mizutani Y, Takahashi H. Carbon deposition behaviour on Ni-ScSZ anodes for internal reforming solid oxide fuel cells. J. Power Sources 2004; 131 (1-2): 285-288.

Chapter 6

Effects of Separation Layer Thickness on Oxygen Permeation and Mechanical Strength of DL-HFMR-ScSZ

Abstract

It has been demonstrated in previous chapters that oxygen permeation through the outer separation layer is the key factor to further improve the performance of the dual-layer hollow fibre membrane reactor, such as higher methane conversion and less coke deposition etc.. With regards to membrane materials, the replacement of YSZ by ScSZ with higher ionic conductivity (Chapter 5) contributes to increase oxygen permeation, and as a result improves the reactor performance. While from the point of view of membrane separation, thinner membrane always facilitates oxygen permeation and results in higher permeation fluxes, although this strategy is limited by the characteristic thickness, L_c, where surface exchange plays a more important role in determining oxygen permeation (Chapter 2). As a result, this chapter mainly investigates the effects of separation layer thickness on oxygen permeation and other properties of DL-HFMR-ScSZ, such as mechanical strength and microstructure, in order to figure out if and how a thinner LSM-ScSZ separation layer can improve the reactor performance. By using the same co-extrusion and co-sintering process, thickness of the outer LSM-ScSZ oxygen separation layer of approximately 8.0 to 72.4 μm can be achieved, further proving the advantages of such membrane fabrication process in controlling the membrane structures.

Key words: Oxygen permeation, co-extrusion and co-sintering, dual-layer ceramic hollow fibre, membrane reactor, methane conversion

6.1 Introduction

Use of dense ceramic membrane with the unique mixed ionic-electronic conducting (MIEC) property to separate highly pure oxygen from air has been widely studied for several decades [1-3]. The oxygen permeation through such membranes normally consists of two processes, i.e. surface changes on membrane surfaces (feed side and permeate side) and bulk diffusion of oxygen ions through the membrane, as shown in the Figure 2.3 of Chapter 2. As the slowest step predominantly determines the overall rate of oxygen permeation, it is important to know which is the rate-determining or controlling step of oxygen permeation, in order to further improve the oxygen permeation flux [4-6].

For many reported MIEC membranes, bulk diffusion is the controlling step of oxygen permeation, and the Wagner equation is usually used to calculate the oxygen permeation flux (J_{O_2}) when the P_{O_2} - difference across the MIEC membrane is small :

$$J_{O_2} = -\frac{R \cdot T}{16 \cdot L \cdot F^2} \int_{\ln P'_{O_2}}^{\ln P''_{O_2}} \frac{\sigma_{el} \cdot \sigma_{ion}}{\sigma_{el} + \sigma_{ion}} d \ln P_{O_2} \qquad (6\text{-}1)$$

where R , T , L and F are the gas constant, temperature, membrane thickness and Faraday constant, respectively, while σ_{el} and σ_{ion} are electronic and ionic conductivity, respectively. In this case, the value of $J_{O_2} \cdot L$ is a thickness-

independent constant at fixed temperature and oxygen partial pressure difference across the membrane.

However, when the surface exchanges can not be neglected, the Wagner equation has to be modified as:

$$J_{O_2} = -\frac{1}{1+(2L_C/L)} \cdot \frac{R \cdot T}{16 \cdot L \cdot F^2} \int_{\ln P'_{O_2}}^{\ln P''_{O_2}} \frac{\sigma_{el} \cdot \sigma_{ion}}{\sigma_{el} + \sigma_{ion}} d \ln P_{O_2} \qquad (6\text{-}2)$$

where $L_C\,(=D_a/K_s)$ is the characteristic membrane thickness, while D_a and K_s are the ambi-polar diffusion coefficient and the surface exchange coefficient, respectively. Apparently, when L >> L_C , or K_s >> D_a , bulk diffusion is the controlling step and the equation 6.2 turns into the Wagner equation. When the value of L decreases to a level that is similar enough to L_C , oxygen permeation is partly governed by surface exchanges, or co-governed by both bulk diffusion and surface exchanges. And when L_C >> L , oxygen permeation reaches the maximum achievable flux and further decreasing the membrane thickness would not increase the oxygen permeation anymore. Surface exchanges thus turn into the controlling step and predominantly determine oxygen permeation.

Such change of oxygen permeation with the membrane thickness can also be presented in the way shown Figure 6.1. As can be seen, when the membrane

is very thick or much thicker than the characteristic membrane thickness (L_C), bulk diffusion is the controlling step and the oxygen permeation flux increases linearly with the inverse of the membrane thickness (L), until the increase of oxygen permeation flux deviates from the straight dashed line with the decreasing membrane thickness, indicating that oxygen permeation is co-governed by both bulk diffusion and surface exchanges processes. Further decrease of L to a level that is much lower than L_C would not increase the oxygen permeation as surface exchanges turn into the controlling step.

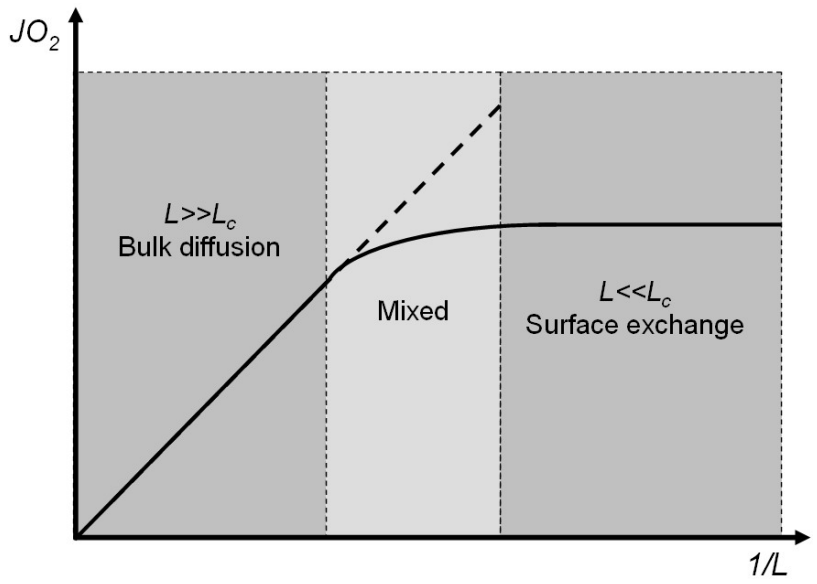


Figure 6.1 Change of oxygen permeation with the membrane thickness

In the previous chapters (Chapter 4 and 5), the replacement of YSZ by ScSZ with higher ionic conductivity majorly contributes to facilitate the migration of oxygen ions through the outer separation, i.e. bulk diffusion step. If the oxygen permeation through the outer separation layer is still not limited by the surface exchange process, reducing the separation layer thickness would contribute

to improve oxygen permeation, and as a result improve the performance of the DL-HFMR-ScSZ for methane conversion.

6.1.1 Objectives

As a result, this chapter focuses on the fabrication and characterization of DL-HFMR-ScSZ with different thicknesses of the outer oxygen separation layer, and investigates the effects of the outer layer thickness on oxygen permeation, microstructure and mechanical strength of the developed dual-layer hollow fibres. The specific objectives are listed as following:

1. Preparing dual-layer ceramic hollow fibre membranes with different outer layer thickness, by using the co-extrusion and co-sintering process.
2. Characterizing the effects of different outer layer thicknesses on the microstructure and mechanical strength.
3. Measuring oxygen permeation rates in order to determine the controlling step of oxygen separation.

6.2 Background

Since bulk diffusion and surface exchanges are the two major steps determining oxygen permeation through the MIEC membranes, lots of investigations have been carried out to explain the mechanisms in order for developing new MIEC materials and membranes for higher oxygen permeation flux, especially for the single-phase MIEC materials. According to

the Wagner theory, the oxygen permeation rate is proportional to $[(\sigma_{el} \cdot \sigma_{ion})/(\sigma_{el} + \sigma_{ion}]$. Therefore, good ionic conductivity and good electronic conductivity are always preferred for higher oxygen permeation. This is also the reason that dual-phase membrane materials consisting of a separate ionic conducting phase and an electronic conducting phase can be used for oxygen separation, although its oxygen permeation mechanism is yet explained as clear as the single phase counterparts.

For the single phase MIEC materials, D_a and K_s are both temperature dependent and increase with elevated temperatures, but at different rates. While K_s also changes with other factors such as the surface morphology (roughness and porosity) and so on. As a result, $L_C (= D_a / K_s)$ changes with temperatures, material compositions and membrane microstructure etc.. Early studies have shown that L_C of some MICE materials can range between μm and mm, and tends to increase with elevated temperatures [7]. There have been a number of ways to measure the values of D_a and K_s [8], in order to determine the value of L_C. But from the point of view of membrane separation, the most straightforward way is to measure the change of oxygen permeation with the membrane thicknesses under certain conditions.

However, the fabrication of self-supported symmetric MIEC membranes of less than several hundred microns is still technically challenging, even for the disk-type membranes that have been widely studied in labs. The idea of

coating a thin separation layer onto a porous support allows the formation of thin MIEC membranes in microns, when there is a reliable way to achieve such design with great membrane integrity. Conventional fabrication processes, such as dip-coating, can hardly achieve a dense MIEC separation layer and a porous substrate layer at the same time, especially when different materials are used in the two layers where cracks, defects and poor adhesion between the layers are always of great concern. But for the single-step co-extrusion and co-sintering process that has been used for the fabrication of dual-layer ceramic hollow fibre membranes (Chapters 3-5), besides the fantastic membrane integrity and great adhesion between the two layers, the thickness of the outer oxygen separation layer can be controlled by varying the co-extrusion parameters. This enables the formation of this separation layer to be less than 100 μm. As a result, a series of such fibres with different separation layer thicknesses can be obtained to investigate the controlling step of the oxygen permeation, in order for higher oxygen permeation and as a result better performance of DL-HFMR-ScSZ for methane conversion.

6.3 Experimental

6.3.1 Materials

$La_{0.80}Sr_{0.20}MnO_{3-\delta}$ (LSM, NexTech Materials Ltd, 5.8 m^2/g), NiO (NexTech Materials Ltd, 5.2 m^2/g) and scandia(10%)-stabilized-zirconia (ScSZ, NexTech Materials Ltd, 9.4 m^2/g) were used as supplied. Polyethersulfone, (PESf, Radel A-300, Ameco Performance, USA), Dimethyl Sulfoxide (DMSO, Sigma, >99.5%) and Arlacel P135 (Uniqema, UK) were used as polymer binder,

solvent and additive functioning as dispersant respectively. DI water and tap water were used as the internal and the external coagulants, respectively, when fabricating the dual-layer hollow fibres.

6.3.2 Fabrication of LSM-ScSZ/NiO-ScSZ dual-layer hollow fibres

The preparation of spinning suspensions as well as the co-extrusion process has been described in previous chapters. In contrast with the previous membrane fabrication process where the extrusion rates of both the inner and outer layers were fixed, the extrusion rate of the inner layer in this chapter was maintained at a certain value, while the one of the outer layer was varied from 5 to 0.5 ml/min, resulting in a series of dual-layer hollow fibre membranes with gradually decreased outer layer thicknesses. Table 6.1 lists suspension compositions and co-extrusion parameters.

Table 6.1 Compositions of spinning suspensions and co-extrusion parameters

	Suspension composition	
	Outer oxygen separation layer (wt.%)	Inner catalytic substrate layer (wt.%)
Ceramics	65.0	68.0
DMSO	28.0	24.7
PESf	6.5	6.8
Additive	0.5	0.5
	Co-extrusion parameters	
	Outer layer suspension	Inner layer suspension
Extrusion rate (ml/min)	0.5 – 5.0	8.0
Temperature (°C)	20	
Air gap (cm)	26	
Internal coagulant (ml/min)	10	

The formed precursor fibres were then cut into the required length, dried and straightened, and finally co-sintered at 1400 °C for 5 h, with heating and cooling rates of 5-10 and 3 °C/min respectively.

6.3.3 Characterizations of dual-layer hollow fibres

Microstructures of the developed dual-layer hollow fibres were visually observed by using a scanning electron microscope (SEM, JEOL JSM-5610LV, Tokyo, Japan). Mechanical strength was examined by a three points bending test (Tinius Olsen H25KS). Samples of around 5.0 cm in length were fixed on sample holder with a 3.0 cm gap. The bending strength (σ_F, MPa) is calculated using the following equation:

$$\sigma_F = \frac{8 \cdot F \cdot L \cdot D}{\pi (D^4 - d_i^{\,4})} \tag{6.3}$$

where F is the measured loading at which fracture occurred (N); L, D, d_i are the length (m), the outer diameter and the inner diameter of the hollow fibres (m), respectively. For the purpose of comparison, some co-sintered fibres were reduced separately (H_2 of 15 ml/min, 600 °C for 30 min) prior to mechanical strength test.

6.3.4 Oxygen permeation and methane conversion of DL-HFMR-ScSZ

Measurements of oxygen permeation and methane conversion were carried out by using the set-up shown in Figure 6.2. Prior to the measurements, the

inner layer was reduced in a hydrogen stream (15 ml/min) at 600 °C for 30 min and turned into a highly porous structure. A gas mixture of CO (10%)/Ar (20 ml/min) was used as the “sweep gas” of oxygen permeation measurement, and the amount of oxygen permeated through the outer layer can be monitored by the amount of CO_2 produced. Methane conversion was also tested, using the similar procedure in Chapter 5.

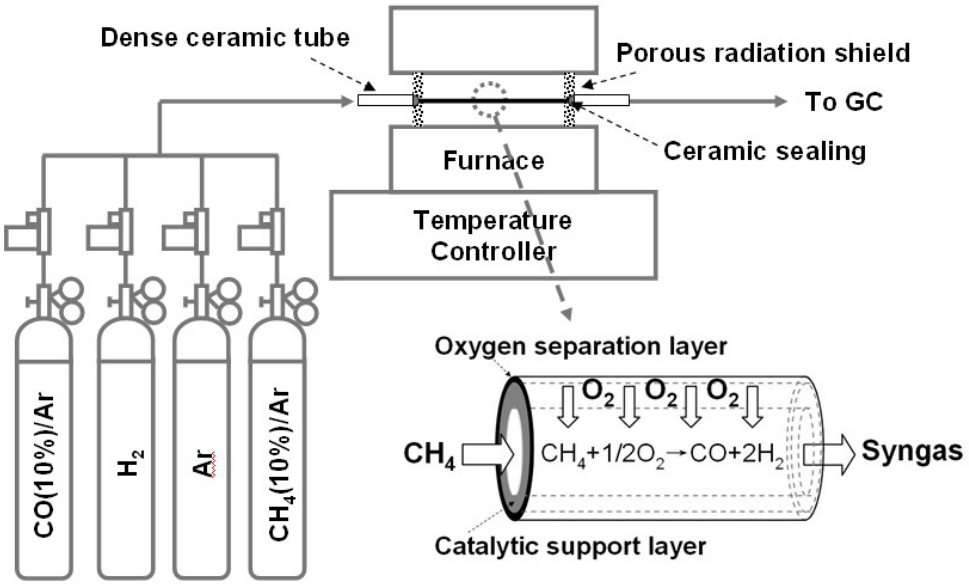


Figure 6.2 Experimental set-up of measuring oxygen permeation and methane conversion

6.4 Results and discussion

6.4.1 Morphology of the precursor dual-layer hollow fibres

Figure 6.3 shows the photographic images of the precursor dual-layer fibres, with the outer layer extrusion rates varied from 0.5 to 5.0 ml/min. As can be seen, the inner catalytic substrate layer is of a typical asymmetric structure, i.e. a sponge-like layer supported on another finger-like layer, while the outer

oxygen separation layer is of a fully sponge-like structure. Meanwhile, there is a clear interface between the two layers, with the outer layer tightly bonded to the inner layer free of any gaps in between, indicating great uniformity of the prepared fibres and adhesion between the two layers.

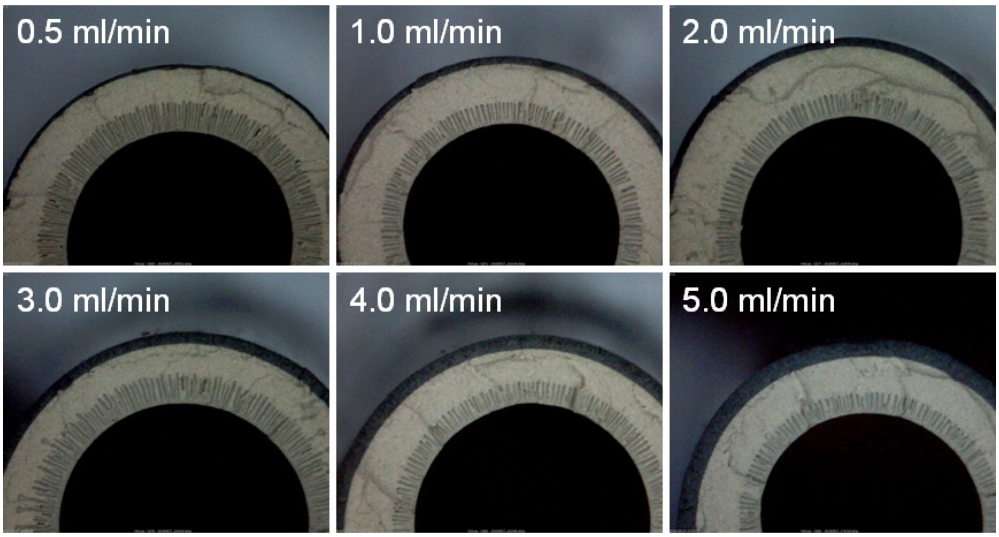


Figure 6.3 Photographic images of the precursor dual-layer fibres with different outer layer extrusion rates (0.5 to 5.0 ml/min)

The thickness of the outer oxygen separation layer keeps increasing with the increasing extrusion rate, while the asymmetric structure of the inner catalytic substrate layer, i.e. a sponge-like layer is support on another finger-like layer, is little affected. This also proves that the co-extrusion process is a well controlled way of fabricating dual-layer ceramic hollow fibres, especially in reducing the thickness of the separation layer (top-layer) to a very low level with great membrane uniformity. It should be noted here that this can still be hardly guaranteed by most of the previous membrane fabrication processes.

6.4.2 Microstructure of the co-sintered dual-layer hollow fibres

Figures 6.4-6.9 show the microstructure of the co-sintered hollow fibres with different outer layer thicknesses. As can be seen in Figure 6.4, all the co-sintered samples are of a uniform hollow fibre configuration, and consist of a symmetric outer layer supported on an asymmetric inner layer. The morphology is very similar to the precursor fibres, except for the smaller inner and outer diameters due to the shrinking at higher temperatures. The change of the outer layer thickness with the different extrusion rates is shown in Figure 6.5, in which a clear interface between the two layers can be found due to the different textures of the each individual layer. Although the thickness of the outer layer keeps increasing with its extrusion rate, the two layers are always closely bonded together, indicating great adhesion of the two layers at high temperatures.

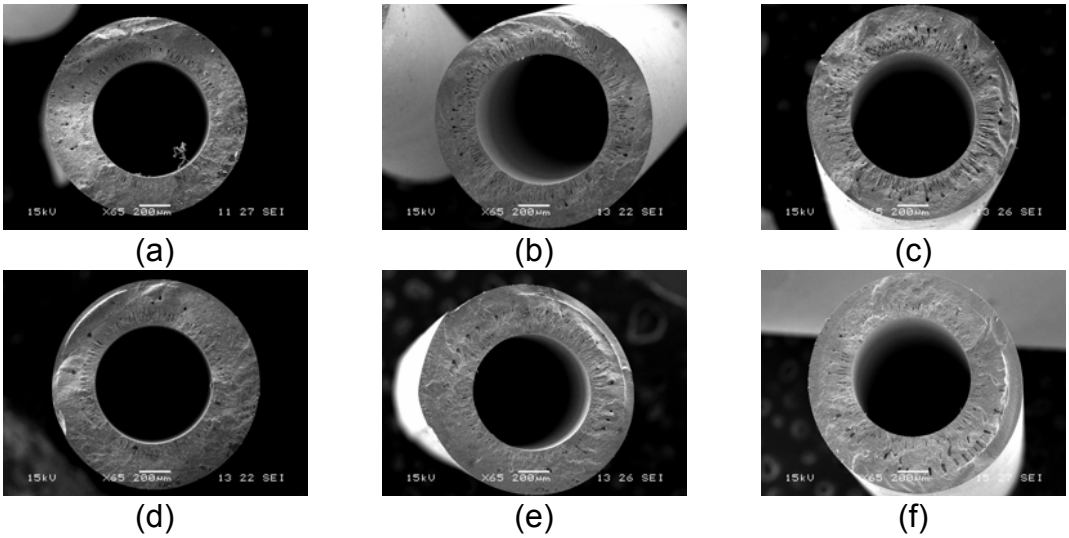
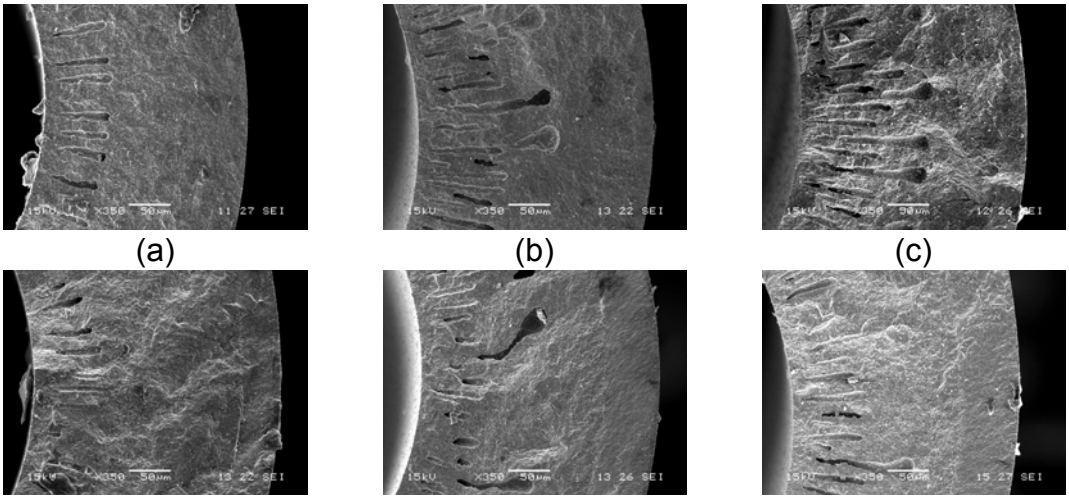


Figure 6.4 SEM images of the co-sintered fibres – whole view (a) 0.5 ml/min, (b) 1.0 ml/min, (c) 2.0 ml/min, (d) 3.0 ml/min, (e) 4.0 ml/min, (f) 5.0 ml/min

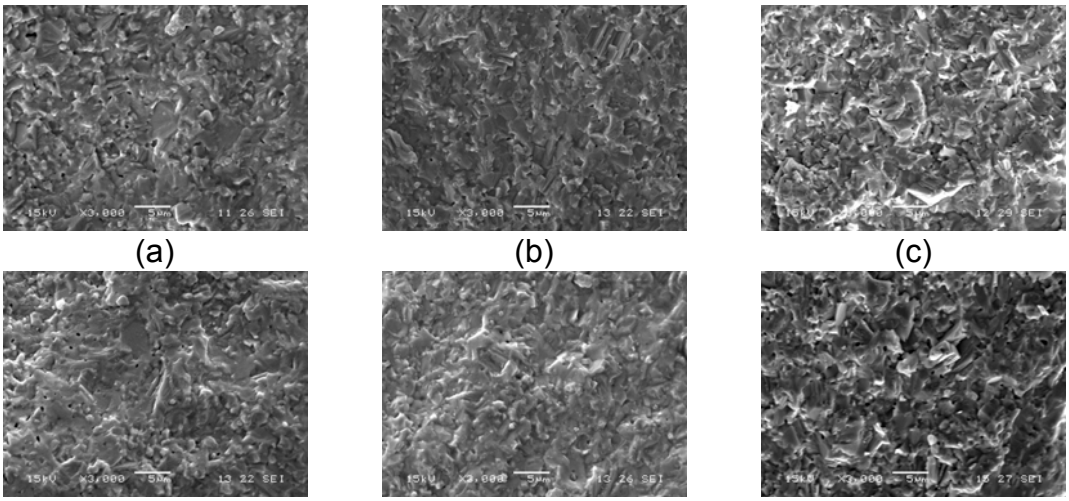


(a) (b) (c)

(d) (e) (f)

Figure 6.5 SEM images of the co-sintered fibres – cross section (a) 0.5 ml/min, (b) 1.0 ml/min, (c) 2.0 ml/min, (d) 3.0 ml/min, (e) 4.0 ml/min, (f) 5.0 ml/min

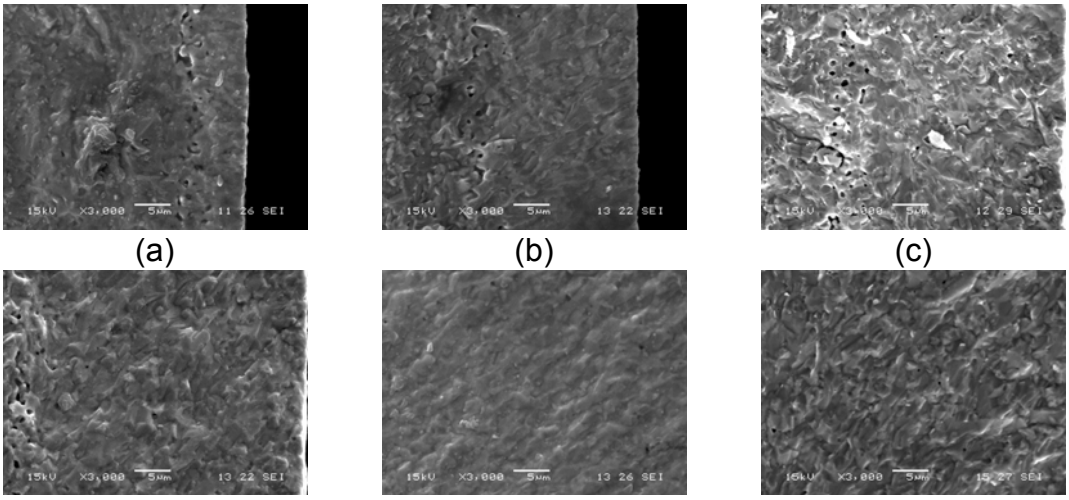
Both the inner and outer layers are densified after the co-sintering (Figures 6.6 and 6.7). And there is little change in the microstructure of the two layers except for the variation of the outer layer thickness.



(a) (b) (c)

(d) (e) (f)

Figure 6.6 SEM images of the co-sintered fibres – inner layer cross section (a) 0.5 ml/min, (b) 1.0 ml/min, (c) 2.0 ml/min, (d) 3.0 ml/min, (e) 4.0 ml/min, (f) 5.0 ml/min

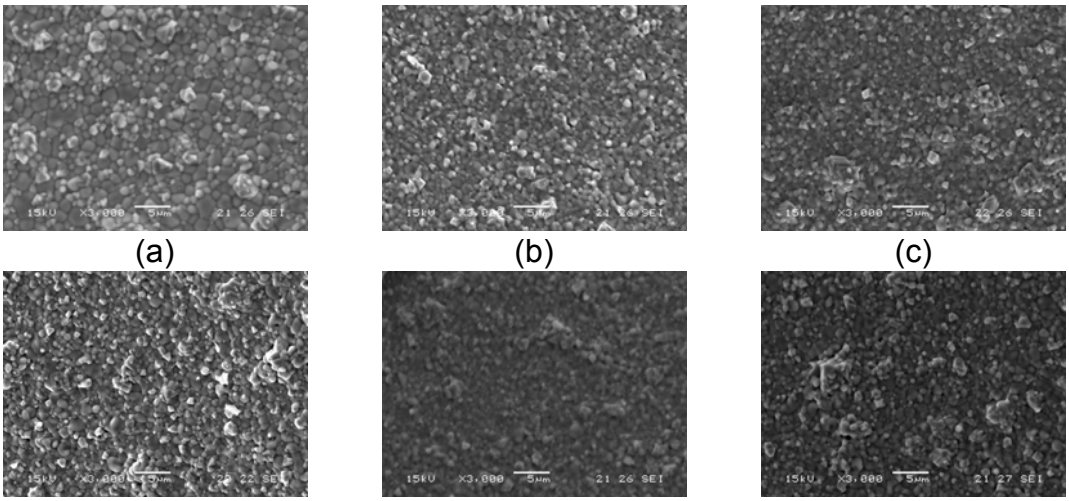


(a) (b) (c)

(d) (e) (f)

Figure 6.7 SEM images of the co-sintered fibres – outer layer cross section (a) 0.5 ml/min, (b) 1.0 ml/min, (c) 2.0 ml/min, (d) 3.0 ml/min, (e) 4.0 ml/min, (f) 5.0 ml/min

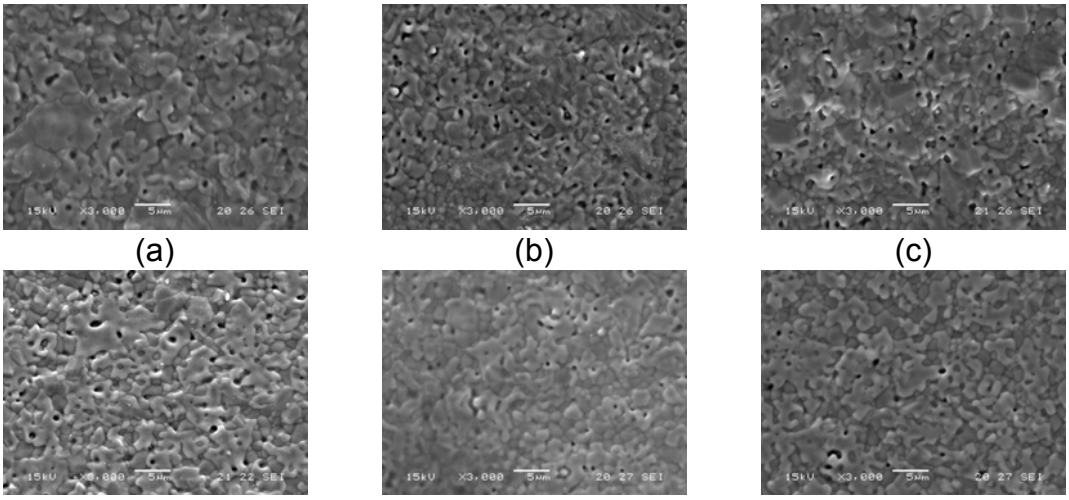
Similarly, the microstructures of both the inner surface and the outer surface are little changes with the different outer layer thickness, as shown in Figures 6.8 and 6.9.



(a) (b) (c)

(d) (e) (f)

Figure 6.8 SEM images of the co-sintered fibres – inner surface (a) 0.5 ml/min, (b) 1.0 ml/min, (c) 2.0 ml/min, (d) 3.0 ml/min, (e) 4.0 ml/min, (f) 5.0 ml/min

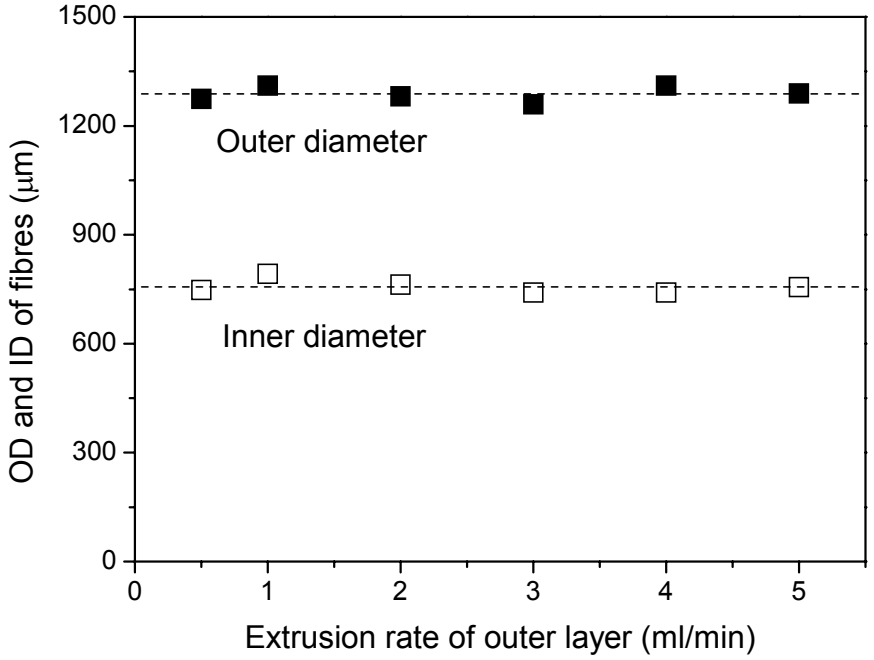


(a) (b) (c)

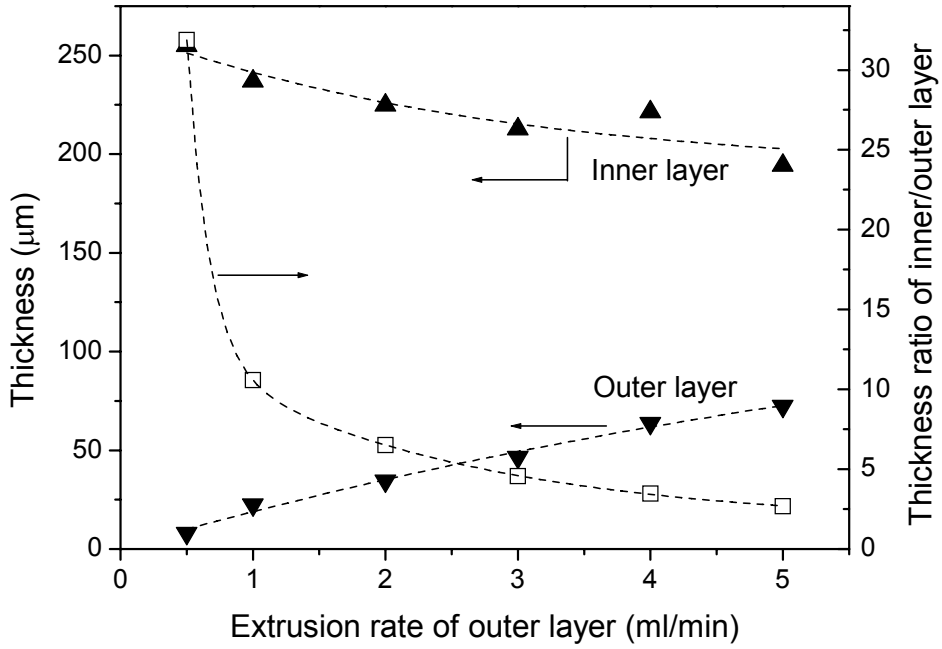
(d) (e) (f)

Figure 6.9 SEM images of the co-sintered fibres – outer surface (a) 0.5 ml/min, (b) 1.0 ml/min, (c) 2.0 ml/min, (d) 3.0 ml/min, (e) 4.0 ml/min, (f) 5.0 ml/min

As a result, it can be concluded that the variation of the extrusion rate of the outer layer during the co-extrusion process would not change the microstructure of the resultant dual-layer hollow fibres, except for the thickness of the two layers. As can be seen in Figure 6.10 (a), the ID and OD of the co-sintered dual-layer hollow fibres with different outer layer thicknesses are actually very close to each other, and are approximately 757 and 1288 μm, respectively. The thickness of the inner layer keeps decreasing with the increasing outer layer extrusion rate (from 0.5 to 5.0 ml/min), while the one of the outer layer keeps increasing (Figure 6.10 (b)). This results in a significant drop of the ratio between the thickness of the inner and the outer layers, especially when the outer layer is very thin (the extrusion rate increases from 0.5 to 2.0 ml/min). When the extrusion rate is increased from 2.0 to 5.0 ml/min, the drop of the thickness ratio slows down.



(a)



(b)

Figure 6.10 (a) ID and OD and (b) thickness of the inner and outer layers of the co-sintered dual-layer hollow fibres with different outer layer extrusion rate

Such a change in the thicknesses of the two layers with the varied extrusion rate of the outer layer is due to co-extrusion process. The current co-extrusion

process is actually based on the conventional dry-wet spinning method that has been widely used to fabricate polymer hollow fibre membranes. In such process, there is an air gap between the spinneret and the external coagulation bath (it is called wet spinning when the air gap is zero, or the spinneret is immersed in the external coagulation bath). And in order for a fully symmetric structure of the outer layer, a big air gap of 26 cm has to be employed. Otherwise, the finger-like voids will develop from the outer surface as well, and results in another morphology shown in Figure 6.11. The finger-like voids in the outer layer can be considered as the defects of the outer oxygen separation layer, and as a consequence decreases the gas-tightness and mechanical property of this layer.

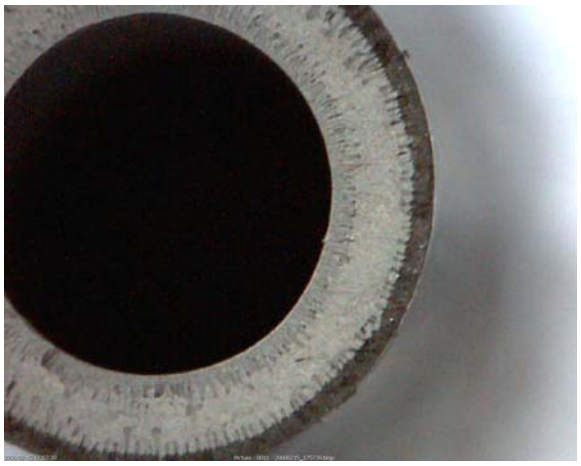


Figure 6.11 Photographic image of precursor dual-layer hollow fibres with finger-like voids developed from both the inner and outer surfaces

The big air gap indicates that the spinning suspension extruded through the spinneret has to vertically pass the distance of 26 cm, prior to accessing the external coagulation bath where the phase inversion can be fully completed.

Within this air gap, the phase inversion process is not completed and as a result the precursor fibre is still very soft. When the extrusion rate of the outer layer is increased (the one of the inner layer is maintained stably by the syringe pump), the precursor fibre in the air gap becomes heavier, which slightly stretches this part and subsequently reduces the thickness of the inner layer. While the increased extrusion rate of the outer layer overweight the slightly stretching of the inner layer, and as a result the thickness of the outer layer still increases with the increasing extrusion rate.

Also due to the variation of the thicknesses of the two layers with the varied outer layer extrusion rate, the mechanical strength of the resultant membranes is changed and is investigated in the following section.

6.4.3 Mechanical strength of the dual-layer hollow fibres

Figure 6.12 shows how the mechanical strength of the developed dual-layer hollow fibres changes with varying thicknesses of the two layers. As can be seen, the mechanical strength of the co-sintered fibres (before reduction in hydrogen) reduces with the decreasing thickness of the inner layer (or increasing thickness of the outer layer), which indicates that the major mechanical strength of the dual-layer hollow fibre is from the inner layer, and agrees with the LSM-YSZ/NiO-YSZ dual-layer hollow fibre in Chapter 4. After reduction, the NiO in the inner layer is converted into Ni and the dense inner layer turns into a highly porous structure. This reduces the mechanical strength of the dual-layer hollow fibre by around 25%.

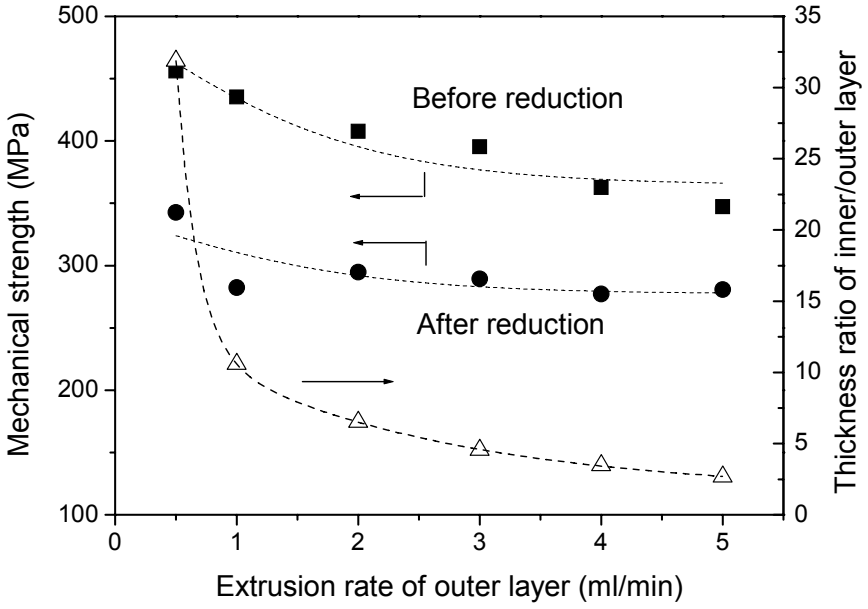


Figure 6.12 Effects of the outer layer extrusion rate on the mechanical strength of the dual-layer hollow fibres

Meanwhile, the major mechanical strength of the reduced dual-layer hollow fibres should also be from the inner layer, as it decreases with the decreasing thickness of the inner layer (or increasing thickness of the outer layer). Furthermore, the drop of the mechanical strength of both the co-sintered and the reduced samples decreases in a gentler way when the extrusion rate of the outer layer is increased from 2.0 to 5.0 ml/min, in agreement with the change of the thickness ratio between the two layers.

6.4.4 Oxygen permeation of the dual-layer hollow fibre membranes

Oxygen permeation of the LSM-ScSZ/Ni-ScSZ was investigated by using the set-up shown in Figure 6.2. A mixture of 10% CO balanced by Ar, instead of pure Ar, was employed as the sweep gas in order to consume the permeated

oxygen, or Ni will be oxidized into NiO and blocks the inner layer. The oxygen permeation rate can be calculated by the amount of CO_2 formed. Three types of membranes with the outer layer extrusion rate of 0.5, 2.0 and 5.0 ml/min were tested, with the thickness of the outer oxygen separation layer of 8.0, 34.5 and 72.4 μm, respectively.

As can be seen in Figure 6.13, for all the membranes tested, the oxygen permeation increases with the elevated operating temperatures. When the operating temperature is below 920 °C, the oxygen permeation rate increases with the decreasing thickness of the outer separation layer, which indicates that bulk diffusion determines or co-determines the oxygen permeation. While at 970 °C, oxygen permeation rate of all the 3 membranes are almost identical, which means that, at or above this temperature, surface exchange is the controlling step of oxygen permeation, and further reduction in the thickness of the separation layer would not increase the oxygen permeation rates. As the inner layer is highly porous after reduction, its mass transfer resistance can be neglected when compared with the one from the separation layer. Although the inner layer thicknesses of the 3 tested membranes are different, it is reasonable to assume that such change in oxygen permeation rate is from the different thicknesses of the outer oxygen separation layer. As a result, bulk diffusion is more likely to be the controlling step of oxygen permeation at lower operating temperatures, while surface exchange is the controlling step at higher temperatures.

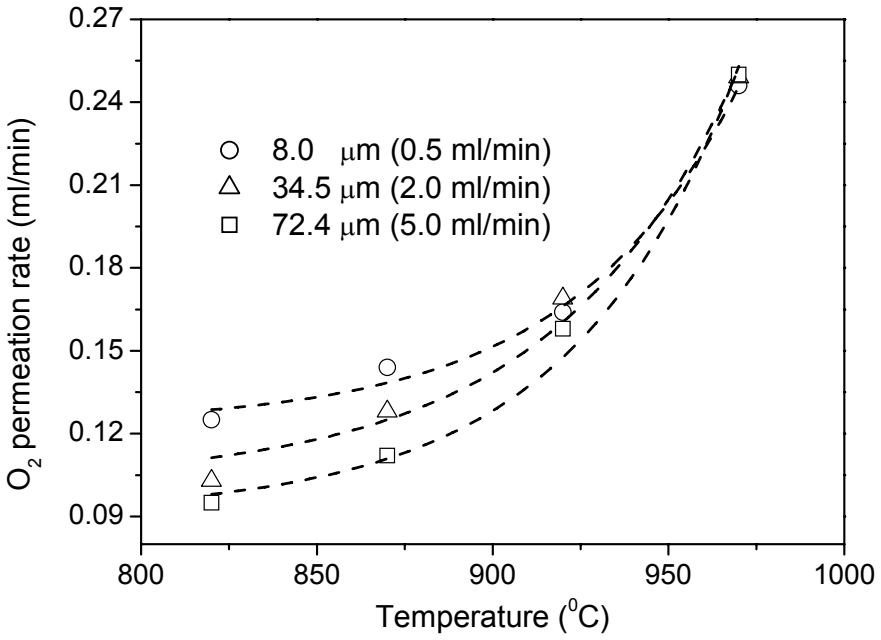


Figure 6.13 Effects of temperature on the oxygen permeation of dual-layer hollow fibre membranes with different separation layer thicknesses

The effects of separation layer thickness on oxygen permeation at different temperatures can also be presented in another way similar to the one shown in Figure 6.1. As can be seen in Figure 6.14, at 970 °C, surface exchange is always the controlling step of oxygen permeation, because the oxygen permeation rate does not change with the separation layer thickness (between 8.0 and 72.4 μm). This indicates that the value of L_c at this temperature is significantly higher than 72.4 μm at this temperature. While at 920 °C, oxygen permeation of the membrane with the separation layer thickness of 72.4 μm should be co-determined by bulk diffusion and surface exchange, i.e. mixed control in Figure 6.1. Pure surface exchange control only occurs when the separation layer is less than 34.5 μm. At further lowered operating temperatures (870 and 820 °C), oxygen permeation of the separation layer thickness of 34.5 μm is co-determined by bulk diffusion and surface exchange,

while the one of the 72.4 μm shift towards the bulk diffusion control although it may still be within the mixed control region.

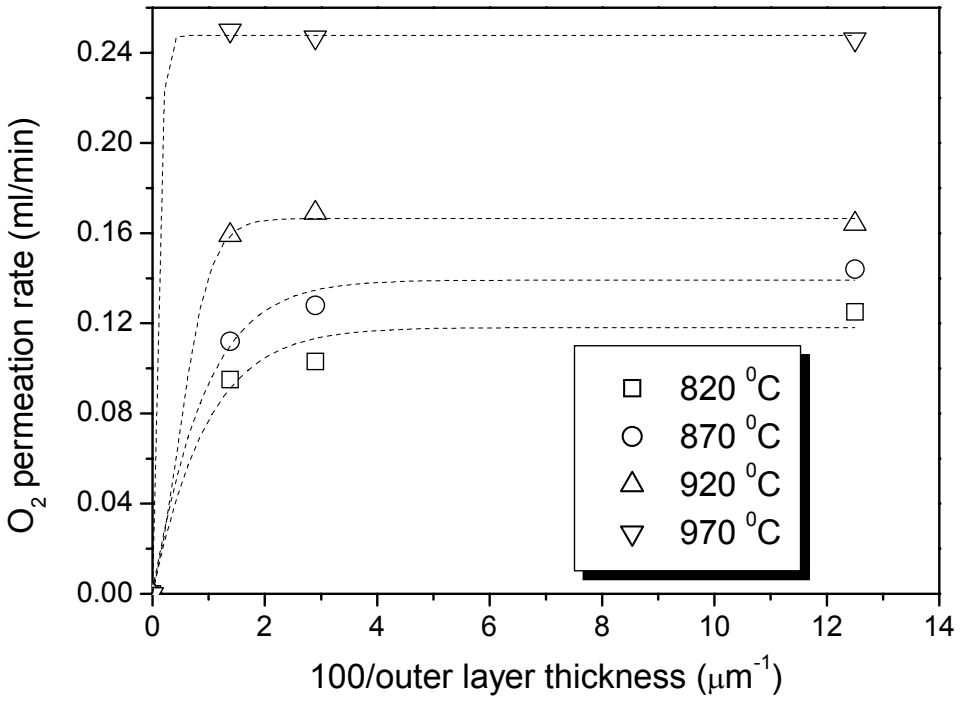


Figure 6.14 Effects of separation layer thickness on oxygen permeation at different temperatures

This indicates that, for the LSM-ScSZ/Ni-ScSZ dual-layer hollow fibre membranes, the value of L_c increases with the elevated temperatures, and as a result, oxygen permeation of the separation layer of 72.4 μm is still controlled by surface exchange processes at 970 °C. While the value of L_c decreases at lowered temperatures, oxygen permeation of the same separation layer thickness keeps shifting towards the bulk diffusion side when the temperature is reduced to 820 °C, although it may still be within the mixed-control range.

Such oxygen permeation behaviour is in agreement with some previous studies. Bouwmeester et. al. [7, 8] collected and compared the values of D_a and K_s of a series of perovskite-type oxides obtained by the O^{18}-O^{16} isotope exchange techniques, and concluded that L_c changes with the different dopant concentrations and there is a slight tendency for the L_c to increase with elevated temperatures. Also, there is a wide range of L_c that can be from 20 μm to 3000 μm at 900 °C for different perovskite-type oxides, which addresses the importance of surface exchange to the oxygen permeation through MIEC membranes. Hong et. al. [9] investigated the oxygen permeation of $Ba_{0.5}Sr_{0.5}Co_{0.8}Fe_{0.2}O_{3-\delta}$ (BSCF) between 750 and 900 °C, with and without a $La_{0.7}Sr_{0.3}CoO_{3-\delta}$ (LSC) coating layer for different surface exchange processes. Besides higher oxygen permeation, L_c of the LSC-coated BSCF membrane is about half of the uncoated counterparts. Furthermore, L_c of LSC-coated and uncoated BSCF membranes increase with the increasing temperatures from 800 to 900 °C. This indicates that with the decreasing membrane thickness or increasing temperature, oxygen permeation of BSCF is more likely to be controlled by surface exchange processes. Chen et. al. [10] investigated the oxygen permeation of $La_{0.7}Sr_{0.3}CoO_{3-\delta}$ (LSC) membrane and the value of L_c increased from 68±20 to 87±21 μm when the temperature is elevated from 1000 to 1100 °C.

However, there are other studies showing different conclusions. Tan et. al. [11-13] investigated the oxygen permeation of $La_{0.6}Sr_{0.4}Co_{0.2}Fe_{0.8}O_{3-\delta}$ (LSCF) hollow fibre membrane and concluded that the controlling step changes from

surface exchange processes at lower operating temperatures to bulk diffusion at higher temperatures. Furthermore, other studies proved that the value of L_c changes with the composition of membrane material [14, 15].

In terms of dense ceramic membranes made of dual-phase materials for oxygen separation, its mechanism of oxygen permeation is less well studied and described when compared with the one made of single phase materials with the perovskite structure. Oxygen transport in a dense membrane made of LSM-yttria-stabilised zirconia (YSZ) was studied by the group of Kilner [16, 17]. Both oxygen diffusion and surface exchange increase with elevating temperatures, which is same as the single-phase materials. Interestingly, surface exchanges of such dual-phase materials were higher than LSM and YSZ, while a higher content of LSM resulted in lower oxygen diffusion. For a disk-type sample (LSM-YSZ, 35-65 wt.%), surface exchange coefficient increased with elevated temperatures (from 803 to 995 °C) in a much faster way than oxygen diffusion, which may indicate that bulk diffusion is more likely to be the controlling step at higher operating temperatures.

The oxygen permeation of the LSM-ScSZ separation layer may not be directly compared with the single phase MIEC membranes and the disk-type LSM-YSZ dual-phase membrane (due to different surface exchange processes). However, by using the principles of oxygen permeation through the dense ceramic membranes, the controlling step of oxygen permeation through LSM-ScSZ should be the bulk diffusion at lower temperatures or for thicker LSM-ScSZ separation layer. Also, by using the co-extrusion and co-sintering process for membrane fabrication, the thickness of the oxygen separation layer can be reduced to such a low level of several microns and surface exchange can easily turn into the controlling step of oxygen permeation,

where the highest possible oxygen permeation can be achieved. If the same knowledge and technique can be transferred to the fabrication of other oxygen permeation membranes, significantly higher oxygen permeation can be expected.

Since surface exchange of LSM-ScSZ is the controlling step of oxygen permeation at high operating temperatures, and high temperatures have to be used in order for more oxygen permeation and subsequently better performance of the DL-HFMR (Chapter 4 and Chapter 5), it is reasonable to predicate that the maximum achievable methane conversions of all DL-HFMR-ScSZ with different thickness of the outer oxygen separation layer are same. But for the purpose of completeness, two DL-HFMR-ScSZ with the outer oxygen separation layer of 8.0 and 63.8 μm were tested for methane conversion at 820 °C, in order to prove that thinner separation layer still contribute to improve the reactor performance at lower operating temperatures, when bulk diffusion co-determines the oxygen permeation.

This time, two dual-layer hollow fibres (14 cm in length) with the same outer layer thickness are bundled together and used as a DL-HFMR-ScSZ for methane conversion, in order to enlarge the membrane surface area and as a result higher oxygen permeation rate. As can be seen in Figure 6.15, under the same operating conditions as the one in Chapter 5, the trend in the changes of methane conversion, coke formation and oxygen permeation rate with time are in agreement with the one in Chapter 4 and Chapter 5. While the

DL-HFMR-ScSZ with thinner oxygen separation layer (8.0 μm) shows higher methane conversion and oxygen permeation rate, together with less coke formation, when compared to the one with thicker oxygen separation layer (63.8 μm). This also agrees with the oxygen permeation measurement shown in Figures 6.13 and 6.14, in which bulk diffusion co-determines oxygen permeation at lower operating temperatures.

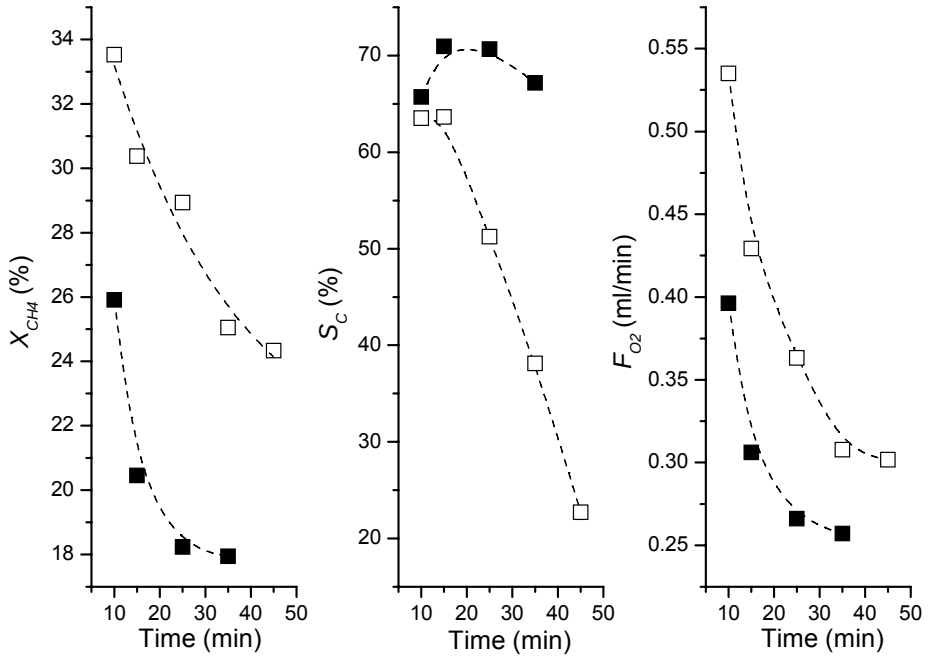


Figure 6.15 Methane conversion, coke deposition and oxygen permeation rate of DL-HFMR-ScSZ with the separation layer of 8.0 μm (blank symbols) and 63.8 μm (solid symbols) at 820 °C

6.5 Conclusions

In this chapter, a series of LSM-ScSZ/NiO-ScSZ dual-layer hollow fibres with the outer oxygen separation layer of approximately 8.0 to 72.4 μm has been fabricated by using the single-step co-extrusion and co-sintering process. The change of the outer layer thickness can be achieved by varying its extrusion

rate and maintaining the one of the inner layer. This results in thicker outer layer and thinner inner layer with the increasing extrusion rate of the outer layer. As the major mechanical strength of such dual-layer hollow fibre is from the inner substrate layer, the fibre with thicker outer layer is weaker than the one with the thinner one. The oxygen permeation of such fibres is co-determined by both bulk diffusion and surface exchange at lower operating temperatures. While surface exchanges turn into the controlling step at high temperatures. Based on the results in Chapters 4, 5 and 6, developing new dual-phase membrane materials is the key step of further improving the performance of DL-HFMR for methane conversion. However, as a new membrane fabrication process, the advantages of the single-step co-extrusion and co-sintering process have been proved. Its potentials in developing more advanced ceramic membranes with more specific functions have also been demonstrated.

References

1. Sunarso J, Baumann S, Serra JM, Meulenberg WA, Liu S, Lin YS, da Costa JCD. Mixed ionic-electronic conducting (MIEC) ceramic-based membranes for oxygen separation. Journal of Membrane Science 2008; 320 (1-2): 13-41.
2. Thursfield A, Metcalfe IS. The use of dense mixed ionic and electronic conducting membranes for chemical production. Journal of Materials Chemistry 2004; 14 (16): 2475-2485.

3. Liu YY, Tan XY, Li K. Mixed conducting ceramics for catalytic membrane processing. Catalysis Reviews-Science and Engineering 2006; 48 (2): 145-198.

4. Kim S, Yang YL, Jacobson AJ, Abeles B. Diffusion and surface exchange coefficients in mixed ionic electronic conducting oxides from the pressure dependence of oxygen permeation. Solid State Ionics 1998; 106 (3-4): 189-195.

5. Virkar AV. Theoretical analysis of the role of interfaces in transport through oxygen ion and electron conducting membranes. Journal of Power Sources 2005; 147 (1-2): 8-31.

6. Kim S, Yang YL, Jacobson AJ, Abeles B. Oxygen surface exchange in mixed ionic electronic conductor membranes. Solid State Ionics 1999; 121 (1-4): 31-36.

7. Bouwmeester HJM, Kruidhof H, Burggraaf AJ. Importance of the Surface Exchange Kinetics as Rate-Limiting Step in Oxygen Permeation through Mixed-Conducting Oxides. Solid State Ionics 1994; 72 185-194.

8. Bouwmeester HJM, Burggraaf AJ, Cot AJBaL, *Chapter 10 Dense ceramic membranes for oxygen separation*, in *Membrane Science and Technology*. 1996, Elsevier. p. 435-528.

9. Hong WK, Choi GM. Oxygen permeation of BSCF membrane with varying thickness and surface coating. Journal of Membrane Science 2010; 346 (2): 353-360.

10. Chen CH, Bouwmeester HJM, vanDoorn RHE, Kruidhof H, Burggraaf AJ. Oxygen permeation of La0.3Sr0.7CoO3-delta. Solid State Ionics 1997; 98 (1-2): 7-13.

11. Tan XY, Liu YT, Li K. Mixed conducting ceramic hollow-fiber membranes for air separation. Aiche Journal 2005; 51 (7): 1991-2000.

12. Tan XY, Li K. Oxygen production using dense ceramic hollow fiber membrane modules with different operating modes. Aiche Journal 2007; 53 (4): 838-845.

13. Tan XY, Li K. Modeling of air separation in a LSCF hollow-fiber membrane module. Aiche Journal 2002; 48 (7): 1469-1477.

14. Geffroy PM, Bassat JM, Vivet A, Fourcade S, Chartier T, Del Gallo P, Richet N. Oxygen semi-permeation, oxygen diffusion and surface exchange coefficient of La((1-x))Sr(x)Fe((1-y))Ga(y)O(3-delta) perovskite membranes. Journal of Membrane Science 2010; 354 (1-2): 6-13.

15. Tenelshof JE, Bouwmeester HJM, Verweij H. Oxygen-Transport through La1-Xsrxfeo3-Delta Membranes .1. Permeation in Air/He Gradients. Solid State Ionics 1995; 81 (1-2): 97-109.

16. Ji Y, Kilner JA, Carolan MF. Electrical properties and oxygen diffusion in yttria-stabilised zirconia (YSZ)-La0.8Sr0.2MnO3 +/-delta (LSM) composites. Solid State Ionics 2005; 176 (9-10): 937-943.

17. Dhallu M, Kilner JA. Oxygen transport in YSZ/LSM composite materials. Journal of Fuel Cell Science and Technology 2005; 2 (1): 29-33.

Chapter 7

Major Findings and Recommendations

7.1 General conclusions

This thesis describes the development of a highly compact dual-layer hollow fibre membrane reactor (DL-HFMR) design for methane conversion, using a new and reliable membrane fabrication process, i.e. single-step co-extrusion and co-sintering. This novel fabrication process was used to control and optimize membrane morphology and microstructure and subsequently to improve the reactor performance.

In addition to the new membrane fabrication process, the functionalization of the hollow fibre membrane with a novel dual-layer structure, i.e. an outer oxygen separation layer supported on an inner catalytic substrate layer, is achieved by using dual-phase membrane materials. As a result, the overall study involves the selection of proper functional membrane materials, the investigation of the key factors in fabricating high quality dual-layer ceramic hollow fibre membranes, the design and control of membrane morphology and microstructures, the measurement of DL-HFMR performance for methane conversion and the determination of the controlling step in the reactor to optimize membrane materials and membrane structures.

Although the efforts of membrane material selection and membrane fabrication in this thesis are directed towards the development of DL-HFMR

for methane conversion, they can be transferred to the development of other advanced membranes with different functions and for other applications of great importance, such as composite hollow fibre membranes for oxygen separation, ceramic hollow fibre substrates with gradient pore structures and micro-tubular solid oxide fuel cells (SOFC) [1-7] etc.

7.1.1 Membrane fabrication – co-extrusion and co-sintering process

A new membrane fabrication process

An asymmetric membrane structure consisting of a thin continuous separation layer supported on a highly porous substrate, also known as a composite or supported membrane, shows great potential for higher permeation flux, stronger mechanical strength and reduced material cost etc. However, before these beneficial potentials can be delivered, proper membrane fabrication processes must be developed. Currently, this is still challenging using most conventional multi-step membrane fabrication processes, due to poor quality control, poor membrane integrity and excessive time and cost. The new membrane fabrication process described in this thesis is not only a reliable approach to overcome the challenges mentioned above for achieving a dual-layer membrane structure, but is also able to realize such structures in a membrane configuration with the highest achievable surface area per unit volume to date, i.e. hollow fibre membranes. From this point of view, the investigation of the feasibility of the single-step co-extrusion and co-sintering process in Chapter 3 is not only a guide to membrane fabrication in the following chapters, but also demonstrates the potential of this membrane

fabrication process for achieving more advanced membrane structures than can be achieved using other membrane fabrication techniques.

The membrane fabrication process involved in this thesis is comprised of two steps, i.e. co-extrusion and co-sintering. Aspects of the membrane morphology such as layer thicknesses and macrostructure are determined in the first step, while mechanical properties, membrane integrity and gas-tightness of the outer separation layer are chiefly determined in the second step.

Co-extrusion

The co-extrusion process is based on the dry-wet spinning of hollow fibres in which phase-inversion and viscous fingering phenomena co-determine the structure of the resultant precursor hollow fibre membranes. As a result, the viscosity of the spinning suspension, air gap, flow rate and nature of the internal coagulant and extrusion rates are the most commonly used parameters to control the membrane morphology and structure. In contrast to previous processes of fabricating ceramic hollow fibre membranes, two spinning suspensions are co-extruded through a triple-orifice spinneret to form a dual-layer structure. This process introduces another controlling parameter during fibre spinning, namely the extrusion rate of the outer layer, which can be varied to adjust the outer layer thickness and is described in Chapter 6.

During the co-extrusion, the two layers are formed together and the polymer matrix formed during phase inversion helps to generate superior bonding between the two layers. This leads to excellent adhesion between the two layers in a much easier way, when compared with conventional coating techniques used to form dual-layer structures. Moreover, the formation of a uniform dual-layer structure in a hollow fibre configuration is more difficult due to the small diameter and high surface curvature, and is extremely challenging for most conventional membrane fabrication processes.

Theoretically, as long as good dispersion of ceramic particles in the spinning suspensions can be guaranteed, any ceramic material can be used to form such dual-layer precursor hollow fibres, as has been shown in Chapter 3, because the hollow fibre structures formed during co-extrusion are governed more by the phase inversion process, rather than the properties of the ceramic particles.

Co-sintering

In conventional fabrication processes, a coating-sintering cycle must be repeated several times to form a proper dual-layer membrane structure, while for dual-layer precursor hollow fibre membranes prepared via co-extrusion, only one sintering step is needed. However, it is still critical to match the sintering behaviour between the two layers. Due to the high surface curvature of hollow fibres, the tolerance in the difference of sintering behaviour is much smaller than for flat-sheet or tubular counterparts. As a result, the

investigation on the sintering behaviours of the membrane materials (Chapters 4 and 5) is necessary to determine the possible membrane materials and their compositions.

In order for good membrane integrity and to minimize the possible formation of cracks or defects during the co-sintering process, the shrinking of the two layers should proceed simultaneously and at the same rate. It is ideal if the final shrinkages of the two layers are identical, which is unfortunately difficult to achieve due to the varying nature of different ceramic materials. The sintering behaviour of a ceramic material is normally composed of four stages (Chapters 3, 4 and 5), and the stages at which the shrinking rate speeds up and reaches the maximum value are considered to be the key stages where the two layers must be matched as close as possible. If not, the fibres cannot even survive the co-sintering process and will consequently break into small pieces. The use of a high heating rate of 10 or even 15 °C/min is helpful when there is a reasonably small gap between the sintering behaviour of the two layers, as it shortens the time window where the shrinkage rate increases quickly to the maximum value. However, this is based on the fact that, for the ceramic materials involved in this thesis, most of sintering is complete before the high temperature dwelling stage (shrinkage rate is reduces to nearly zero). If this is not the case, the effects of dwelling temperature and time also play an important role in membrane integrity.

Basically, co-sintering is more related to aspects of the membrane material because it is determined by how membrane materials are sintered at certain temperatures. For this reason, the selection of membrane materials and the determination of material compositions are not only dependent on membrane function, but also on the co-sintering behaviour of the dual-layer hollow fibre membranes.

7.1.2 Membrane functionalization – dual-phase membrane materials

The single-step co-extrusion and co-sintering process offers a reliable way of fabricating ceramic hollow fibre membranes with controllable dual-layer structures. However, the use of such membranes as a highly compact membrane reactor design for methane conversion still requires the functionalization of each membrane layer. It is shown in Chapter 3 that single-phase membrane materials are not suitable as the sintering behaviour of the two layers is significantly different (sintering behaviour of a ceramic material is a function of material property, particle size and particle shape etc). As a result, dual-phase membrane materials have to be employed. Besides the possibility of better chemical, thermal and mechanical properties, another important benefit of using dual-phase membrane materials is the ability to adjust the ratio between the two components (or material compositions) to match the sintering behaviour of two layers made from different materials.

To turn the outer layer into a dense oxygen separation layer, a mixture of Yttria-Stabilized Zirconia (YSZ) and $La_{0.80}Sr_{0.20}MnO_{3-\delta}$ (LSM) (Chapter 4), and

another mixture of Scandia-Stabilized-Zirconia (ScSZ) and LSM (Chapters 5 and 6) are employed as the outer layer materials. Such dual-phase membrane material design is based on a membrane with a separate ionic-conducting phase (YSZ or ScSZ) and an electronic-conducting phase (LSM) for oxygen separation. Although better membrane stability in reducing atmospheres is one of the key advantages, especially in a membrane reactor, oxygen permeation lower than many single-phase perovskite ceramics must be tolerated.

Similarly, the inner catalytic substrate layer is also made of a dual-phase material, i.e. an ionic-conducting ceramic with NiO, such as YSZ-NiO (Chapter 4) or ScSZ-NiO (Chapters 5 and 6). The mixture of YSZ-NiO or ScSZ-NiO is normally densified together with the outer oxygen separation layer during the co-sintering process. Due to the nature of NiO, it turns into a highly porous structure when reduced into Ni, which creates a porous inner layer substrate at the same time. Moreover, Ni and the ionic-conducting phase can function as a catalyst layer for the partial oxidation of methane (POM) to Syngas.

Furthermore, the same ionic-conducting ceramic phase in both layers functions as a continuous inorganic matrix throughout the whole membrane, which significantly improves the adhesion between the two layers, especially at high operating temperatures (Chapters 4, 5 and 6). This is very important to extend the life time of such membrane reactor designs at high temperatures.

This can be considered as another important advantage over conventional membrane fabrication processes.

7.1.3 Application – Functional DL-HFMR for methane conversion

The employment of proper membrane materials to functionalize each membrane layer allows the use such dual-layer ceramic hollow fibre membranes as a compact membrane reactor design for methane conversion. A membrane reactor is a unit combining membrane separation and catalytic reactions into one step, where one of the two processes can be the controlling step in the reactor. For the DL-HFMR design described in this thesis, oxygen separation is in many cases the controlling step due to the relatively low oxygen permeation of the dual-phase membrane materials. In comparison, the highly porous structure of the inner layer and its good catalytic activity guarantees a sufficiently rapid consumption of the permeated oxygen. From this point of view, further optimization of the outer oxygen separation layer is needed in order for higher oxygen permeation which is able to match the capability of the inner catalytic layer for methane conversion.

In contrast to most conventional membrane reactor designs, in which additional catalyst has to be packed on the membrane surface, the DL-HFMR is a much more compact design. This means that, per unit volume of a reactor, more membrane surface area can be provided so that higher processing capacity can be achieved.

7.1.4 Approaches to improved DL-HFMR performance

The benefits of the new membrane fabrication process described in this thesis have been investigated using two approaches, from the point of view of membrane material and membrane structure in chapters 5 and 6, respectively, to improve the performance of DL-HFMR designs for methane conversion.

It has been demonstrated in Chapter 4 that higher oxygen permeation and less coke formation are the two key factors in improving reactor performance. Since the outer oxygen separation layer in Chapter 4 is made of YSZ-LSM, the replacement of YSZ by ScSZ, which has higher ionic conductivity and better resistance to coke-formation, would contribute to enhance oxygen permeation and alleviate catalyst deactivation, respectively. Such improvements were proved in Chapter 5, with a clear conclusion that high oxygen permeation can suppress the coke-formation that deactivates the catalytic substrate layer, although high operating temperatures are needed for sufficient oxygen permeation.

From the point of view of membrane structure, these results guide the study in Chapter 6 to reduce the separation layer thickness for higher oxygen permeation. Although a thinner oxygen separation layer would contribute to improve oxygen permeation at low temperatures, high operating temperatures are still needed for sufficient oxygen permeation even if the separation layer can be reduced to around 8 μm. This is because the surface exchange at such high temperatures is the controlling step for oxygen permeation.

7.2 Recommendations

It has been clearly shown that excellent control of dual-layer membrane structure and quality can be achieved using the co-extrusion and co-sintering process. Therefore, to further improve the performance of DL-HFMR designs for methane conversion, further optimization of membrane materials should be undertaken. Other possible membrane materials for the outer oxygen separation layer should be stable dual-phase materials with higher oxygen permeation flux that can possibility function at lower operating temperatures, such as $Bi_{1.5}Y_{0.3}Sm_{0.2}O_{3-\delta}$-$La_{0.8}Sr_{0.2}MnO_{3-\delta}$ [8], $Zr_{0.84}Y_{0.16}O_{1.92}$- $La_{0.8}Sr_{0.2}MnO_{3-\delta}$ [9] and $Ce_{0.8}Sm_{0.2}O_{2-\delta}$-$La_{0.8}Sr_{0.2}MnO_{3-\delta}$ [10] etc. However, NiO may still be the choice for the inner catalytic substrate layer, due to its change in structure during the reduction process and its catalytic activity for POM reaction.

Since the surface exchange process is the controlling step for oxygen separation which determines the performance of the current DL-HFMR design, surface modification can be used to further speed up surface exchange to give higher oxygen permeation. This requires the coating of a third, porous active functional layer onto the oxygen separation layer, which can be done either by brush-coating the co-sintered fibres or by co-extrusion of triple-layer hollow fibre membranes. A triple-layer hollow fibre fabricated by such a co-extrusion process, but for a different application, has recently been developed, as shown in Figure 7.1. Although it demonstrates the feasibility of fabricating triple-layer hollow fibres, more investigations on the sintering behaviour of the membrane materials are necessary, before such membrane structures can be used as a membrane reactor design for methane conversion.

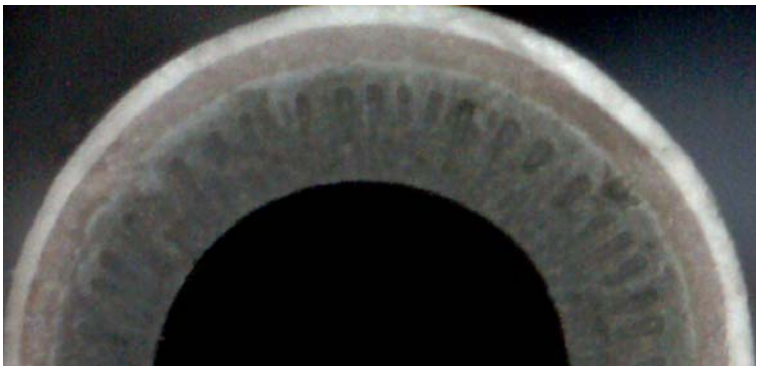


Figure 7.1 Photographic image of a triple-layer hollow fibre fabricated by co-extrusion and co-sintering process

Since the co-extrusion and co-sintering process has been proved to be a good way of fabricating dual-layer ceramic hollow fibre membranes in this thesis, it can be used to prepare multi-layer alumina hollow fibre membranes with a gradient pore structure [11]. For example, alumina of different particle sizes can be used to form different layers, and after the co-sintering a gradient pore structure throughout a membrane of this type can be obtained. Although this differs from the membranes discussed in this thesis, in which the outer layer needs to be densified, the control of pore size in each individual layer is the major concern and is also related to the investigation of the sintering behaviour of the membrane materials.

Further study can also be carried out to develop dual-layer ceramic hollow fibre membranes for oxygen separation. As discussed in Chapter 6, the thickness of the outer oxygen separation layer can be reduced to a very low level by using the co-extrusion and co-sintering process. If a membrane

structure of this type can be achieved using MIEC materials with extremely high oxygen permeation flux, such as $Ba_{0.5}Sr_{0.5}Co_{0.8}Fe_{0.2}O_{3-\delta}$ (BSCF) which has been well studied, a further improvement in oxygen separation can be expected. However, proper design of the inner substrate layer material must be achieved first.

References

1. Othman MHD, Droushiotis N, Wu ZT, Kelsall G, Li K. Novel fabrication technique of hollow fibre support for micro-tubular solid oxide fuel cells. Journal of Power Sources 2011; 196 (11): 5035-5044.

2. Othman MHD, Droushiotis N, Wu ZT, Kelsall G, Li K. High-Performance, Anode-Supported, Microtubular SOFC Prepared from Single-Step-Fabricated, Dual-Layer Hollow Fibers. Advanced Materials 2011; 23 (21): 2480-+.

3. Kanawka K, Othman MHD, Wu ZT, Droushiotis N, Kelsall G, Li K. A dual layer Ni/Ni-YSZ hollow fibre for micro-tubular SOFC anode support with a current collector. Electrochemistry Communications 2011; 13 (1): 93-95.

4. Othman MHD, Wu ZT, Droushiotis N, Doraswami U, Kelsall G, Li K. Single-step fabrication and characterisations of electrolyte/anode dual-layer hollow fibres for micro-tubular solid oxide fuel cells. Journal of Membrane Science 2010; 351 (1-2): 196-204.

5. Othman MHD, Droushiotis N, Wu ZT, Kanawka K, Kelsall G, Li K. Electrolyte thickness control and its effect on electrolyte/anode dual-layer

hollow fibres for micro-tubular solid oxide fuel cells. Journal of Membrane Science 2010; 365 (1-2): 382-388.

6. Kanawka K, Dal Grande F, Wu ZT, Thursfield A, Ivey D, Metcalfe I, Kelsall G, Li K. Microstructure and Performance Investigation of a Solid Oxide Fuel Cells Based on Highly Asymmetric YSZ Microtubular Electrolytes. Industrial & Engineering Chemistry Research 2010; 49 (13): 6062-6068.

7. Droushiotis N, Othman MHD, Doraswami U, Wu ZT, Kelsall G, Li K. Novel co-extruded electrolyte-anode hollow fibres for solid oxide fuel cells. Electrochemistry Communications 2009; 11 (9): 1799-1802.

8. Yang CL, Xu QM, Liu C, Liu JJ, Chen CS, Liu W. Bi(1.5)Y(0.3)Sm(0.2)O(3)-La(0.8)Sr(0.2)MnO(3-delta) dual-phase composite hollow fiber membrane for oxygen separation. Materials Letters 2011; 65 (23-24): 3365-3367.

9. Li W, Liu JJ, Chen CS. Hollow fiber membrane of yttrium-stabilized zirconia and strontium-doped lanthanum manganite dual-phase composite for oxygen separation. Journal of Membrane Science 2009; 340 (1-2): 266-271.

10. Li W, Tian TF, Shi FY, Wang YS, Chen CS. Ce(0.8)Sm(0.2)O(2-delta)-La(0.8)Sr(0.2)MnO(3-delta) Dual-Phase Composite Hollow Fiber Membrane for Oxygen Separation. Industrial & Engineering Chemistry Research 2009; 48 (12): 5789-5793.

11. de Jong J, Benes NE, Koops GH, Wessling M. Towards single step production of multi-layer inorganic hollow fibers. Journal of Membrane Science 2004; 239 (2): 265-269.

Appendix - I: symbols and abbreviations

D	outer diameter	m	113
D_a	ambi-polar diffusion coefficient		162
d_i	inner diameter	m	113
F	measured loading	N	113
$F_{CH4inlet}$	methane flow rate at inlet	$ml \cdot min^{-1}$	114, 140
$F_{CH4outlet}$	methane flow rate at outlet	$ml \cdot min^{-1}$	114, 140
F_{CO}	carbon monoxide flow rate at outlet	$ml \cdot min^{-1}$	140
F_{CO2}	carbon dioxide flow rate at outlet	$ml \cdot min^{-1}$	140
J_{O2}	oxygen permeation flux		161, 162
K_s	surface exchange coefficient		162
L	sample length	m	113
L_c	characteristic membrane thickness		162
P_{O2}	oxygen partial pressure		161, 162
r_A	mean ionic radii of A-site cations		36
r_B	mean ionic radii of B-site cations		36
r_O	mean ionic radii of oxygen ions		36
S_C	selectivity to carbon	%	140
S'_{CO}	selectivity to carbon monoxide (including coke formation)	%	114
S_{CO}	selectivity to carbon monoxide (excluding coke formation)	%	140
s_F	bending strength	MPa	113
t	tolerance factor		36
$t_{electron}$	transport numbers of electronic defects		37
t_{ion}	transport numbers of ionic defects		37
t_k	transport (or transference) number of carrier k		37
X_{CH4}	methane conversion	%	114, 140
$\sigma_{Electron}$	electronic conductivity		37, 161
σ_{ion}	ionic conductivity		37, 161
σ_k	Conductivity of carrier k		37
σ_{Total}	total conductivity		37

List of publications

Journal publications evolved from this thesis

1. Zhentao Wu, Alan Thursfield, Ian Metcalfe and Kang Li, Effects of Separation Layer Thickness on Oxygen Permeation and Mechanical Strength of DL-HFMR-ScSZ, Journal of Membrane Science, in press

2. Wu ZT, Wang B, Li K. Functional LSM-ScSZ/NiO-ScSZ dual-layer hollow fibres for partial oxidation of methane. International Journal of Hydrogen Energy 2011; 36 (9): 5334-5341.

3. Wu ZT, Wang B, Li K. A novel dual-layer ceramic hollow fibre membrane reactor for methane conversion. Journal of Membrane Science 2010; 352 (1-2): 63-70.

4. Wu ZT, Li, K. Dense Ceramic Membranes for Separation and Reaction Recent Patents on Engineering 2007; 1 (3): 228-237.

Journal publications related to this thesis

5. Othman MHD, Droushiotis N, Wu ZT, Kelsall G, Li K. Novel fabrication technique of hollow fibre support for micro-tubular solid oxide fuel cells. Journal of Power Sources 2011; 196 (11): 5035-5044.

6. Othman MHD, Droushiotis N, Wu ZT, Kelsall G, Li K. High-Performance, Anode-Supported, Microtubular SOFC Prepared from Single-Step-Fabricated, Dual-Layer Hollow Fibers. Advanced Materials 2011; 23 (21): 2480-+.

7. Kanawka K, Othman MHD, Wu ZT, Droushiotis N, Kelsall G, Li K. A dual layer Ni/Ni-YSZ hollow fibre for micro-tubular SOFC anode support with a current collector. Electrochemistry Communications 2011; 13 (1): 93-95.

8. Hatim MDI, Tan XY, Wu ZT, Li K. Pd/Al(2)O(3) composite hollow fibre membranes: Effect of substrate resistances on H(2) permeation properties. Chemical Engineering Science 2011; 66 (6): 1150-1158.

9. Othman MHD, Wu ZT, Droushiotis N, Kelsall G, Li K. Morphological studies of macrostructure of Ni-CGO anode hollow fibres for intermediate temperature solid oxide fuel cells. Journal of Membrane Science 2010; 360 (1-2): 410-417.

10. Othman MHD, Wu ZT, Droushiotis N, Doraswami U, Kelsall G, Li K. Single-step fabrication and characterisations of electrolyte/anode dual-layer hollow fibres for micro-tubular solid oxide fuel cells. Journal of Membrane Science 2010; 351 (1-2): 196-204.

11. Othman MHD, Droushiotis N, Wu ZT, Kanawka K, Kelsall G, Li K. Electrolyte thickness control and its effect on electrolyte/anode dual-layer hollow fibres for micro-tubular solid oxide fuel cells. Journal of Membrane Science 2010; 365 (1-2): 382-388.

12. Kingsbury BFK, Wu ZT, Li K. A morphological study of ceramic hollow fibre membranes: A perspective on multifunctional catalytic membrane reactors. Catalysis Today 2010; 156 (3-4): 306-315.

13. Kanawka K, Dal Grande F, Wu ZT, Thursfield A, Ivey D, Metcalfe I, Kelsall G, Li K. Microstructure and Performance Investigation of a Solid Oxide Fuel Cells Based on Highly Asymmetric YSZ Microtubular Electrolytes. Industrial & Engineering Chemistry Research 2010; 49 (13): 6062-6068.

14. Gbenedio E, Wu ZT, Hatim I, Kingsbury BFK, Li K. A multifunctional Pd/alumina hollow fibre membrane reactor for propane dehydrogenation. Catalysis Today 2010; 156 (3-4): 93-99.

15. Zydorczak B, Wu ZT, Li K. Fabrication of ultrathin $La_{0.6}Sr_{0.4}Co_{0.2}Fe_{0.8}O_{3-\delta}$ hollow fibre membranes for oxygen permeation. Chemical Engineering Science 2009; 64 (21): 4383-4388.

16. Wu ZT, Hatim IMD, Kingsbury BFK, Gbenedio E, Li K. A Novel Inorganic Hollow Fiber Membrane Reactor for Catalytic Dehydrogenation of Propane. Aiche Journal 2009; 55 (9): 2389-2398.

17. Wang B, Zydorczak B, Wu ZT, Li K. Stabilities of $La_{0.6}Sr_{0.4}Co_{0.2}Fe_{0.8}O_{3-\delta}$ oxygen separation membranes-Effects of kinetic demixing/decomposition and impurity segregation. Journal of Membrane Science 2009; 344 (1-2): 101-106.

18. Wang B, Wu ZT, Livingston AG, Li K. A novel phase transition technique for fabrication of mesopore sized ceramic membranes. Journal of Membrane Science 2009; 339 (1-2): 5-9.

19. Koonaphapdeelert S, Wu ZT, Li K. Carbon dioxide stripping in ceramic hollow fibre membrane contactors. Chemical Engineering Science 2009; 64 (1): 1-8.

20. Gimeno MP, Wu ZT, Soler J, Herguido J, Li K, Menendez M. Combination of a Two-Zone Fluidized Bed Reactor with a Pd hollow fibre membrane for catalytic alkane dehydrogenation. Chemical Engineering Journal 2009; 155 (1-2): 298-303.

21. Droushiotis N, Othman MHD, Doraswami U, Wu ZT, Kelsall G, Li K. Novel co-extruded electrolyte-anode hollow fibres for solid oxide fuel cells. Electrochemistry Communications 2009; 11 (9): 1799-1802.

22. Koonaphapdeelert S, Tan XY, Wu ZT, Li K. Solvent distillation by ceramic hollow fibre membrane contactors. Journal of Membrane Science 2008; 314 (1-2): 58-66.

Book chapters

23. Zhentao Wu, Mohd Hafiz Dzarfan Othman, Benjamin F. K. Kingsbury and K. Li. *Chapter 16: Functional Ceramic Hollow Fibre Membranes for Energy Utilization*, Advanced membrane science and technology for

sustainable energy and environmental applications, Woodhead Publishing Series in Energy No. 25, 2011, ISBN 1 84569 969 6

24. Benjamin F. K. Kingsbury, Zhentao Wu and K. Li, *Chapter 3: Inorganic Hollow Fibre Membranes for Chemical Reaction*, Membranes for Membrane Reactors: Preparation, Optimization and Selection, Wiley, 2011, ISBN: 978-0-470-74652-3

Manuscripts in process

25. Zhentao Wu, Guangru Zhang, Wanqin Jin and Kang Li, Asymmetric Nb_2O_5-doped $SrCo_{0.8}Fe_{0.2}O_{3-\delta}$ Hollow Fibre Membrane for Oxygen Separation